Review of Experimental and Computational Studies on Spray, Combustion, Performance, and Emission Characteristics of Biodiesel Fueled Engines

Avinash Kumar Agarwal[1]
Engine Research Laboratory,
Department of Mechanical Engineering,
Indian Institute of Technology Kanpur,
Kanpur 208016, India
e-mail: akag@iitk.ac.in

Sungwook Park
School of Mechanical Engineering,
Hanyang University,
222, Wangsimni-ro, Seongdong-gu,
Seoul 04763, South Korea

Atul Dhar
School of Engineering,
Indian Institute of Technology Mandi,
Mandi 175005, India

Chang Sik Lee
School of Mechanical Engineering,
Hanyang University,
222, Wangsimni-ro, Seongdong-gu,
Seoul 04763, South Korea

Suhan Park
School of Mechanical Engineering,
Chonnam National University,
77 Yongbong-ro, Buk-gu,
Gwangju 61186, South Korea

Tarun Gupta
Department of Civil Engineering,
Indian Institute of Technology Kanpur,
Kanpur 208016, India

Neeraj K. Gupta
Department of Civil Engineering,
Indian Institute of Technology Kanpur,
Kanpur 208016, India

Biodiesel has emerged as a suitable alternative to mineral diesel in compression ignition (CI) engines in order to ensure global energy security and to reduce engine out emissions in near future. Biodiesel derived from various feedstocks available worldwide fits well in the current fuel supply arrangement for transport sector. However, biodiesel as an alternative transportation fuel has been extensively investigated because of differences in its important fuel properties compared with baseline mineral diesel. Since fuel properties greatly influence spray development, combustion, and emission formation in internal combustion (IC) engines, a number of experimental and computational studies on biodiesel usage in CI engines have been performed to determine its brake thermal efficiency (BTE), gaseous emissions, durability, etc., by various researchers using variety of engines and feedstocks. In the present paper, a critical review of the effect of biodiesel's fuel properties on engine performance, emissions, and combustion characteristics in existing diesel engines vis-a-vis conventional diesel has been undertaken. In addition, the progress and advances of numerical modeling involving biodiesel are also reviewed to determine the effect of fuel properties on spray evolution and development of reaction mechanisms for biodiesel combustion simulations. Fuel properties are discussed in two categories: physical and chemical properties, which are key parameters affecting spray and combustion processes. Subsequent sections review spray, combustion, emissions, and performance characteristics of biodiesels under various engine operation conditions. In the last section of this review paper, numerical modeling of biodiesel covering recent numerical models and schemes to understand the behavior of biodiesel combustion and pollutants formation is included. This review paper comprehensively summarizes biodiesel fuel's (BDFs) spray, combustion, and emission characteristics using experimental and numerical approaches. Limitations and scope for future studies are discussed in each section. [DOI: 10.1115/1.4040584]

Keywords: biodiesel, spray characteristics, modeling, combustion, regulated emissions, unregulated emissions

1 Introduction

For ensuring energy security in near future and to mitigate life threatening consequences of energy utilization such as climate change, herculean research efforts are being made for developing viable alternative fuels [1–4] and suitable engine technology [5–10] for the global transport sector. Infrastructure investment requirement favors the use of renewable alternatives for fueling existing vehicles and it fits well in the current fuel supply scenario as well. Biodiesels derived from various feedstocks available worldwide are being considered as the most suitable candidates in near future for full/partial replacement of mineral diesel. Though the fuel properties of biodiesel are fairly close to mineral diesel, stringent emission norms for modern diesel engines require fuel property within a very narrow band. Production of biodiesel from a large variety of locally available feedstocks is an environment friendly option; however, the final properties of biodiesel produced depend on the feedstock properties and the production process adapted to a great extent. In general, biodiesels are fatty acid methyl esters derived from various vegetable oils and animal fats. Composition of biodiesel has significant influence on its physical properties such as density, viscosity, and surface tension. Engine performance and emission characteristics are dependent on biodiesel properties. For ensuring successful implementation of various biodiesels on a large scale, different performance parameters, gaseous and particulate emission characteristics, combustion characteristics such as pressure rise rate, engine knock, degradation of lubricating oil, and engine durability need to be comprehensively studied for biodiesel fueled engines. For fulfilling this requirement, the effects of biodiesel properties on performance, combustion, and emissions characteristics of compression ignition (CI) engines vis-à-vis conventional diesel are comprehensively reviewed.

2 Biodiesel Properties

2.1 Physical Properties. Biodiesel is typically characterized by important fuel properties such as density, viscosity, surface tension, flash point, cetane number (CN), and heating value. Fuel

[1]Corresponding author.

Contributed by the Internal Combustion Engine Division of ASME for publication in the Journal of Energy Resources Technology. Manuscript received April 8, 2018; final manuscript received June 9, 2018; published online August 30, 2018. Editor: Hameed Metghalchi.

properties of biodiesels are comparable to conventional mineral diesel; therefore, biodiesels can be used with negligible or no hardware modifications to the existing fuel injection equipment (FIE) and the main combustion system of the CI engine. In order to use it in CI engines, biodiesels derived from vegetable oils, animal fats, and waste cooking oils should meet statutory requirements set by various biodiesel standards such as ASTM D6751 in USA and EN 14214 in Europe, as listed in Table 1 [11,12].

Some of the important biodiesel properties are discussed in the following subsections (2.1.1–2.1.5).

2.1.1 Density. Density of biodiesel is one of the most important fuel properties affecting its use in automotive engines. Density is defined as the mass per unit volume of a substance at specified pressure and temperature. Fuel density is an important physical property that directly affects fuel indicators such as heating value and cetane number [13]. The densities of biodiesels are usually higher than conventional mineral diesel and depend on their composition and purity. As shown in Table 1, the legislated density ranges of biodiesels and mineral diesel at 15 °C are 860–900 and 820–845 kg/m^3, respectively [11,12]. These density values are related to the fatty acid saturation level and carbon chain length of the hydrocarbon chains present in biodiesel. Biodiesel density increases with decreasing chain length (number of carbon atoms) and increasing number of double bonds (unsaturation degree) [14,15]. Giakoumis [15] showed that the average densities of 25 investigated biodiesels, except castor oil biodiesel ($\rho = 917.6$ kg/m^3), were between 870.8 and 891.5 kg/m^3 with an overall mean value of 880.2 kg/m^3. Composition of biodiesel has a significant influence on its physical properties such as density, viscosity, and surface tension [16]. Density of fuel in a CI engine primarily affects spray characteristics such as spray tip penetration, spray momentum, and distribution of the fuel-air mixture in the combustion chamber. Density of biodiesel depends on the fatty acid content, molar mass, water content, and temperature. Density of biodiesel is particularly influenced by the feedstock used in its production. Soybean, rapeseed, and palm oils are commonly used; however non-edible oils such as jatropha and karanja

Table 1 Specifications of mineral diesel and biodiesels [11,12]

		Mineral diesel (ASTM D975-12a)		Biodiesel (ASTM D6751-15b)		Biodiesel (EN 14214)	
Property	Units	Specification	Test method	Specification	Test method	Specification	Test method
Flash point	°C	52 min[a]	D93	93 min	D93	101 Min.	EN ISO 2719
Water and sediment	% vol	0.05 max[a]	D2709	0.05 max	D2709	0.05 max	EN ISO 12937
Calcium and magnesium, combined	ppm (μg/g)			5 max	EN14538	5 max	EN 14538
Distillation temperature (90% vol. recovered)	°C	2D: 282 min 338 max	D86	360 max	D1160	—	—
Kinematic viscosity at 40 °C	mm^2/s	2D: 1.9 min 4.1 max	D445	1.9-6.0	D445	3.5–5.0	EN ISO 3104 / EN 14105
Density, 15 °C	kg/m^3	820–845[b]		860–900[c]		860–900	EN ISO 3675 / EN ISO 12185 / EN12185.
Ramsbottom carbon residue on 10% distillation residue	mass, max	0.35	D524	0.010	D524	0.3 max.	EN ISO 10370
Ash	%mass max	0.01	D482	—	—	—	—
Sulfated ash	%mass max			0.02 max	D874	0.02 max	ISO 3987
Sulfur	ppm (μg/g)	15 ppm	D5453	0.0015 max (15 ppm)	D5453	10	EN ISO 20846 / EN ISO 20884.
Copper strip corrosion rating	Max 3 h at 50 °C	No.3 max	D130	No.3 max	D130	Class 1	EN ISO 2160
CN		40 min	D613	47 min	D613	51 min.	EN ISO 5165
Cloud point or LIFT/CFPP	°C max	Regional requirement	D2500 D4539 /D6371	Report	D2500	—	—
Carbon residue	%mass	2D:0.35	D524	0.05 max	D4530	0.3	EN ISO 10370
Acid number	mg KOH/g			0.5 max	D664	0.5 max	EN 14104
Sodium and potassium, combined	ppm (μg/g)			5 max	EN14538	5 max	EN 14108 / EN 14109 / EN 14538
Oxidation stability	hours			3 min	EN14112	6 Min,	EN 14112
Methanol	%mass			0.2max	EN14110	0.2 Max.	EN 14110
Phosphorous	ppm			10 max	D4951	4 Max.	EN14107
Lubricity, HFRR at 60 °C	Mm	520 max	D6079 D7688	—	—	—	—
Conductivity	pS/m Unit (C.U.) min	25	D2624/D4308	—	—	—	—
Free glycerine Total glycerine	%mass %mass	—	—	0.02 max 0.240 max	D6584 D6584	0.02 max 0.25 max.	EN 14105 / EN 14106

[a]min refers to minimum and max refers to maximum.
[b]EN: Diesel 820-845 kg/m^3, EN ISO3675, 12185.
[c]EN Biodiesel 860-900 kg/m^3, EN ISO-3675, EN-12185.

Table 2 Density ranges of biodiesels from different feedstocks

Biodiesel feedstock	Density (kg/m^3)	Temperature (K)	Reference
Soybean	894.6–832.5	278.15–363.15	[18]
Sunflower	888.16–834.05	288.15–363.15	[20]
Rapeseed	893.3–831.4	278.15–363.15	[18,21]
Cotton seed	884.1–837.2	288.15–358.15	[22]
Palm oil	875.9–821.5	288.15–363.15	[18–19]
Lard Fatty Acids	871.86–824.92	298.15–363.15	[20]
Peanut+ sunflower	886.9–828.8	293.15–373.15	[23]
Mineral diesel	849.23–777.97	273.15–373.15	[21]

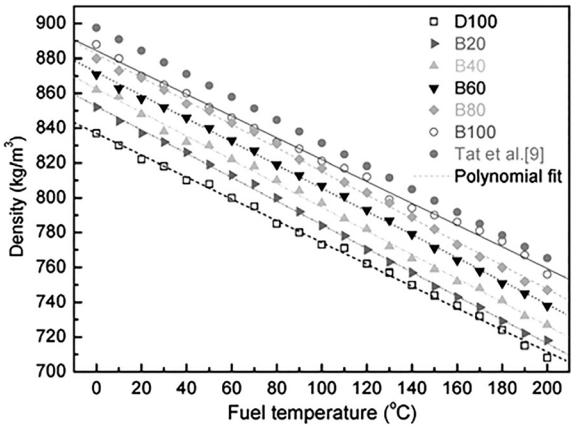

Fig. 1 Relationship between fuel density and fuel temperature [25–26]

have also been investigated as suitable feedstocks for biodiesel production [16,17]. Density is a significant factor in choosing feedstock for the production of biodiesel using established production processes and standards. The densities of biodiesels at various temperatures are given in Table 2. As shown in this table, the density of various biodiesels was in the ranges of 894.6–832.5, 875.9–821.5, 893.3–831.4, and 884–837.2 kg/m^3 for soybean [18], palm [19], rapeseed [18], and cottonseed oils [22], respectively.

The density of biodiesel, ρ_b (g/cm^3) can be calculated using the following equation [24]:

$$\rho_b = \sum_{i=1}^{n} w_i \left(1.069 + \frac{3.575}{M_i} + 0.0113N_i - 7.41 \times 10^{-4}T\right) \quad (1)$$

where w_i, M_i, N_i, and T are the mass fraction, molecular weight (g/mol), number of double bonds in the fatty acid chain, and temperature (K), respectively.

Pure biodiesel is denoted as B100 and the blending percentage (v/v) of biodiesel with mineral diesel set to 0, 10, 20, 30, and 40% and so forth are denoted as B0, B10, B20, B30, and B40, respectively. In Table 2, the densities of select biodiesels are in the range of 824–893 kg/m^3. The densities of mineral diesel (D100), biodiesel (B100), and B20-B80 at various temperatures are compared in Fig. 1 [25,26]. The densities of biodiesel blends increased with biodiesel blending ratio. In the measured temperature range, many investigations showed that densities of B100, D100, and biodiesel blends decreased with increasing temperature and the slopes of their density versus temperature variation curves showed similar reduction rates [24–29].

2.1.2 Viscosity. In the analysis of liquid motion and flow behavior near the solid boundary in a fuel injection system, the viscosity, which is a measure of resistance to fluid deformation by shear stress, is an important fuel property. In this case, the shear resistance in a flow field is caused by intermolecular friction. There are two related fluid viscosities: dynamic (absolute) viscosity and kinematic viscosity. Dynamic viscosity is the resistance of a medium to fluid flow, which is caused by a shear stress in the fluid flowing by a solid boundary. Therefore, the dynamic viscosity μ(Ns/m^2, Pa·s or kg/ms) can be expressed as $\tau = \mu dc/dy$. In this equation, τ is the shear stress (N/m^2) and dc and dy are the velocity and unit distance between layers (m), respectively. The kinematic viscosity, ν (m^2/s), is the ratio of dynamic (or absolute) viscosity to the fuel density ($\nu = \mu/\rho$).

In general, the viscosity of biodiesel ranges from 3.5 to 5.0 mm^2/s at 40 °C, which is slightly higher than conventional mineral diesel as reflected in biodiesel standards (e.g., EN ISO 3104). The dynamic viscosity of biodiesel and its blends is highly dependent on the fuel temperature. As listed in ASTM D6751-15, the kinematic viscosity range of B100 at 40 °C is in a broader range of 1.9–6.0 mm^2/s, whereas a narrower range of 1.9–4.1 mm^2/s is shown by mineral diesel. Higher fuel viscosity affects both the spray characteristics and the combustion characteristics of biodiesel fueled engine [21,27].

The viscosities of biodiesels derived from soybean oil, rapeseed oil, and soybean and rapeseed oil mixtures [28] at 293.15 K and 393.15 K are shown in Table 3. A highly viscous biodiesel would take longer time to evaporate and mix with the air in the combustion chamber. Therefore, the fuel-air mixture quality deteriorates compared to that from low viscosity fuel.

Shahabuddin et al. [29] showed that the viscosity of palm oil methyl ester (PME) increased from 4.92 to 5.971 cSt after a storage duration of 2160 h at 40 °C. In their study, the viscosities of jatropha oil methyl ester and coconut oil methyl ester showed an increasing trend and this rate was lower than that in the case of PME. Mineral diesel showed a slightly increased viscosity of 0.49 cSt (from 3.20 to 3.69 cSt) with storage duration, because oxidation did not affect fuel viscosity significantly. The viscosity of biodiesels is dominated by the chain length (number of carbon atoms) of the methyl esters [29]. Ramirez-Verduzco et al. [30] showed that kinematic viscosity of biodiesel increases with chain length (number of carbon atoms) and there is a linear relationship between kinematic viscosity and molecular weight of the constituent molecules of biodiesel. As shown in Table 4, kinematic viscosity of fatty acid methyl esters increases with the increasing number of carbon atoms of constituent methyl esters of biodiesel.

The viscosity of biodiesels, μ_b (mPa·s), can be estimated using the following equation [30]:

Table 3 Dynamic viscosities of biodiesels

	Dynamic viscosity (mPa s)			
Biodiesel feedstock	293.15 K	393.15 K	Pressure (MPa)	Reference
Soybean	6.33	1.35	0.1	[28]
Rapeseed	6.93	1.33	0.1	[28]
Fatty acids from lard	5.913	1.466	0.1	[20]
Soybean + Rapeseed[a]	6.76	1.49	0.1	[28]
Peanut+ Sunflower[b]	3.50	0.89	0.1	[21]

[a]Mixture of soybean and rapeseed.
[b]Mixture of peanut and sunflower.

Table 4 Density and kinematic viscosity of fatty acid methyl esters

Methyl ester	ρ (g/cm^3) at 20 °C [26]	η (mm^2/s) at 40 °C	η (mm^2/s) at 40 °C [30]
C10:0	0.8726	1.71[a]	1.72
C12:0	0.8692	2.43[a]	2.45
C14:0	0.8665	3.30[b]	3.33
C16:0	0.8664	4.38[a]	4.37
C16:1	0.8764	3.67[a]	3.59
C18:0	0.8627	5.85[a]	5.59
C18:1	0.8746	4.51[a]	4.60
C18:2	0.8865	3.65[a]	3.79

[a]Gerhard Knothe [31].
[b]Saiban and Brown [32].

$$\ln \mu_b = \sum_{i=1}^{n} w_i \left(-18.354 + 2.362 \ln M_i - 0.127 N_i + \frac{2009}{T} \right)$$

where w_i, M_i, N_i, and T are the mass fractions, molecular weight (g/mol), number of double bonds in the fatty acid chain, and temperature (K), respectively.

Essentially, the viscosity of biodiesels decreases with increasing fuel temperature. Therefore, heating biodiesel reduces its viscosity, and hence the pumping work requirement by the fuel injection system, while it improves biodiesel's spray and atomization characteristics. To reduce energy loss due to viscous friction caused by interaction between biodiesel and fuel injection pump, a minimal fuel viscosity is required. Fuel viscosity plays an important role in preventing fuel leakage from the high-pressure fuel lines of the fuel injection system. During the injection period, higher viscosity of biodiesel reduces fuel leakage from the high-pressure fuel injection system [33]. To analyze properties of biodiesel, Yoon et al. [25] measured the density and kinematic viscosity of soybean biodiesel and blends in a temperature range from 0 to 200 °C. Their results showed that the kinematic viscosity of soybean biodiesel was 6.954 mm^2/s at 20 °C. Essentially, viscosity of biodiesel decreased with increasing fuel temperature. As the blending ratio of biodiesel increased, the viscosity of test blend increased slightly.

2.1.3 Surface Tension. In general, intermolecular forces are dependent on the liquid fuel type such as gasoline, mineral diesel, or biodiesel. Surface tension is defined as the energy required to increase the surface area of a liquid and it depends on intermolecular forces. The surface tension of biodiesel is an important factor in the analysis of fuel's spray, atomization, and vaporization characteristics because higher surface tension influences the disintegration of injected liquid fuel spray [34–36]. The surface tension of conventional mineral diesel and biodiesel were measured to be approximately 28.0 and 31.7 mN/m respectively at 293 K [37].

In a diesel engine, fuel spray and atomization are the first stage leading up to fuel's combustion in the combustion chamber. The oxygen of the intake air reacts with the atomized droplets of injected fuel on the surface and combustion generated heat is released to the surroundings. In the spray droplet formation and spray breakup of biodiesel, surface tension, viscosity, and droplet inertia are the most relevant factors, which govern the effective spray evolution. In a study on the effect of fuel viscosity and surface tension on the spray breakup and coalescence for four different liquid fuels, Davanlou et al. [38] showed that spray diameter decreased with lowering surface tension.

The surface tension of biodiesel is closely related to its molecular structure and is influenced by the length of fatty acid hydrocarbon chains and the number of unsaturated bonds [36,39]. Long chains of fatty acid hydrocarbons in the molecular structure lead to higher surface tension. Table 5 shows a comparison of calculated and experimental values of surface tension. The calculated values of surface tension in this table are taken from the study by Phankosol et al. [39] and experimental results from the study by Freitas et al. [40]. It may also be noted from the table that the surface tension of biodiesels decreased linearly with increasing fuel temperature.

2.1.4 Flash Point. Flash point is defined as the lowest temperature at which a fuel can form a combustible mixture in the air, when exposed to a flame or spark. The fire point is the minimum temperature at which inflammable vapors will continue to form and steadily burn. In other words, fire point is similar to the flash point except that the flame continues to burn for at least 5 s (DIN ISO 2592). The flash point is therefore an important fuel property to be considered in handling, storage, and safe management of biodiesel. According to biodiesel standards, flash points of mineral diesel [ASTM D975] and biodiesel (ASTM D6751) should be above 52 and 93 °C, respectively. As shown in Table 6, flash point of soybean biodiesel is 178 °C [41], and for castor biodiesel, it is 285.71 °C [42], which is the highest among biodiesels. Comparing these values with mineral diesel, the mean value of flash point of biodiesels in Table 6 is 182.10 °C, which is 2.53–3.03 times that of mineral diesel (60–72 °C). From this data, it is clear that

Table 5 Surface tension of biodiesels at various temperatures [39,40]

	Surface tension, σ (mN/m)						
Biodiesel feedstock oil	Temp 303.15 (K)	Temp 313.15 (K)	Temp 323.15 (K)	Temp 333.15 (K)	Temp 343.15 (K)	Temp 353.15 (K)	Reference
Soybean[a]	31.10	30.21	29.32	28.43	27.54	26.65	[39]
Soybean[b]	30.89	29.74	28.66	27.98	26.97	25.97	[40]
Rapeseed[a]	30.89	30.03	29.16	28.29	27.43	26.56	[39]
Rapeseed[b]	32.18	31.17	30.14	28.60	27.39		[40]
Palm[a]	30.13	29.30	28.48	27.65	26.83	26.00	[39]
Palm[b]	31.89	30.55	29.86	28.62	27.84		[40]
Sunflower[a]	31.13	30.24	29.35	28.47	27.58	26.69	[39]
Sunflower[b]	–	31.15	29.39	28.29	27.47	26.04	[40]
Soybean+Rapeseed[a]	30.95	30.08	29.20	28.32	27.44	26.57	[39]
Soybean+Rapeseed[b]	31.57	30.55	29.54	28.50	27.59	26.57	[40]
Soybean+Palm[a]	30.60	29.74	28.89	28.03	27.17	26.32	[39]
Soybean+Palm[b]	–	30.74	29.70	28.50	27.71	26.89	[40]
Rapeseed+Palm[a]	30.47	29.62	28.78	27.93	27.09	26.25	[39]
Rapeseed+Palm[b]	–	30.74	29.70	28.50	27.71	26.89	[40]
Soybean+Rapeseed+Palm	31.53	30.49	29.40	28.56	27.29	26.07	[40]

[a]Calculated value.
[b]Experimental value.

Table 6 Flash point, cloud point, and pour point of biodiesels

Biodiesel feedstock	Flash point (°C)	Cloud point (°C)	Pour point (°C)	Reference
Soybean oil	178	−0.5	−3.8	[41,44]
Peanut oil	176	5	—	[41]
Palm oil	151.71	16	12	[45,46]
Castor oil	285.71	−12	−32	[45,47]
Sunflower seed oil	139	1.0	−1	[41,48,49]
Rapeseed oil	170	−4.0	−13	[42,44]
Jatropha oil	184.5	4	3	[46,50]
Tallow	117	12	9	[44,47]
Karanja oil	237	—	2	[51,52]
# 2 mineral diesel	60–72	−15 to 5	−35 to −15	[44]

biodiesel has significantly higher flash point than mineral diesel. Higher blending ratios of biodiesels increase the flash point of test blends. Especially, residual alcohol from biodiesel production process has significant influence on the flash point temperature [43] of biodiesel and higher residual alcohol decreases the flash point.

When considering biodiesel usage for transportation sector, a higher flash point is safer for storage and handling of the test fuel; therefore, higher flash point ensures greater safety of both biofuels and the passengers.

2.1.5 Cloud Point and Pour Point. Cloud point of fuel is defined as the temperature at which a cloud of wax crystals first appears in the liquid fuel that is cooled under specified conditions prescribed by ASTM D2500. Pour point is defined as the temperature of the gelling of the liquid fuel (ASTM D97) and it indicates the lowest temperature, at which the fuel will begin start to flow under specified conditions. Pour point of biodiesel is always lower than the cloud point as defined by ASTM D97. In cold climate regions, one of the major concerns of biodiesel usage is its relatively unfavorable cold flow properties compared to mineral diesel. Table 6 shows that biodiesels derived from soybean, rapeseed, and castor oils have lower cloud and pour points, while tallow methyl ester has higher cloud and pour points. The cloud point of biodiesel depends on the feedstock and its values are in a range of −12 °C for castor biodiesel and 16 °C for palm biodiesel [48]. Generally, addition of flow improving additives in biodiesel can decrease the size by restraining the formation of wax crystallites when the test fuel is cooled. Also, suitable additives can significantly reduce the gelling temperature. As shown in Table 6, cloud and pour points of biodiesels are 20–25 °C higher than mineral diesel [50]. In biodiesels, the freezing temperature is affected by the structural properties of the constituents such as the chain length, degree of unsaturation, and degree of branching. Blending of biodiesels with mineral diesel is widely used to resolve the flow problems in cold weather conditions. Mineral diesel component in biodiesel blended fuels acts as a solvent for precipitated crystals, waxes, or gels formed at low temperature [48], thus effectively reducing cold weather related issues.

2.1.6 Fuel Lubricity. Lubrication system in a diesel engine plays an important role in reduction of friction and an effective engine operation. In general, biodiesels provide superior lubrication properties than mineral diesel [53], e.g., the coefficient of friction (COF) in friction and wear tests showed that biodiesels offer significantly lower COF than mineral diesel [54]. Mosarof et al. [54] reported that biodiesel showed lower COF because it contains methyl esters, which are more effective in protection of surfaces from scuffing compared to mineral diesel. In an unsteady condition, Calophyllum inophyllum biodiesel (CIB100) and its blends exhibited lower COF among tested fuels. Comparing the COF of mineral diesel and biodiesels in unsteady test, mineral diesel showed 84.5% and 39.4% higher COF values than CIB100 and PB100 (palm oil biodiesel), respectively. In steady-state condition, all biodiesel blends showed similar COF, and the COF of mineral diesel indicated 79.2% and 76.1% higher values than CIB100 and PB100 respectively.

According to a study on improvement of lubricating properties using sunflower biodiesel, addition of 1% biodiesel to low-sulfur diesel ensures lubrication properties that meet the requirements set by the European standard (EN590) [55]. In this study, lubrication properties significantly improved but the power output of the engine did not change significantly. This was primarily due to presence of longer carbon chains among biodiesel fatty acids, leading to improved lubrication properties.

Lubricity of biodiesel is strongly dependent on its chemical composition, wherein oxygen atoms are bound in the ester molecule [56]. In the scoffing load ball-on-cylinder lubricity evaluator of test for estimating the lubricating quality of fuels [ASTM D6078], biodiesel (soy methyl ester (SOE)) showed a performance enhancement by nearly 1.68-fold over the baseline mineral diesel [57]. In another experimental investigation involving 250 h endurance test for determining diesel engine wear using Karanja biodiesel [58], biodiesel blends showed relatively lower wear than mineral diesel because of the presence of free fatty acids, oxygenated moieties, and unsaturated molecules in biodiesel. However, the presence of sodium hydroxide in biodiesel can sometimes reduce its lubricity [59].

2.2 Chemical Properties

2.2.1 Oxygen Content. One of the major difference in chemical structure and composition of mineral diesel and biodiesel is its oxygen content. A significant advantage of biodiesels compared to mineral diesel is that biodiesels have higher oxygen content (∼11–12% w/w) in their molecular structure [60,61]. The variations in oxygen content are attributed to the degree of oxygenation of different feedstocks and their chemical composition. Highly saturated oils used as feedstocks for biodiesel production are more oxygenated, hence they burn cleanly and are stable. Oxygen content of biodiesels enhances the combustion rate and in turn shortens the combustion duration. Therefore, the oxygen content of biodiesels results in improved combustion efficiency, and reduced emissions of CO, HCs, and other harmful species [47,53]. Presence of biodiesel in the test blend plays an important role in reducing harmful engine-out emissions. Oxygen content of test blends increases with increasing biodiesel blending ratio [62]. It was shown that in the exhaust emissions from a diesel engine, the reduction in PM emissions was proportional to the oxygen content of the biodiesel containing test blend.

2.2.2 Cetane Number. As an indicator of ignition and combustion characteristics, the CN is measured by a dimensionless index according to test standards ASTM D613 and ISO 5165. In a CI engine, ignition and combustion properties are the most important quality factors for test fuels. Generally, CN is related to the ignition delay period and is dependent on composition and degree of unsaturation of the test fuel [63]. Higher CNs advance the combustion timing because of shorter ignition delay [30,63]. The relationship between CN and ignition delay shows that higher CNs

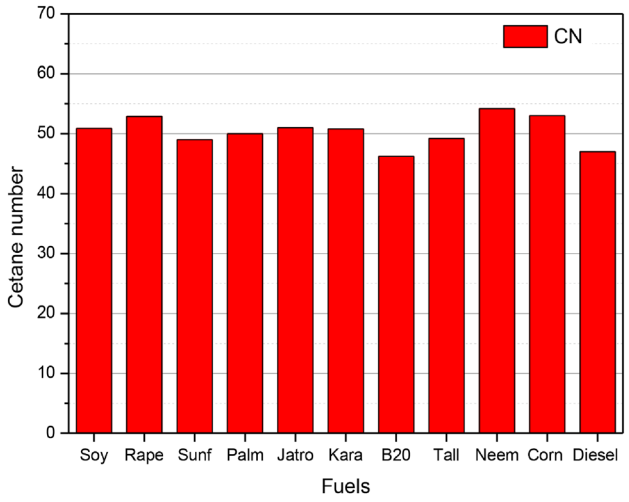

Fig. 2 Comparison of CN of biodiesels vis-a-vis mineral diesel [15,30,44,66,67,70]. (Soy: soybean, Rape: rapeseed, Sunf: sunflower, Palm: palm, Jatr: jatropha, Kara: karanja, Tall: tallow, and B20: 20% v/v biodiesel blend).

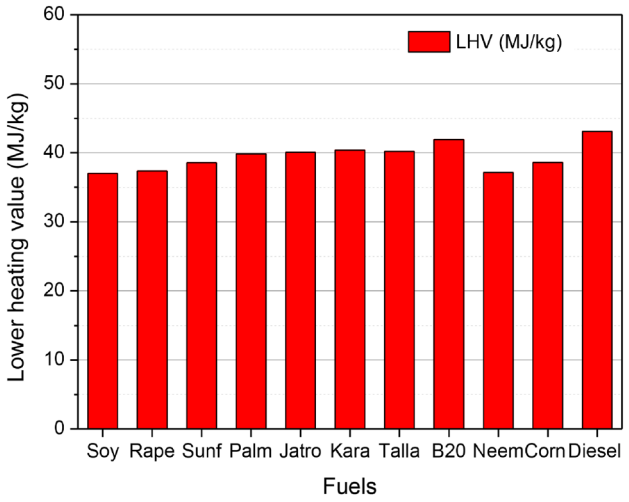

Fig. 3 Comparison of LHV of biodiesels and mineral diesel [42,44,68–70,73,74,77,78,80–82] (Soy: soybean, Rape: rapeseed, Sunf: sunflower, Palm: palm, Jatr: jatropha, Kara: karanja, Tall: tallow, and B20: 20% biodiesel blend)

Table 7 CN and calorific value of biodiesels

Fuel	LHV(MJ/kg)	CN	Reference
Soybean	35.6	50.9	[44]
Rapeseed	35.9	52.9	[44]
Sunflower	38.6	49.0	[44]
Palm oil	39.8[a]	50	[72]
Tallow	40.2[a]	58.8	[44]
B20 (Soy)	41.6	46.2	[72,76]
Jatropha	40.1	51.0	[75,77]
Karanja	40.4	50.8	[74,78]
Animal fat	37.3	63	[57,76]

[a]Higher heating value.

result in shorter ignition delays. In addition, CN is influenced by the chain length of fatty acids and the number of double bonds. The CN of biodiesel increases with increasing chain length and decreases with increasing number of double bonds [64]. Biodiesels have higher CNs [62–70] than mineral diesel [71] and higher CNs tend to increase the peak combustion temperature due to shorter ignition delay [57,73,74]. Figure 2 shows the CNs of biodiesels and mineral diesel. As shown in Fig. 2, most biodiesels exhibit higher CN than mineral diesel.

The CN of biodiesel derived from soybean oil is 50.9 (Table 7), while karanja and jatropha biodiesels are 50.8 and 51, respectively [74,75].

2.2.3 Heating Value. The heating value of a fuel can be further categorized as higher heating value (HHV) and lower heating value (LHV). The HHV or gross calorific value is defined as the amount of heat released when unit mass of fuel (maintained initially at 25 °C) is completely combusted under stoichiometric fuel-air conditions at constant pressure with combustion products being cooled to the initial temperature of 25 °C and any water vapor produced in the combustion products being condensed. Therefore, HHV includes latent heat of vaporization contained in the water produced as well. In this case, stoichiometric combustion ensures that the condition of excess air did not occur during combustion. LHV or net calorific value is similarly determined, except that any water produced as byproduct of combustion is not condensed and remains in vapor state. Thus, LHV does not include the latent heat of vaporization of the water produced during combustion reactions.

In determining the suitability of biodiesel for CI engine, one of the most significant properties is the heating value of the test fuel. LHV of soybean biodiesel is 37.04 MJ/kg, which is 14.05% lower than that of mineral diesel (43.07 MJ/kg) [44,79]. Figure 3 shows the comparative LHV of biodiesels vis-à-vis baseline mineral diesel.

The heating value of biodiesel blends is dependent on the blending ratio of biodiesel in the test blend. In order to compensate for the lower LHV of biodiesel/blends, it becomes necessary to inject larger fuel quantity in every engine cycle for providing same engine power output. The heating value of biodiesel is influenced by its molecular weight and number of double bonds. In general, the HHV of biodiesel increases with increased number of carbon atoms and decreases with increased number of double bonds [30].

2.2.4 Oxidation Stability. Oxidation reactions are an important factor, which determine biodiesel quality during extended storage. The storage ability of biodiesels is influenced by storage conditions, including exposure to ambient air, water content, and exposure to sunlight and temperature. The thermal and oxidative instability of biodiesels can cause darkening and an increase in viscosity due to formation of gums and sediments [28]. The formation of sediments and gums during biodiesel storage can lead to significant problems during its usage such as fouling and plugging of fuel filtration equipment, and deposits in the fuel line. These can also lead to fouling of fuel pump and fuel injectors.

Oxidative stability of biodiesel is assessed using either the oxidative stability instrument index method (OSI, AOCS Cd12b-92) or the Rancimat method (EN 14112). Most commonly used oils for biodiesel production such as vegetable oils, animal fats, or waste cooking oils possess fatty acid profiles consisting mainly of C_{16}–C_{18} fatty acids [80]. Changes in biodiesel properties due to its oxidation cause an increase in acid and peroxide values as well as fuel viscosity, while the methyl ester content and iodine value (IV) decrease. Currently, biodiesels used in diesel engines are primarily blends ranging from B5 to B20, depending on weather conditions. A study on oxidation stability and its impact on the deterioration of metallic and polymeric materials by Zuleta et al. [80] concluded that in automotive engines, excellent solvent properties of biodiesels can dissolve elastomers and also cause swelling of nitrile rubber components. Their results indicated that materials such as brass, bronze, copper, aluminum, tin, and zinc may oxidize biodiesels and create sediments, thus rendering them

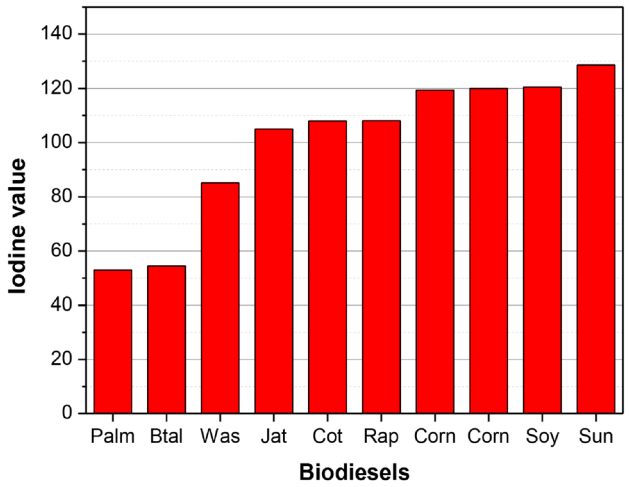

Fig. 4 Comparison of iodine values of various biodiesels [14,75,83] (Btal: beef tallow, Was: waste cooking oil, Jat: jatropha, Cot: cotton seed, Rap: rapeseed, Soy: soybean, and Sun: sunflower)

biodiesel incompatible. Polyunsaturated methyl esters containing biodiesels such as from croton, safflower, linseed, soybean, and sunflower oils, rich in linoleic and linolenic acids, are more prone to oxidative degradation [69,79,81].

Agarwal and Khurana [81] reported the long-term storage oxidation stability of karanja biodiesel using various antioxidants. In their work, the effectiveness of five anti-oxidants were tested for the long-term storage oxidation stability of karanja oil methyl esters under different storage conditions such as dark/sunlight exposure, with air/without air exposure, and with/without metal exposure.

2.2.5 Iodine Value. The IV of biodiesels is determined by measuring the degree of unsaturation (number of double bonds) in the fatty acid constituents [78,82]. In this measurement, a higher IV indicates that the oil is highly unsaturated (e.g., canola oil); hence, the biodiesels will exihibit a low cloud point (this property is good for winter biodiesels). In contrast, higher IVs lead to shorter oxidation stability of fuel. A lower IV indicates that biodiesel has a lower degree of unsaturation; therefore, a lower IV results in a higher cloud point and improved oxidation stability compared to a higher IV biodiesel. The maximum acceptable IV according to EN 14214 is 120 mg I_2/100 g FAME. IV has been linked to the formation of engine deposits and problems in the fuel storage [57]. In general, biodiesels easily meet the IV requirement (Fig. 4).

As shown by the comparison of IV for various biodiesels, Sunflower biodiesel (Sun) has a higher IV (128.6 mg I_2/100 g), which is approximately 2.43 times higher than palm biodiesel (53 mg I_2/100 g) [15,75]. The IVs of sunflower, soybean, rapeseed, jatropha, and corn biodiesels have higher IVs than those of palm, beef tallow (Btal), and waste cooking oil (Was) biodiesels, indicating that the earlier group has higher unsaturation levels than the later group.

3 Spray Characteristics of Biodiesel

Review of biodiesel properties indicated that biodiesels have different properties such as density, viscosity, and surface tension compared to conventional mineral diesel. These differences lead to different spray behaviors, which influence combustion and emissions characteristics of biodiesels, when used in CI engines. In this section, studies related to fuel injection, spray behavior, and atomization characteristics of biodiesels are summarized.

3.1 Fuel Injection Rate. Biodiesels exhibit higher density, viscosity, very high pour point, higher cetane number, and LHV compared to baseline mineral diesel. These properties lead to problems in cold starting of the engine in addition to significantly influencing fuel injection, spray atomization, and spray droplet evaporation characteristics.

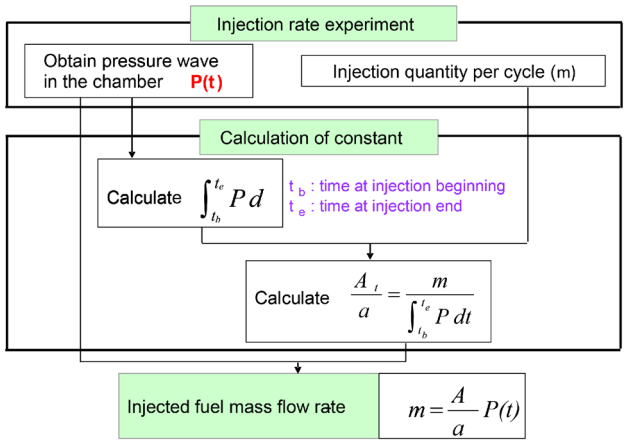

Fig. 5 Flow chart for fuel injection rate analysis [85]

3.1.1 Measurement System and Procedure. Injection rate describes progression of fuel mass injected into the combustion chamber as a function of time [84]. In the analysis of the fuel injection system and fuel sprays, fuel injection rate is one of the most important parameters. The maximum fuel flow rate, injection delay (both closing and opening), and actual injection duration can be evaluated from injection rate characteristics. In addition, it can be utilized for designing the fuel injection systems and combustion chamber shapes.

The injection rate is mainly obtained by using Bosch principle [73], in which pressure variations in a tube are monitored as fuel is injected into this tube. The pressure profile can be converted into the injection rate profile by a correlation using total injected mass, measured using a precision scale. The detailed experimental procedure for measuring injection rate of biodiesel is given in Fig. 5 and the schematic of the measuring system is shown in Fig. 6.

As shown in Fig. 6, the fuel injection rate measurement system consists of an adapter, a long measuring tube (5 or 10 m), a pressure vessel, a relief valve, and a throttle valve.

During the measurement, pressure in the measuring tube is fixed to a constant value. A data acquisition system is used for acquisition of injection profiles and injection quantity from the mean value of many continuous injections. A piezo-resistive type absolute pressure sensor is used to measure the pressure variations in the tube. Besides

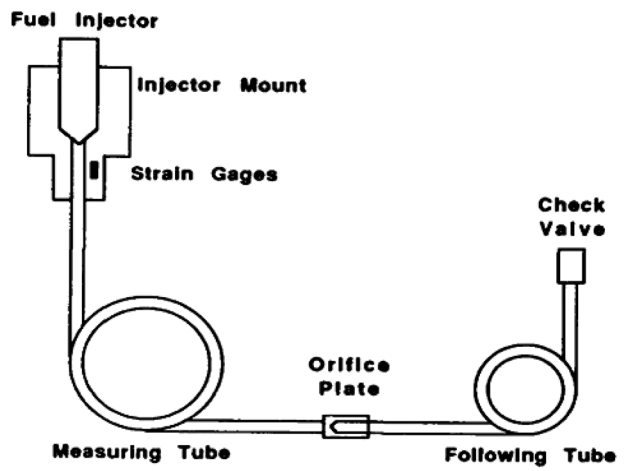

Fig. 6 Schematic of the Bosch rate of injection meter [73]

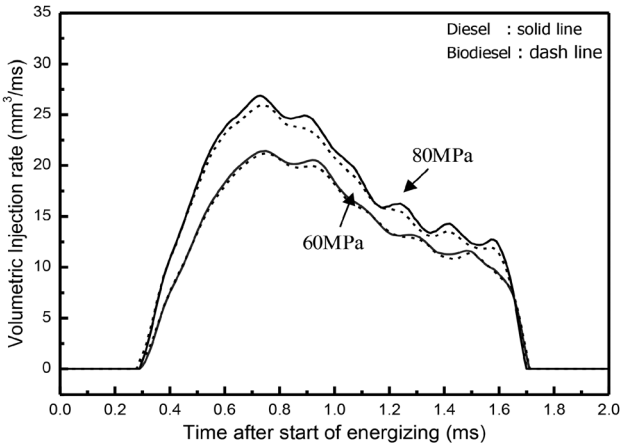

Fig. 7 Comparison of volumetric injection rate of mineral diesel and biodiesel (P_{inj} = 60 MPa, 80 MPa, P_{amb} = 4.0 MPa, and t_{eng} = 1.2 ms) [85]

the Bosch method, there are various other methods/techniques to measure the fuel injection rate such as membrane [86], spray momentum flux [87], charge [82], and Zeuch [88] methods.

3.1.2 Injection Rate Profile. Compared to conventional mineral diesel, different densities and kinematic viscosities of biodiesels influence the fuel injection rate profile. Park et al. [85] and Tinprabath et al. [89] studied the injection rate characteristics of biodiesels and mineral diesel. Park et al. [85] reported higher injection rate of biodiesel compared to mineral diesel and they suggested that the injection delay of both fuels was almost similar; however, the closing delay of biodiesel was slightly longer than mineral diesel (Fig. 7). Similar trend was also reported in the study by Tinprabath et al. [89]. They also reported that the injection delay (hydraulic delay) of both test fuels was almost same, while the closing delay increased with biodiesel content in the test blend because of variations in needle behavior due to higher viscosity of biodiesel. These results were supported by the study conducted by Moon et al. [90] using ultrafast X-ray phase contrast technique. As shown in Fig. 8, the needle motion of mineral diesel and biodiesel showed almost same trend in the initial stage of injection, while the needle lift of mineral diesel in transient and steady-state steps was higher than that of biodiesel. This phenomenon resulted in higher maximum injection rate of biodiesel. In addition, the needle lift of biodiesel in the closing step was higher than mineral diesel and the needle after injection closed later compared to mineral diesel. This resulted in longer closing delay, as shown in Fig. 8.

3.1.3 Parameters Influencing Injection Rate. The peak injection rate, injection delay, and closing delay are mainly affected by fuel properties such as viscosity, density, bulk modulus, and sonic velocity; and injection parameters such as fuel injection pressure (FIP), ambient pressure, and solenoid energizing duration. Increasing fuel injection pressure induces an increase in injection momentum and initial exit velocity, thus the peak injection rate also increases. In addition, increasing fuel injection pressure causes advanced start of injection [90]. Energizing duration has an insignificant effect on the injection rate because spray momentum, which affects initial spray behavior at the initial stage, is quite similar.

3.2 Macroscopic and Microscopic Spray Characteristics. Combustion in diesel engines influences thermal efficiency and formation of pollutants, particularly nitrogen oxides (NO_x) and particulates. Quality of combustion is largely influenced by quality of fuel-air mixture formation [84]. Fuel spray behavior and atomization characteristics generally exhibit different aspects according to various injection and ambient conditions such as fuel

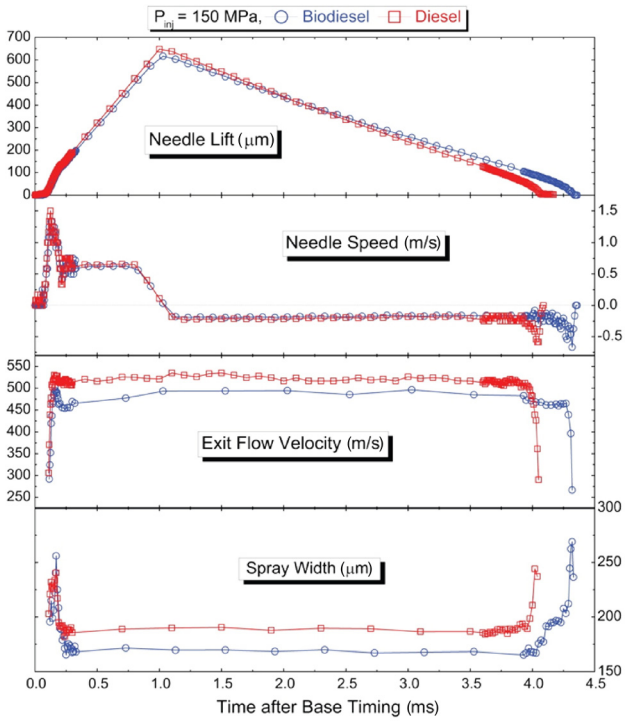

Fig. 8 Needle-lift, needle speed, exit velocity, and spray width of mineral diesel and biodiesel through an entire injection process (P_{inj} = 150 MPa, P_{amb} = 0.1 MPa, and T_{amb} = 300 K) [90]

injection pressure, ambient pressure, energizing duration, and injection quantity. When fuel is injected via a nozzle tip, various forces, including inertia, viscosity and surface forces, act on the fuel spray, causing it to deform and ultimately breakup. Since the mechanism that leads to breakup of the spray jet is very complicated, full understanding of it still remains insufficient. Therefore, many researchers have made efforts to investigate and clarify spray behavior and atomization mechanisms under various injection and ambient conditions, including real time engine operating conditions [73,91–94]. Biodiesel has significantly different fuel properties compared to mineral diesel such as higher viscosity, specific gravity, density, and cloud point. These fuel properties have a significant influence on fuel spray, atomization, and evaporation characteristics. Therefore, it is essential to understand the effect of biodiesel properties on overall spray characteristics. In this section, macroscopic and microscopic spray characteristics including the spray evolution process, spray tip penetration, spray cone angle, droplet size, and droplet velocity of biodiesel in a CI engine are discussed.

3.2.1 Spray Evolution, Spray Tip Penetration, and Fuel Distribution. Figure 9 shows temporal variation of spray evolution process with entrained gas velocity distribution of biodiesel and mineral diesel. As shown in the figure, the spray evolution process of both fuels is almost similar. However, the spray tip penetration and the spray cone angle of biodiesel are longer and narrower respectively, compared to baseline mineral diesel due to higher fuel density and kinematic viscosity. Similar results were also reported by many other researchers [85,95–99]. Kuti et al. [98] used laser-induced florescence—particulate image velocimetry (LIF-PIV) technique to study the spray characteristics of biodiesel derived from Palm oil. They reported that spray tip penetration and spray cone angle of both mineral diesel and biodiesel increased under the influence of ultra-high fuel injection pressure and micro-hole nozzles. As a result of higher fuel viscosity, which influences the spray breakup and atomization process, biodiesel produces longer spray tip penetration and smaller spray cone angle compared to baseline mineral diesel. In addition,

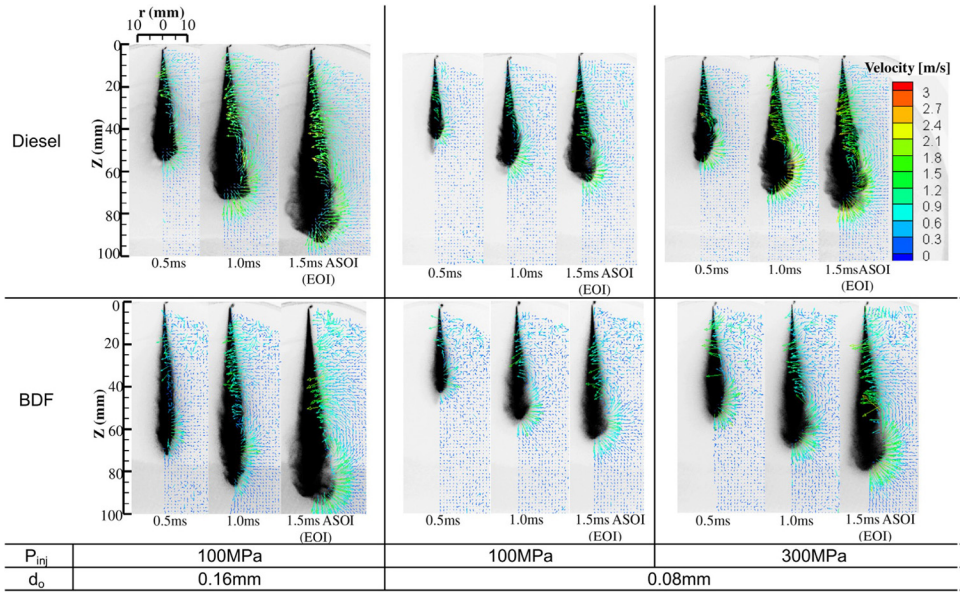

Fig. 9: Temporal spray evolution process and velocity distribution of ambient gas around the fuel spray [98]

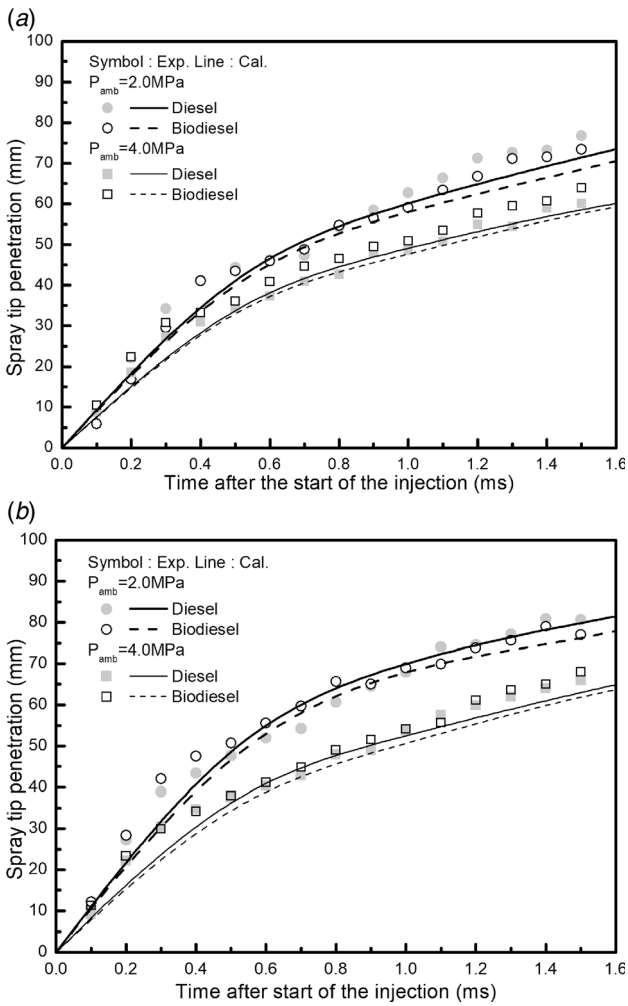

Fig. 10 Comparison of experimental and numerical results for mineral diesel and biodiesel sprays ($t_{eng} = 1.2$ ms and $T_f = 293$ K) [85]: (*a*) $P_{inj} = 60$ MPa and (*b*) $P_{inj} = 80$ MPa

inferior atomization of biodiesel caused relatively lower normal spray droplet velocity and total mass of entrained gas.

Mohan et al. [97] investigated spray characteristics such as spray tip penetration, spray cone angle, spray velocity, and spray morphology using biodiesel derived from waste cooking oil. They reported that biodiesel sprays exhibited longer spray tip penetration and smaller spray cone angle. In addition, they reported that the deviation in spray tip penetration reduced under higher ambient pressures. The spray shape of mineral diesel and biodiesel were different because of the cavitation phenomenon inside the injector nozzle hole. Park et al. [85] studied the effect of fuel injection and ambient pressures on biodiesel spray characteristics. They reported that higher ambient pressures induced shorter spray tip penetration (Fig. 10) and reduction in spray area in case of biodiesel sprays. Hong et al. [100] compared spray characteristics of mineral diesel and biodiesels at high fuel injection pressure. They reported that spray tip penetration of biodiesel was longer than that of mineral diesel, but the spray cone angle was relatively narrower. They also reported that reduction in spray cone angle was related to increased spray tip penetration. Tinprabath et al. [101] studied the impact of cold flow conditions on biodiesel and its blends with mineral diesel in the fuel injection process. They reported that cold flow conditions induced reduction in discharge coefficient. It was reported that both, the spray tip penetration and the spray angle of biodiesel strongly reduced under cold flow conditions. Mo et al. [102] investigated biodiesel spray characteristics using high-speed Schlieren technique. They reported that test fuel with higher biodiesel content showed larger spray area and spray volume as well as longer spray tip penetration.

Advancement in diagnostic technologies allowed deeper understanding of fuel sprays and atomization characteristics. Recently, ultrafast X-ray techniques enabled access to the first several millimeters of the optically dense regions of the fuel spray. Through X-ray techniques, the needle motion of a real injector, spray morphology, breakup process, and exit flow velocity in a flow-field very close to the nozzle tip was investigated experimentally. Figure 11 shows comparison of near-exit flow structure of biodiesel and mineral diesel sprays during steady-state. Through analysis of near-exit spray morphology, differences in wavelength and breakup process in mineral diesel and biodiesel sprays can be observed and analysed. As shown in the figure, the spray structure of biodiesel was less turbulent than mineral diesel because of its higher viscosity, lower exit velocity, and corresponding lower Reynold number

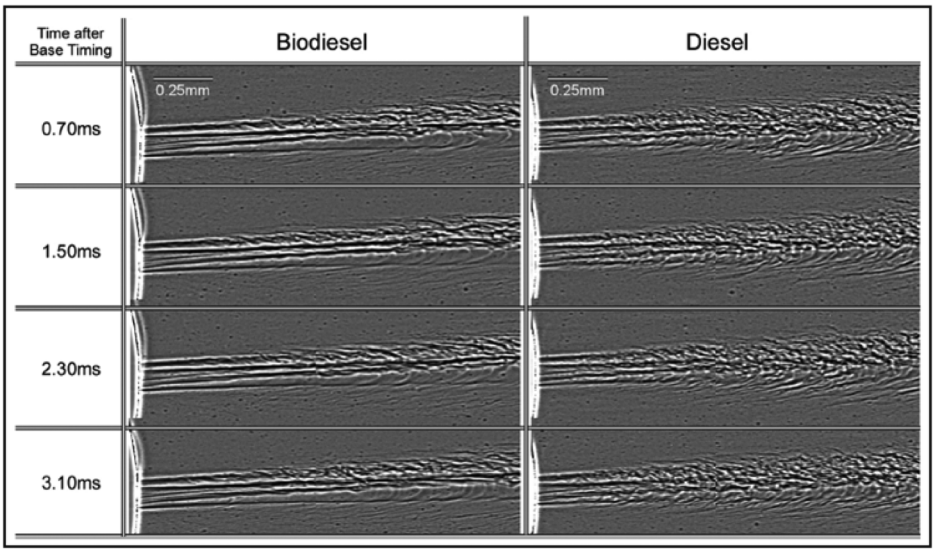

Fig. 11 Near-exit flow morphology of biodiesel and mineral diesel during steady-state (P_{inj} = 150 MPa, P_{amb} = 0.1 MPa, and T_{amb} = 300 K) [90]

(Re) [90]. Further, it can be conjectured that less turbulent flow characteristics of biodiesel cause less active interactions with the surrounding air in the spray periphery. Hence, smaller detectable spray width and dense core regions were observed.

3.2.2 Spray Breakup and Atomization Characteristics. In a combustion system, producing fine fuel droplets is quite important because it has significant influence on homogeneous fuel-air mixture formation and combustion characteristics in the combustion chamber. In order to study droplet size distribution and spray atomization performance, phase Doppler particle analyzer (PDPA) system is mainly used. This system can measure fuel droplet size and velocity distributions in liquid phase. The breakup and atomization processes are mainly affected by fuel viscosity and surface tension as well as injection conditions, such as fuel injection rates and ambient pressures. From this viewpoint, biodiesel has weaker atomization performance because of its higher viscosity and surface tension. The spray atomization performance is generally represented by Sauter mean diameter (SMD), which is the ratio of the average volume-to-average surface area of spray droplets averaged over the entire droplet size distribution range, and it characterizes a number of important processes involving droplet penetration and heat and mass transfer [103].

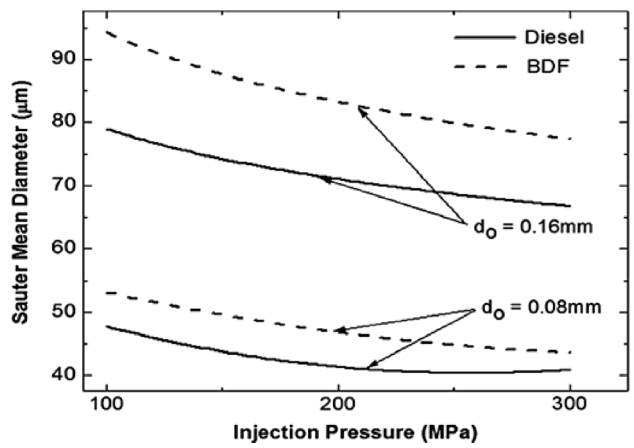

Fig. 12 Variation of SMD for mineral diesel and biodiesel at different FIP and nozzle hole diameters (P_{inj} = 100, 200, and 300 MPa; d_o = 0.08 and 0.16 mm) [98]

Figure 12 shows the variation in SMD of mineral diesel and biodiesel according to fuel injection pressure and nozzle hole diameter. As shown in the figure, increasing fuel injection pressure and reducing nozzle hole diameter induced reduction in SMD of the fuel sprays of both test fuels. This was primarily because high fuel injection pressure induced higher momentum in the spray droplets. However, biodiesel still exhibited higher SMD compared to baseline mineral diesel. These observations were attributed to higher viscosity and density of biodiesel. Lee et al. [53] and Agarwal et al. [27,70] also obtained similar experimental results.

Figure 13 shows the effect of mixing ratio of biodiesel on SMD distribution. Lee et al. [53] used unpolished Rice oil and Soybean biodiesel in this study. As shown in the figure, biodiesel blends showed higher SMD than mineral diesel. It was concluded that

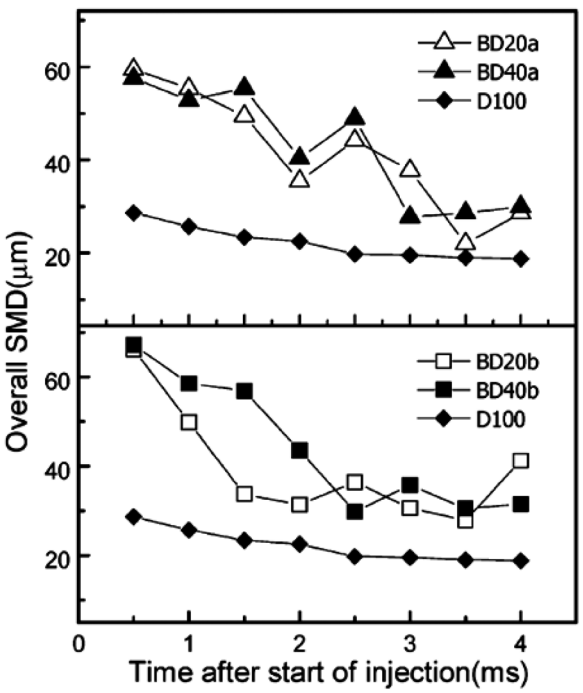

Fig. 13 Mean droplet size distribution of biodiesel-blended fuels (P_{inj} = 60 MPa) [53]

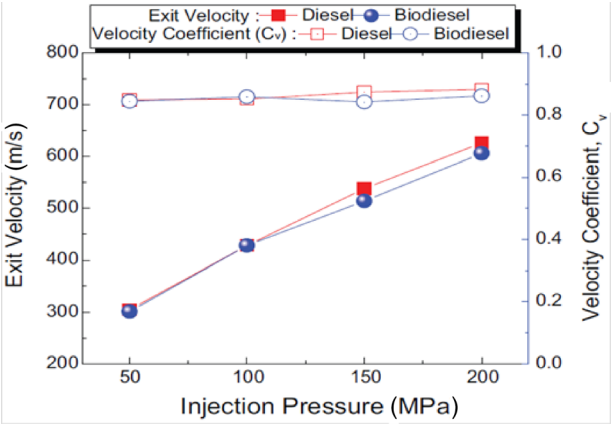

Fig. 14 Axial velocity of mineral diesel and biodiesel sprays at different FIPs [90]

the atomization characteristics of spray and droplets were mainly affected by the Weber number and the injection velocity. Since biodiesel has higher surface tension, its spray has lower Weber number than mineral diesel. In addition, higher kinematic viscosity of biodiesel induced lower spray injection velocity because of increased friction between the nozzle surface and the fuel. This was also experimentally proved by Moon et al. [90] and Lee et al. [53] who used X-ray phase contrast technique and PDPA technique to prove that the exit flow velocity of biodiesel was lower than that of mineral diesel. Ejim et al. [34] compared atomization characteristics of biodiesel and blends. They confirmed that the most influential fuel property for atomization was 'fuel viscosity'. This property exerted the largest influence on the change in droplet size distribution, whereas the contribution of density was the lowest. Therefore, there was a need to reduce the fuel viscosity in order to achieve finer droplet size distribution in the spray for engine applications.

The axial velocity and the velocity coefficient of mineral diesel and biodiesel fuel sprays at 5 mm distance from the nozzle exit are shown in Fig. 14. As shown in the figure, the axial exit velocity of both mineral diesel and biodiesel increased with increasing fuel injection pressure, as expected. Up to 100 MPa, the effect of fuel properties on axial velocity was insignificant. However, the exit velocity of biodiesel slightly decreased and the velocity coefficient of biodiesel reduced compared to mineral diesel above 100 MPa fuel injection pressure [90].

There are many methods to improve spray atomization performance of biodiesel. One of them is to increase the fuel temperature. In fact, the increase in fuel temperature affects the evaporation characteristics thus homogeneous fuel-air mixtures can be formed in the combustion chamber. Park et al. [104] investigated the effect of temperature on biodiesel's atomization characteristics. They increased the fuel temperature up to 360 K using steam in a duplication tube. It was reported that biodiesel droplet size distribution increased with temperature because of active fuel evaporation and increased temperature influenced the formation of a homogeneous mixture of the injected fuel droplets and ambient air. Manin et al. [105] also reported similar results, wherein the combined effect of temperature on coalescence and aerodynamic drag led to increased SMD with penetration of mineral diesel fuel spray. In addition, increasing the fuel injection pressure was a promising strategy to improve the spray atomization performance of biodiesel.

4 Combustion Characteristics of Biodiesel

Due to almost similar fuel related properties of biodiesel and mineral diesel, the combustion characteristics of biodiesel and its blends are not significantly different from baseline mineral diesel [106]. Peak cylinder pressures were higher for biodiesel blends (waste cooking oil, rapeseed, and corn biodiesels) compared to mineral diesel [107]. Operation of a four stroke, vertical, air-cooled diesel engine with waste cooking oil methyl ester and mineral diesel blends (20, 40, 80, and 100% v/v) resulted in an increase in brake-specific energy consumption, and peak cylinder pressure, while reduction in peak heat release rate (HRR) [108]. Peak cylinder pressures for different blends (PME20, PME40, PME60, and PME80) of Pongamia biodiesel were quite similar to that of mineral diesel. The peak pressure was ~2 to 3% higher for PME20, and HRR was lower compared to mineral diesel along with shorter ignition delay [109].

4.1 Effect of Chemical Composition. Lin et al. [110] investigated the effect of carbon chain length of biodiesel on the ignition delay in an unmodified diesel engine. They reported that Palm kernel oil methyl ester and palm oil methyl ester (PME), which have shorter carbon chain lengths and more saturated bonds, had superior ignition quality, i.e., higher CN in comparison to mineral diesel as well as other biodiesels with longer carbon chain lengths and higher degree of unsaturation [110]. Lahane et al. [111] reported advanced start of combustion (SOC) timings with increasing concentration of biodiesel (Karanja oil methyl ester) in blends with mineral diesel due to the advancement of fuel injection timing and higher CN of biodiesels. They also reported that combustion duration increased marginally for lower biodiesel blends (up to B25), whereas it increased significantly for higher biodiesel blends (B50 and B100) due to requirement of longer injection duration because of lower calorific value of biodiesel. The use of rice bran methyl ester blend in direct injection diesel engine resulted in lower HRR during premixed combustion, lower maximum rate of pressure rise, and longer combustion duration [112].

In optical visualization combustion investigations, SOC is indicated by the first appearance of luminous flames in the image sequence. Combustion chamber images of mineral diesel and biodiesel blends also confirmed relatively earlier start of combustion in case of 20% and 50% biodiesel fueled engines (Fig. 15) [113]. Oxygenated molecules of biodiesel ensure higher reactivity that results in earlier SOC. This behavior is also confirmed by higher CN of biodiesel compared to baseline mineral diesel as discussed in Sec. 2.2.2. Comparison of mineral diesel and biodiesel combustion images showed that white regions were marginally larger for mineral diesel compared to biodiesel at full and half load conditions. This indicated that soot particles occupied lesser area biodiesel images due to their relatively higher oxidation rates, while combustion was still progressing in an engine cycle [114], which can be attributed to the presence of oxygen in the molecular structure of biodiesel.

In the combustion investigations of Canola biodiesel blends (10, 20 and 30% v/v), it was shown that there was reduction in cylinder pressure and indicated mean effective pressure (IMEP) at low engine speeds with increasing blend ratio, while above 2000 rpm engine speed, cylinder pressure and IMEP increased with increasing blend ratio in a four-cylinder DI diesel engine. Increasing cylinder pressure with biodiesel blends at higher engine speed was caused by accelerated combustion of test fuel, which was finally atomized by higher fuel injection pressure and fuel oxygen in case of biodiesel. At lower engine speeds, due to comparatively lower fuel temperature in the fuel injection equipment, spray atomization characteristics deteriorated with increasing biodiesel blending ratio, resulting in lower peak in-cylinder pressure. Further, with the use of 0, 10, 20, and 30% exhaust gas recirculation (EGR), cylinder pressure and IMEP decreased with increasing biodiesel blending ratio at all engine speeds [115].

Cottonseed biodiesel (25, 50, 75, and 100%) blends with mineral diesel exhibited superior combustion because of higher fuel oxygen content. Cottonseed biodiesel blends also exhibited higher peak cylinder pressure, peak pressure rise rate, and peak HRR compared to mineral diesel in a naturally aspirated diesel engine [116].

Addition of 5, 10, and 15% ethanol in Rapeseed oil methyl ester (biodiesel) blend in a four-stroke, four-cylinder, naturally

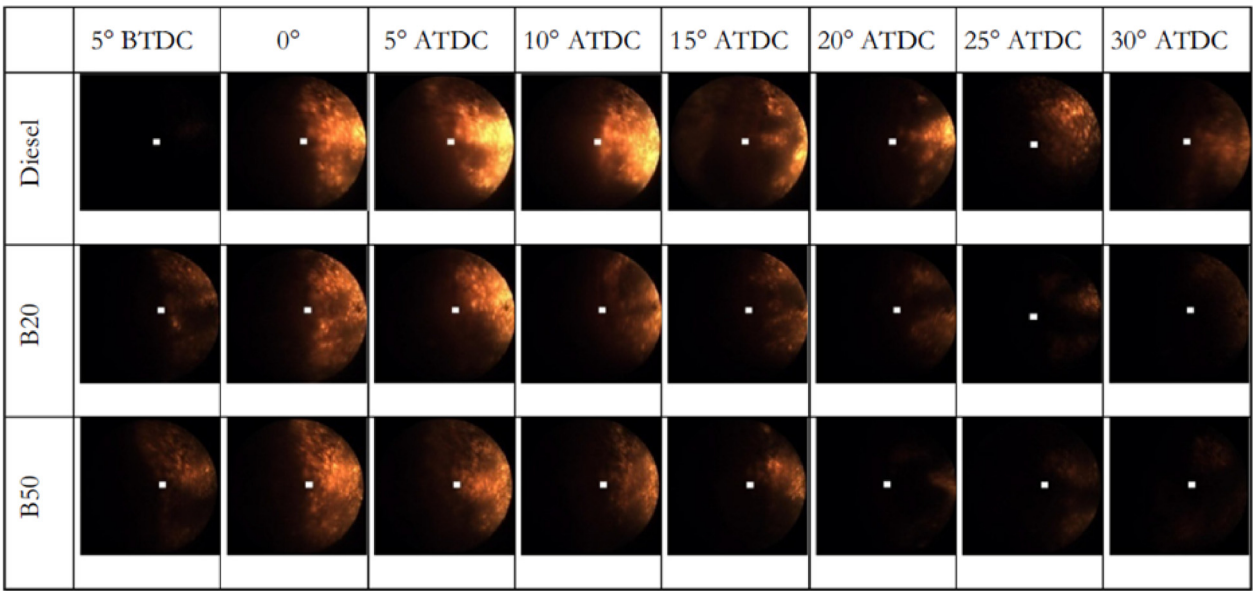

Fig. 15 Spatial and time-resolved combustion endoscopy images of biodiesel blends and diesel at 50% load at various crank angles in an engine cycle [113]

aspirated DI diesel engine of 60 kW rating resulted in lower peak cylinder pressures at lower engine speed and higher values of relative air-fuel ratios [117] but higher peak cylinder pressure was observed at higher engine loads. The influence of ethanol's oxygen content on maximum cylinder pressure was rather ambiguous and was dependant on many variables including temperature inside the engine cylinder, turbulence intensity, swirl, air–fuel ratio, and fuel oxygen. At low ethanol content, slower engine speed and lower in-cylinder gas temperature; ethanol misses the main advantage because fuel evaporation occurs slowly and the flame front propagates in lean fuel-air mixtures with limited speed. The use of biodiesel-butanol-mineral diesel blend (20% biodiesel 5% butanol and 75% mineral diesel) resulted in lower peak cylinder pressure and peak HRR at 0.17 MPa BMEP in a common rail direct injection (CRDI) diesel engine [118].

4.2 Effect of Fuel Injection Strategies. Investigations of combustion characteristics of Karanja biodiesel blends (KOME10, KOME20, and KOME50) and mineral diesel [70] showed that start of heat release slightly advanced for KOME10 compared to other test fuels at 300 and 500 bar FIP. This advancement was higher at advanced start of injection (SoI) timings (−15 deg CA SoI timing) (Fig. 16). It appears that KOME10 was the optimum blend percentage that ensured adequate fuel-air mixing characteristics and took advantage of oxygen content of biodiesel during combustion. Maximum premixed heat release for KOME20 was comparable to mineral diesel, while that of KOME50 was slightly lower than mineral diesel. It was also observed that maximum cylinder pressure increased with increasing FIP at fixed SoI timing for all test fuels and SoC advanced for lower biodiesel blends in comparison to mineral diesel. For lower biodiesel blends, combustion duration was relatively shorter than mineral diesel, but at higher FIPs, combustion duration of KOME50 was relatively longer.

For all injection timings in multiple fuel injection mode, combustion duration of KOME20 and KOME50 were longer than

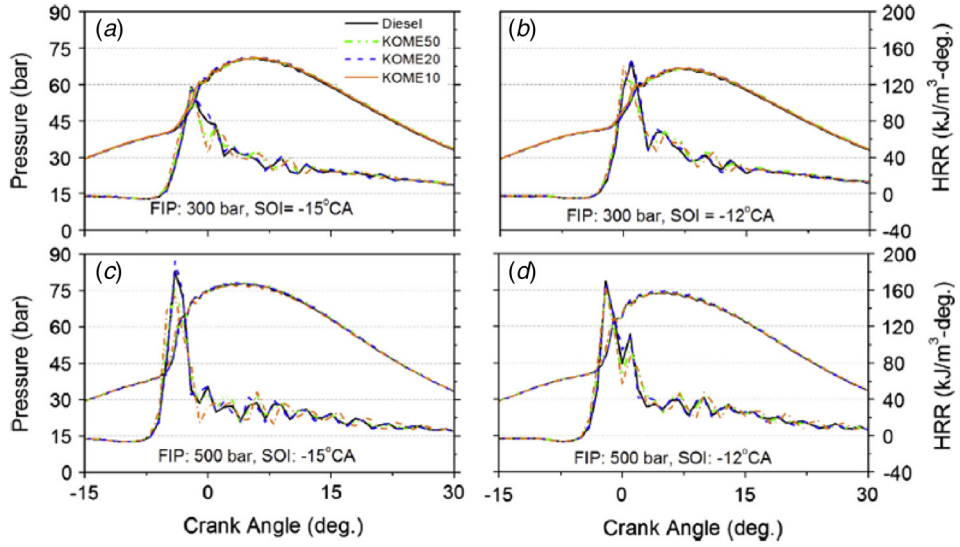

Fig. 16 Effect of FIP and SoI timing on cylinder pressure and HRR of biodiesel blends vis-à-vis mineral diesel [70]

Table 8 Effect of biodiesels on BTE and specific fuel consumption

SN	Fuel	BTE	BSFC	Ref.
1	Waste cooking oil, Rapeseed and Corn biodiesels-mineral diesel blend	Decreased	Increased	[107]
2	Canola biodiesel blend (10%, 20%, and 30% v/v) with mineral diesel	Decreased	Increased	[115]
3	Cottonseed biodiesel (25%, 50%, 75%, and 100%) blend with mineral diesel	Increased	Increased	[116]
4	5, 10, and 15% ethanol + Rapeseed oil methyl ester-mineral diesel blend	No change	Increased	[117]
5	5% Palm and 5% Jatropha biodiesel and 90% mineral diesel	Increased	Reduced	[120]
6	5% and 15% Coconut biodiesel blended with mineral diesel	Decreased	Increased	[121]
7	Blend of Moringa oleifera biodiesel (B10 and B25)	Slightly decreased	Increased	[122]
8	Blends of Moringa oleifera biodiesel (B10 and B20)	Decreased	Increased	[123]
9	Blends of Moringa oleifera biodiesel (B0 and B10)	No change	Increased	[124]
10	Blend of Moringa oleifera biodiesel (B5 and B10)	Decreased	Increased	[125]
11	Waste cooking oil methyl ester and mineral diesel blend (20%, 40%, 80%, and 100% v/v)	Decreased	Increased	[109]
12	Pongamia biodiesel	Decreased	Increased	[110]
13	Soybean biodiesel	Decreased	Increased	[126]
14	Cottonseed biodiesel	Decreased	Increased	[127]

mineral diesel due to relatively inferior fuel-air mixing characteristics and requirement of larger fuel quantity compared to mineral diesel with increasing concentration of biodiesel in test blends [119].

5 Performance Characteristics of Biodiesels

Performance characteristics of biodiesels and baseline mineral diesel are compared by comparison of brake thermal efficiency (BTE) and brake specific fuel consumption (BSFC) of these test fuels. Due to slightly lower calorific value and higher density of biodiesels compared to baseline mineral diesel, in general BSFC for biodiesels and blends is higher than mineral diesel. This is also reported by various studies and summarized in Table 8.

5.1 Engine Power Output. Lahane et al. [111] reported marginal reduction of <1% engine peak torque and power for lower biodiesel blends (up to B25) and significant (~2%) reduction for higher biodiesel blends (B50 and B100) of karanja biodiesel. Dhar and Agarwal [128] investigated the effect of karanja biodiesel blends on maximum engine torque and reported that lower blends did not have any adverse effect on maximum torque. However, reduction of 1.4 and 2.1% engine torque was observed for higher biodiesel blends (KOME50) and biodiesel (KOME100), respectively, compared to baseline mineral diesel (Fig. 17).

Citrus sinensis biodiesel (5, 10, and 20%) blend with mineral diesel resulted in reduction in both power and torque output from a DI diesel engine [121]. Coconut biodiesel (5 and 15%) blend with mineral diesel reduced both, the brake power and the torque output from a four stroke, naturally aspirated DI diesel engine, whereas BSFC increased compared to baseline mineral diesel [129]. There was 4.65% average increase in brake power output with the use of 10% biodiesel (5% Palm and 5% Jatropha) blend

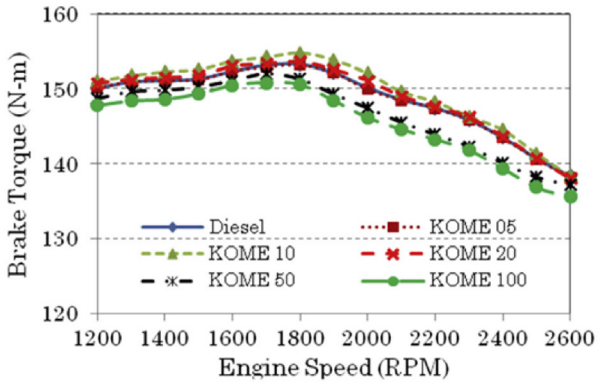

Fig. 17 Effect of Karanja biodiesel blend concentration on engine brake torque [128]

in a single cylinder, DI diesel engine [120]. Azad et al. [130] concluded that the use of different blends of Moringa oleifera biodiesel blend with mineral diesel in a diesel engine resulted in reduction in maximum brake power and BTE, and increased the BSFC.

5.1.1 Effect of Chemical Composition. Lin et al. [110] reported that the change in carbon chain length and degree of unsaturation in the carbon chain length of feedstock did not have any significant effect on peak engine power, while comparing the maximum engine power produced by eight biodiesels (Soybean, Peanut, Corn, Sunflower, Rapeseed, Palm, Palm kernel, and Vegetable oil based waste cooking oil). Chemical composition of these blends was quite varied, ranging from Palm kernel biodiesel having ~50% of carbon-chains present as C_{12}, Palm oil methyl ester having ~50% of carbon chains present as C_{16}, while other biodiesels having more than ~60% carbon chains present as C_{18} [110].

Different test blends such as mineral diesel 80%-micro-algae biodiesel 20%; mineral diesel 70%-micro-algae biodiesel 20%-butanol 10%; and mineral diesel 60%-micro-algae biodiesel 20%-butanol 20% produced relatively lower power outputs compared to baseline mineral diesel in a DI diesel engine [131]. Lower calorific values of biodiesels were partly compensated by their higher density. Hence, fuel injection systems, which generally measure fuel on volume basis, experienced no significant drop in mass of the fuel injected, hence no significant drop in mass of the fuel injected, hence no significant drop in peak engine power output from biodiesel blends due to different compositions. However for butanol like fuels, which have both lower calorific value and density in comparison to biodiesel, significant drop in peak engine power output was observed. Ternary fuel blends (10, 15, and 20% each) of pentanol and Calophyllum inophyllum (CI) biodiesel with mineral diesel tested in a single-cylinder, four-stroke, light-duty engine showed that ternary blends (CI10P10, CI15P15, and CI20P20) exhibited an average 10.4% higher brake power output compared to CI20 blend [132]. Heating value and density of pentanol is closer to biodiesel. Due to lower boiling point of pentanol, its addition into biodiesel blend leads to accelerated vaporization and enhanced the spray atomization effectively. Addition of antioxidants and nano-particles as additives in biodiesel led to improvement in BTE along with reduction in emissions [133]. Higher brake power output of pentanol-blended biodiesel can be attributed to increased accessibility of fuel-bound oxygen in the test blend and superior atomization characteristics. Addition of 5, 10, and 15% (v/v) ethanol in Rapeseed oil methyl ester-mineral diesel blend in a four stroke, four-cylinder, naturally aspirated, DI diesel engine of 60 kW rated power resulted in higher BMEP compared to baseline mineral diesel [117].

5.1.2 Effect of Fuel Injection Strategies. In the investigations of optimization of SoI timing, 2 deg crank angle (CA) retardation in SoI timing resulted in 2.8% increase in peak torque and 5%

reduction in peak cylinder pressure for B50 (Soybean biodiesel blend) in comparison to standard injection timing for mineral diesel, while 1 deg CA retardation in SoI for B100 resulted in negligible increase in torque and 4.4% reduction in peak cylinder pressure. Further, lower ignition delay in both blends resulted in lower peak cylinder pressures for the same engine load [134]. The in-line FIP increased with increasing percentage of biodiesel in test blend. Lahane et al. [111] reported that the peak in-line FIP of all Karanja methyl ester blends (B5: 484.28, B10: 487.62, B15: 490.85, B20: 495.45, B25: 493.48, B50: 496.32, and B100: 505.9 bar) was higher than baseline mineral diesel (472.31 bar) due to relatively lower compressibility of biodiesel (i.e., higher bulk modulus), resulting in automatic advancement of injection timing. In order to maintain the same power output, fuel flow rate needs to be increased. The enhanced fuel flow rate requirement due to lower calorific value of biodiesel is also one of the reasons to increase the in-line FIP for biodiesel blends. Due to this effect of changed FIP and injected fuel quantity with change in fuel, which affects other mixing parameters discussed in Sec. 3, the optimization of fuel injection strategy increases the peak power output from the biodiesel blend fueled engine.

5.2 Brake Thermal Efficiency

5.2.1 Effect of Chemical Composition. Cottonseed biodiesel (25, 50, 75, and 100%) blends exhibited higher BTE and higher BSFC at higher load compared to mineral diesel in a naturally aspirated, DI diesel engine [116]. For 100% Neem biodiesel, 2–13% improvement in BTE was observed in comparison to mineral diesel [135]. Experimental investigations of mineral diesel and Jatropha biodiesel in a two-cylinder, four-stroke, CI engine indicated that maximum BTE for mineral diesel was 29.6%, whereas for Jatropha biodiesel, it reduced to 21.2% [136]. Lin et al. [110] reported that the increase in BSFC for biodiesel blends with shorter carbon chain length was higher due to their lower density, but the observed BTE improved in comparison to mineral diesel. Earlier completion of combustion for biodiesels with shorter combustion duration produced favorable combustion phase shift in an unmodified engine compared to an optimized baseline mineral diesel fueled engine.

Blend of 81% Jatropha methyl ester and 15% Wood pyrolysis oil mixed with 4% surfactant (by volume) resulted in an emulsion, which exhibited 11.3% higher BTE in comparison to mineral diesel in a DI diesel engine [137]. Experimental investigations on a Lister Peter, two-cylinder, four-stroke, DI diesel engine with different blends of Canola biodiesel (0, 5, 10, 20, 50, and 100%)–mineral diesel, Canola biodiesel-mineral diesel-additive (Wintron XC 30 (2 vol.%)), and kerosene-biodiesel (0,5, 10, 20, 50 and 100%)–mineral diesel blends showed that there was an increase in BSFC and reduction in BTE [138] due to blending. There was a 2.8% reduction in BTE and 4% increase in BSFC due to addition of 5 and 10% waste cooking oil biodiesel to mineral diesel in a single cylinder, four stroke, natural aspirated, DI diesel engine [139]. There was an average increase of 15% in BTE up on using higher biodiesel blending ratio, e.g. 20% mineral diesel and 80% biodiesel (40% Palm and 40% Jatropha) in a single cylinder, DI, diesel engine [120].

Yilmaz [140] reported that BSFC for biodiesel (waste cooking oil)-alcohol-mineral diesel blends was generally higher compared to baseline mineral diesel. It was also shown that biodiesel-ethanol-mineral diesel blend exhibited lower BSFC in comparison to biodiesel-methanol-mineral diesel blend. Yasin et al. [141] reported that BSFC was higher for Palm biodiesel (20%)-methanol (10%)-mineral diesel (70%), and biodiesel (20%)-methanol (5%)-mineral diesel (75%) blends compared to baseline mineral diesel. At the same time, it was demonstrated that addition of 5% methanol was more effective compared to addition of 10% methanol. Yilmaz et al. [142] reported that BSFC increased with butanol and butanol-biodiesel (waste cooking oil biodiesel) blends (butanol 20, 10, and 5%-biodiesel 80, 90, and 95%, respectively) compared to baseline mineral diesel in a four-stroke, naturally aspirated, water-cooled, IDI diesel engine. The addition of 10% n-propanol to mineral diesel increased the BTE by 11.78% compared to baseline mineral diesel at full load in a Kirloskar DI, naturally aspirated, water cooled diesel engine [143]. In low temperature combustion (LTC) mode, a 20% ethanol-mineral diesel-biodiesel blend exhibited higher BTE and advanced injection timing compared to mineral diesel in a four-stroke, heavy-duty diesel engine [144]. Coconut biodiesel-mineral diesel blend (20% biodiesel and 80% mineral diesel) and biodiesel-bioethanol-mineral diesel blend (20% biodiesel-5% bioethanol and 75% mineral diesel) exhibited higher BTE (with highest improvement of 5.4% at medium load) but higher BSFC compared to baseline mineral diesel in a CRDI diesel engine [118]. Imdadul et al. [132] investigated the performance of 10, 15, and 20% pentanol and Luminophyllum (Calophyllum inophyllum) (CI) biodiesel blends with mineral diesel in a single cylinder, four-stroke, light-duty engine. It was shown that the modified pentanol blends exhibited 8.7% lower BSFC and ~15% higher BTE compared to CI20 blend. Addition of 5, 10, and 15% ethanol in Rapeseed oil methyl ester biodiesel-mineral diesel blend in a four-stroke, four-cylinder, naturally aspirated DI diesel engine of 60 kW rated power resulted in an increased BSFC [117]. Blending 5, 10, and 15% butanol (by volume) into a 20% Palm oil methyl ester blend ultra-low sulfur mineral diesel blend in a stationary diesel engine showed that there was an increase in thermal efficiency at medium and high loads and slight increase in BSFC, when butanol was added up to 10% [145]. Performance of Mahua biodiesel incorporating additive (dimethyl carbonate) in 85, 90, 95, and 100% biodiesel blends with mineral diesel was tested in a single cylinder, water-cooled diesel engine at varying loads from 20 to 100%. It was found that BTE increased and BSFC decreased with percentage of additives for all prepared test blend. BTE values at full load for biodiesel blends (B100, B95, B90, and B85) were 30.09, 26.63, 28.01, 29.74, and 29.97%, respectively [146].

Canola biodiesel blends (10, 20, and 30%) with mineral diesel showed that both BSFC and brake-specific energy consumption increased with increasing biodiesel concentration and 10, 20, and 30% EGR [115]. Can et al. [147] showed that with application of 15% EGR, there was a maximum 3% reduction in BTE and a maximum 6% increase in BSFC of a Soybean (20%)-mineral diesel blend fueled single cylinder, four-stroke DI diesel engine. Mofijur et al. [148] concluded that the use of ethanol in biodiesel-mineral diesel blends resulted in higher fuel consumption than mineral diesel fueled engine.

5.2.2 Effect of Fuel Injection Strategies. Investigation of the effect of FIP and SoI timing on BTE in a single cylinder research engine showed that BTE of lower Karanja biodiesel blends (KOME10 and KOME20) was higher than KOME50 [170]. Singh et al. also reported that BTE of lower soybean biodiesel (20% v/v) blend was higher than 40% v/v blend in the tested FIP range of 400–700 bar [149]. BTE was the highest at −15 deg CA SoI timing for all test fuels at 300 and 500 bar FIP (Fig. 18). At a fixed SoI timing, it was observed that increasing FIP generally improved the BTE of test fuels. Increasing FIP was more effective in increasing BTE of mineral diesel compared to Karanja biodiesel blends, which suggested that higher FIP was more effective in improving the spray characteristics of the test fuels with lower viscosity, which was mineral diesel in this case.

Investigations of the effect of pilot injection timing on the efficiency of Karanja biodiesel by Dhar and Agarwal [119] showed that BTE was more sensitive to variations in start of main injection timings. Start of pilot injection timings were used to control the thermodynamic condition of the in-cylinder charge at the time of main injection, which controlled the HRR during the main injection and consequent combustion. Higher FIP led to finer atomization of test fuels. This subsequently improved the droplet vaporization; therefore the rate of pressure rise became higher in cases of advanced SoI timings. Multiple injections were effective in extending the range of SoI timings by keeping the rate of

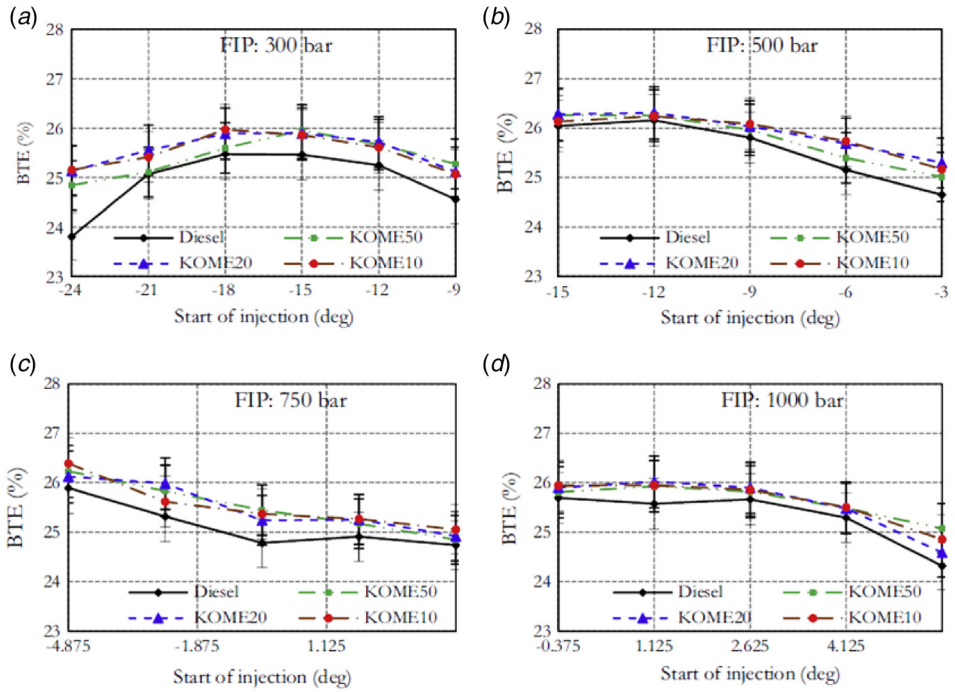

Fig. 18 Effect of FIP and SoI timings on BTE of biodiesel blends vis-à-vis mineral diesel [70]

pressure rise within acceptable limits. In multiple injection mode, BTE of biodiesel blends was generally higher than mineral diesel. This indicated that the oxygen content of biodiesel helped in improving the combustion in the engine cylinder. It was also observed that the thermal efficiency of KOME10 and KOME20 were higher than mineral diesel as well as KOME50. This was explained by deterioration of atomization and fuel-air mixing characteristics of test fuels with higher concentration of biodiesel due to higher viscosity, density, and relatively inferior volatility characteristics of biodiesel compared to baseline mineral diesel.

6 Emission Characteristics of Biodiesels

Engine exhaust emissions consist of both organic and inorganic species, which are present as a mixture of particles and gases. Exhaust emissions in the environment is a harmful consequence of large number of mineral diesel fueled vehicles. These are in turn a result of exponential economic growth of the global economy in last few decades. Mineral diesel fuelled engine-out emissions can be broadly classified into regulated (particles, carbon monoxide, HCs, and oxides of nitrogen) and unregulated emissions (such as benzene, toluene, xylene, carbonyls, polycyclic aromatic HCs (PAHs), and organic acids) [150,151]. There are some specific benefits of using biodiesel, e.g., negligible fuel sulfur content, higher fuel oxygen, and negligible fuel aromatics, which eventually lead to lower emissions of particulate and other gaseous pollutants [152]. Negligible sulfur in biodiesel leads to lower sulfate formation in the engine cylinder, leading to lower particulate emissions.

6.1 Regulated Emissions. The products formed due to partial combustion contribute to either gaseous or particulate form of the engine exhaust. Composition of engine exhaust varies, depending on the type of engine, engine operating conditions, biodiesel blending ratio, and the fuel-lubricant combination. Carbon monoxide (CO), carbon dioxide (CO_2), oxides of nitrogen (NO_x), and PM are the main regulated pollutants formed due to incomplete/partial combustion of automotive fuels.

6.1.1 CO, NO_x, and HC Emissions. A fraction of compounds in the fuel escape unburnt in the exhaust such as HC, CO, and particulates. Few compounds are formed in the combustion, leading for formations of chamber due to incomplete combustion, leading for formations of organic particulates. The organic fractions of the gaseous emissions and particulates contain numerous species which can be collectively analysed by the CHONS analyses, i.e., by using the five element system [153]. The organic fraction in the gaseous form and particulates depends on carbon-to-hydrogen ratio of the fuel [154]. Some of these subfractions are gaseous, some are oily and viscous, while some are solids [155]. The oxygen content in the organic fraction may be higher if it is found in the test fuel. It indicates the presence of other partial reaction products and leads to production of oxygenated HCs during combustion. Compounds with $\sim C_{23}$–C_{24} are the dividing line between particulate phase and vapor phase hydrocarbons [156]. PAHs present in the particles possess five or more rings [157]. While there has not been much research done in the field of size measurement of the organic fractions, it can be better understood by understanding the nucleation-mode particles [158].

The relationship between the parent fuel based organic compounds and those present in the exhaust (HCs, organic and carbonaceous compounds) is depicted in Fig. 19 [159].

Significantly lower unburnt hydrocarbon emissions have been reported from Rapeseed methyl ester (RME) [160]. This was largely attributed to the presence of oxygen in the biodiesel molecules. Generally with biodiesel usage, lower emission of CO and higher emissions of NO_x is reported in most experimental studies. EGR has been used for controlling the NO_x formation and emissions from biodiesel fuelled engine [161].

6.1.2 Particulate Emissions. Mineral diesel and biodiesel particulates are agglomerates of primary spherical particles made of solid carbonaceous matter, and metallic ash along with adsorbed hydrocarbons and sulfates. Diesel particulate matter (DPM) is largely composed of elemental carbon (EC), organic carbon (OC), nitrates, sulfates, heavy metals, trace metals, water, and other hazardous hydrocarbon species in minor concentrations.

Classical mechanism of particle formation is depicted in Fig. 20. In an IC engine, the combustion chamber witnesses pyrolytic breakdown of hydrocarbon fuel molecules [162]. These pyrolytic products rearrange themselves into aromatic species [163] through

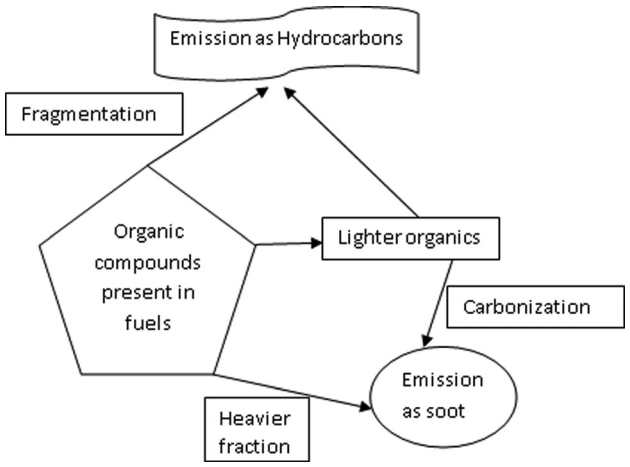

Fig. 19 Schematic showing possible pathways for organic compounds present in the fuels

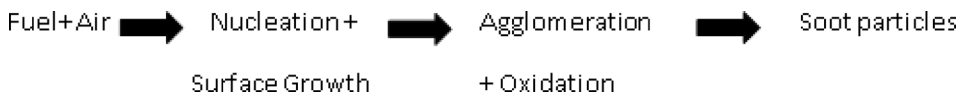

Fig. 20 Classical flow-chart of soot formation steps [164]

cyclization of aliphatic compounds [164] in which benzene is the basic molecular building unit [165–167]. Hydrogen is depleted out of benzene rings, resulting in formation of graphitic structures. These products act as nuclei and soot settles down over these surfaces, which then rolls over to form spherules. Surface growth results in an increase in soot mass, while keeping the number of particles more or less the same. These spherules collide and stick together as a result of thermal coagulation; hence, the number concentration of particles decreases but their mass remains constant. Figure 20 represents a classical schematic of soot formation in the engine combustion chamber and as exhaust emanates from the tailpipe.

Upon cooling and dilution, volatile materials present in the exhaust transform into liquid and solid phases. Nucleation, condensation, and absorption are the principal modes of transformation. Mode of transformation as well as the amount of volatile materials converting in to particles depends upon temperature of the exhaust gas and prevailing dilution conditions [151].

Tiny exhaust particles provide enormously large surface area per unit mass for adsorption of organic and inorganic species [151]. Composition of typical diesel particulate is shown in Fig. 21. Contributions to PM from combustion of lubricating oil, mineral diesel and biodiesel were examined using various parametric tests by several researchers [168,169]. Soluble organic fraction (SOF) primarily comprises of unburnt fuel and lubricating oil. In addition, a small fraction is also formed by pyrolysis and incomplete combustion of fuel. Ultrafine particles emanating from mineral diesel and biodiesel fueled engines serve as adsorption sites for condensation of other contaminants because of the large surface area they offer [151]. It has been demonstrated in a study using mass spectrometry [170] that unburnt lubricating oil is the main source of organic components present in the engine-out nano-particles. Another study [171] demonstrated that ~1% of the total SOF comprises of mono-carboxylic acids, of which ~90% are either unbranched or cyclic alkanes. Rest of the particle is made up of refractory materials such as oxides of metals (ash).

Engine exhaust has ~90% of total PM mass in two distinct modes: accumulation mode (56–1000 nm) and nuclei mode (7.5–56 nm) [172]. The nuclei mode particles are dominated by elemental carbon (EC). Accumulation mode particle formation takes place due to adsorption of organic substances on primary carbon spheres along with sulfates [168]. It has been observed from several experimental studies that formation of numerous nuclei-mode particles takes place because of higher sulfur content in the test fuel [173,174].

In comparison to conventional gasoline engines and engines equipped with catalytic converters, diesel engines emit 10 and 30–70 times more particulate mass per km, respectively [175]. Majority of particles in the DPM are smaller than 1 μm. The duration for which these particulates remain suspended in the atmosphere varies from a few hours to several days, depending on their size. DPM, due to their small size and mass, may travel to far-off places and they have the capacity to penetrate into deeper regions of the lungs of living beings. Ultrafine particles can eventually enter into the blood stream and affect vital organs [176,177].

Differential mobility analyzers and various electrical/optical measurement techniques have been employed for measuring particle size-number distribution in the engine exhaust [178–180]. Semi-volatile fractions are usually sampled and collected on polyurethane foam, which is used as an absorbent, whereas samples of exhaust particles are collected on pre-weighed filters using inertial impactors. Initially, scanning mobility particle sizer was used to measure particle size-number distribution from diesel engines [154,167]. However, there were disadvantages of these measurements. Scanning mobility particle sizer cannot be used for dynamic sampling of exhaust particles because it has high sampling time, which is of the order of few minutes. Condensation

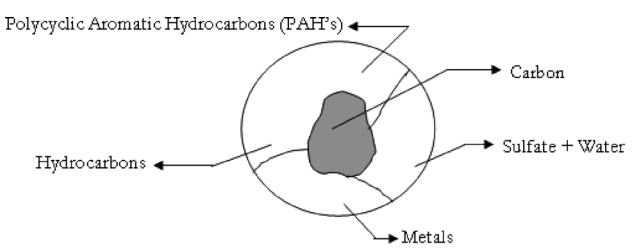

Fig. 21 Typical composition of diesel particulates

particle counter helped detect particles with diameter in the range of 2.5–3000 nm. Therefore, condensation particle counter was used to measure the particle size-number concentration of the exhaust gas. Engine exhaust particle sizer is an instrument (size range 5.6–560 nm), which is designed for dynamic sampling of diesel engine exhaust. It is designed to measure at a sampling frequency of 10 Hz; therefore it can even measure particle size distributions in transient conditions.

Various studies reported particle size-number distributions in the engine exhaust from diesel engines fueled by biodiesel and mineral diesel [152,181–184]. Majority of exhaust nano-particles were composed of OC formed due to incomplete combustion inside the engine. Particle size-number distributions have been reported from a study using CRDI system fueled by Rapeseed biodiesel blended with mineral diesel [183]. It reported that emitted particles were mostly smaller than 300 nm. In addition, bimodal particle number-size distribution was observed for biodiesel blends, with majority of them being in nanoparticle size range. Another study revealed higher particle number concentration, when the engine was fueled by KB100 (Karanja biodiesel) compared to mineral diesel [181]. However, almost similar particle numbers were obtained from mineral diesel and KB20. Agarwal et al. [185] reported that with increasing FIP, number, and mass of particulates decreased at all loads.

Another study showed measurable reduction in particle number concentrations in the engine exhaust, when fueled by Soy biodiesel blends [182]. Jung et al. [182] examined the effect of biodiesel (SME) blends on particulate emissions at 1400 rpm engine speed and 75% load. 38% reduction in accumulation mode particle number concentration and 82% reduction in particle volume compared to baseline mineral diesel were reported. Kawano et al. [152] reported uni-modal accumulation mode particle number-size distribution for mineral diesel and RME at different engine loads. At higher engine loads, the peak particle number concentration for RME decreased. On the contrary, higher engine loads actually increased the peak particle number concentration for mineral diesel. This indicated that biodiesel origin particles were primarily made of OC, which burnt completely at high temperature conditions prevailing at higher engine loads in the combustion chamber. Variations in emission levels were mainly due to variations in fuel (mineral diesel and biodiesel) atomization characteristics. Higher viscosity and density of biodiesel led to larger spray droplets sizes, which formed lower number of larger particles. However, the oxygen content of biodiesel improved the oxidation of fuel droplets and which reduced the size and number of particles emitted [152,181,183–185].

Mineral diesel and biodiesel exhaust particles mainly consisted of EC and OC. In general, contribution of EC to the particle composition varies in the range of ~50–75% and contribution of OC varies in the range of ~19–43% [186]. Partially burned particulate phase HCs are a result of heterogeneous combustion in the engine. A fraction of these fuel-based HCs are present in the fuel-rich zones in the engine combustion chamber. These pyrolyzed inside the engine under the influence of high temperature and pressure, which resultsed in the formation of tiny particulate nuclei. EC core formation was due to selective removal of hydrogen atoms from the resultant soot in hydrocarbon chains, which takes place rapidly. Cyclization of carbon results in formation of graphite-like layered sheet structures that finally roll-over to form spherules and nano-tube-like structures [187]

Solid and dry soot particles provide nucleation sites and condensation surfaces, over which semi-volatile organic materials condense. These particles further grow by sorption and undergo surface oxidation to form the SOF.

Zielinska et al. [188] showed that at lower engine loads, ultrafine particulates mainly comprise of the OC. Larger particles produced under lower engine loads are mostly heterogeneous in their composition [169]. At higher engine loads, exhaust particles are dominating composed of the EC. Kweon et al. [189] investigated the effect of engine load on emitted OC concentration from a heavy-duty diesel engine. At idling, light and medium loads, dominance of OC in the exhaust particles was observed, which mostly originated from fuel pyrolysis. Gangwar et al. [190] investigated the toxicity of biodiesel origin particulates and reported that biodiesel blend origin particulates have more benzene soluble organic fraction (BSOF; which is a marker of toxicity) compared to mineral diesel [190]. Comparison between mineral diesel and vegetable oil origin particulates showed that vegetable oil origin particulates contain lesser toxic metals, in addition to lower soot formation [191].

6.2 Unregulated Emissions. Total hydrocarbon emissions are regulated However, individual hydrocarbon species are unregulated since they are not yet covered under any emission regulation. It is challenging to accurately detect, identify, and quantitatively determine the concentration of each and every individual hydrocarbon species. This is the prime reason that such individual hydrocarbon species are currently studied for academic and research purposes only. However, there are a few studies, which have reported unregulated tailpipe emissions from various new fuels and conventional fuels [192,193]. A number of these investigations related to unregulated emissions have been carried out via gravimetric analysis. Past studies have reported lower unregulated emissions from biodiesel blends fuelled engines compared to baseline mineral diesel fuelled engines [194,195]. Unregulated emissions such as PAHs, benzene, toluene, ethyl benzene and xylene (BTEX), and carbonyls are important due to their severe adverse health effects on humans [187].

6.2.1 Carbonyl Compounds. A large number of organic compounds emitted by diesel and biodiesel engines have not yet been measured quantitatively. The term carbonyl suggests –C = O functional group, i.e., a divalent group comprising a carbon atom attached to the oxygen with a double bond. Engine exhaust has a significant amount of carbonyls and these emissions have been evaluated using its derivatives with 2, 4-di-nitro-phenyl-hydrazine (DNPH) in various studies [196–199].

The presence of carbonyls in the engine exhaust increases their overall physiological and toxicological effects on humans [200]. Pang et al. [200] studied the properties of carbonyl emissions originating from a diesel engine fueled by a biodiesel–ethanol–mineral diesel blend. It was found that acetaldehyde, formaldehyde, acetone, propionaldehyde, and benzaldehyde were the dominant carbonyl species emitted. Due to blending of mineral diesel with biodiesel, nearly 1–12% enhancement in total carbonyl emissions was reported for varying engine loads and speeds.

He et al. [201] observed that the contribution of formaldehyde emissions were 46 and 62% from Sunflower biodiesel and mineral diesel, respectively, in the emission of total carbonyl compounds. In addition, significant concentrations of acetaldehyde, acrolein, acetone, etc., were observed. Karavalakis et al. [202] measured unregulated emissions in two driving cycles (Athens driving cycle: ADC and New European driving cycle: NEDC) using Soy biodiesel blended (5, 10, and 20%) with mineral diesel. They found that carbonyl emissions reduced from a diesel engine operating on ADC and NEDC test cycles, when fueled by the blends of Soy biodiesel. In another study, it was reported that lower blends of biodiesel from different feedstocks (Rapeseed, Soy, Sunflower, Palm, and waste cooking oils) blended with mineral diesel (B10) did not affect carbonyl emissions in the exhaust [203].

Magara-Gomez et al. [204] measured emissions from Sunflower biodiesel blends (B0, B50, and B100) and beef tallow biodiesel (BT50 and BT100). They reported that there was significant reduction in different unregulated emissions such as toluene, ethyl benzene, and m-, p- and o-xylenes. It was also reported that formaldehyde emissions reduced by 23, 42, and 40% for B50, B100, and BT100 respectively, compared to baseline mineral diesel. Further, the use of both biodiesels reduced carbonyl emissions. Cheung et al. [195] tested methanol blends (5, 10, and 15%) with biodiesel and

reported that acetaldehyde, formaldehyde, and unburned methanol emissions were observed to be relatively higher compared to baseline mineral diesel.

Formaldehyde emerged as one of the main pollutant, closely followed by acetaldehyde and acetone, among 15 carbonyl species identified and measured by Ho et al. [205]. 54.8–60.8% of total carbonyl compounds in the exhaust were identified as formaldehyde. Secondary organic aerosol (SOA) formation in the ambient atmosphere takes place due to formation of oligomers from parent carbonyl emissions. Several samples were collected from the ambient atmosphere in the Hong-Kong city during summer. It was found that measured formaldehyde concentrations were significantly different from the theoretically predicted ones. This is possibly due to photochemically excessive production of SoA namely formaldehyde in the ambient atmosphere due to oxidation of more complex volatile organic compounds.

6.2.2 Benzene, Toluene, Ethyl-Benzene, and Xylene. Cheung et al. [195] investigated BTEX emissions at 1800 rpm at varying engine loads from a diesel engine fueled by biodiesel and methanol blended with mineral diesel. Significant emissions of BTEX obtained were attributed to higher oxygen content of biodiesel. BTEX levels reduced at higher engine loads.

Di et al. [206] and Takada et al. [207] also reported relatively lower BTEX emissions at higher engine loads. In another study, relatively lower aromatic emissions from biodiesel were reported [208,209]. Higher carbonyl emissions were correlated with increasing biodiesel content ($R^2 > 0.96$) [198]. The prime source of these carbonyl emissions might be the esters present in biodiesel. At lower engine loads, carbonyl emissions were relatively higher than those measured at higher engine loads [195,210]. Xue et al. [211] also reported that biodiesel usage led to reduction in emission of aromatic and polyaromatic compounds but higher carbonyl emissions.

6.2.3 Polycyclic Aromatic Hydrocarbons. As a result of incomplete combustion of fuel, PAHs that are highly carcinogenic are produced. Ravindra et al. [186] put together a database to recognize and characterize these engine-out PAHs in their study. PAHs that are human carcinogens, were found to be adsorbed onto the particulate surface. Keeping this in view and the adverse impact of PAHs on the human health, these pollutants should get due attention in the emission legislations in the future.

Molecular structure of PAHs is responsible for their toxicity. Different toxicity behaviors have been seen with two isomers of PAHs of different structures. Therefore, EPA classified these PAH compounds into different categories [186]. Lea-Langton et al. [212] collected particulate samples of mineral diesel, biodiesel, and waste cooking oil for comparison and analyzed particulate bound PAH emissions from a heavy duty DI diesel engine. It was observed that biofuels emitted lower particulate bound PAHs. This was more prominent at lower engine loads. Most of the larger PAHs such as benzo(a)anthracene, chrysene, benzo(b)fluoranthene, and benzo(k)fluoranthene were oxidized by diesel oxidation catalysts in the engine tail-pipe. Further, pyrolytic formation of fluoranthene in the engine combustion chamber was reported in the study since there was no fluoranthene present in mineral diesel; however, it was found to be present in the emitted soot.

Zielinska [213] assessed physical and chemical transformation of primary mineral diesel engine origin emissions. It was observed that primary mineral diesel exhaust reacted primarily with OH radicals, ozone, and NO_x radicals present in the ambient air in presence of sunlight. It was also observed that monocyclic aromatics from primary mineral diesel exhaust produced various aromatic compounds such as phenols, glyoxal, quinones, nitro-PAHs, and aromatic aldehydes, when they reacted with OH radicals. It was concluded in this study that PAHs were produced due to incomplete combustion of fuel.

Detailed speciation of PAHs adsorbed on diesel particulate has been presented by researchers [214,215], wherein it was observed that during the collection of particulates, adsorption of semi-volatile PAHs could also occur along with chemical transformation of the semi-volatile compounds. PAHs and PAH-derivatives present in diesel engine-out emissions are formed at high temperature and are thus present in both, gas and particle phase [216]. When PAHs react with ambient NO_x, they transform into nitro-PAHs. Major sources of emitted PAHs are unburned PAHs present in the fuel and electrophilic nitration of PAHs in the engine and crankcase oil. Diesel exhaust thus contains a wide variety of both gas and particulate phase PAHs [217–219]. Majority of nitro-PAH formation takes place during the expansion/exhaust stroke. Heavy-duty diesel engine powered vehicles emit PAHs in much higher concentration than light-duty gasoline engine powered vehicles [171].

In another study, PAH and nitro-PAH emissions originating from a Cummins engine fueled by mineral diesel, biodiesel (B100, Soy methyl ester), and B20 were compared [215]. These emissions from mineral diesel and biodiesel were measured by gas chromatography-mass spectrometry (GC_MS) technique. It was reported that B100 produced significantly lower PAH and n-PAH emissions than mineral diesel. B20 fueling also resulted in substantially lower PAH and *n*-PAH emissions than mineral diesel in most cases.

Agarwal et al. [169] estimated individual PAH species from the total PAH load using the method provided by Pan et al. [215] (Fig. 22). In addition, the toxic equivalent factors of 8 PAHs and 2 nitro-PAHs were also calculated. This experimental study was performed on mineral diesel and Karanja biodiesel (B20) for both primary as well as secondary emissions, emanating from a CRDI diesel engine. A custom-built UV light illuminated photochemical chamber having 2 h residence time was employed to measure the SoA emissions. It was observed that B20 emitted lower particulate bound PAHs compared to mineral diesel. Marginally higher toxic potential of total PAHs for mineral diesel was observed compared to B20. Primary particles demonstrated lower toxicity when compared to those from secondary emissions for both test fuels [169].

7 Biodiesel Engine Simulations

Now-a-days, simulations based on computational fluid dynamics (CFD) are being developed and used in various research domains. The CFD investigation protocols have expanded to the domain of development of IC engines and combustion as well. CFD computations technology reproduces complex in-cylinder engine phenomenon and allows researchers to overcome the limitations experienced in experimental investigations. There are various tools to model complicated IC engine phenomenon, which include commercial software programs and open-source software

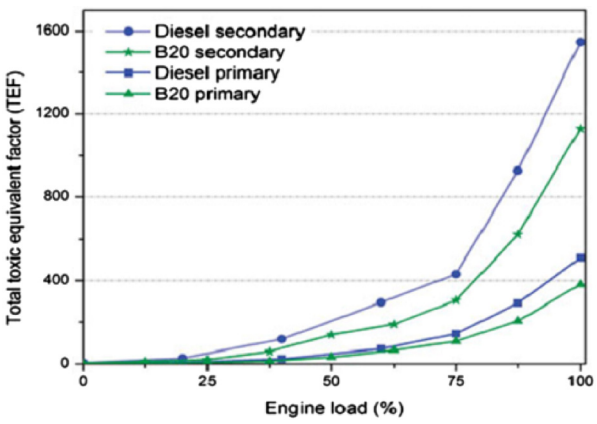

Fig. 22 Total toxic equivalent potential of PAHs emitted by mineral diesel and biodiesel (B20) fueled engine particulates (Primary and secondary) [169]

Table 9 Methodologies and equations to determine physical properties of biodiesel [227]

Property	Method	Equation
Critical temperature	Ambrose's method	$T_{cm} = \frac{1}{V_{cm}^{1/4}} \sum_i \sum_j y_i y_j V_{cij}^{1/4} T_{cij}$
Critical pressure	Ambrose's method	$V_{cm} = \sum_i \sum_j y_i y_j V_{cij}$
Critical volume	Lydersen's method	$P_{cm} = (0.2905 - 0.085\omega_m) RT_{cm}/V_{cm}$
Vapor pressure	Pitzer method	$\ln P_{vPr} = f^{(0)}(T_r) + \omega_m f^{(1)}(T_r)$
Latent heat of vaporization	Pitzer acentric factor correlation	$\Delta H_v = RT_{cm}\left[7.08(1-T_r)^{0.354} + 10.95\omega_m(1-T_r)^{0.456}\right]$
Liquid density	Modified Rackett equation	$\rho = 0.8976 \times 0.2370288^{-\varnothing}$
Surface tension	Allen's method	$\sigma_m = \sum_i^n w_i \sigma_i x_i$
Liquid viscosity	Orrick and Erbar method	$\ln \frac{\eta_L}{\rho_L M} = A + \frac{B}{T}$

codes. Many scientists and engineers have developed new computational skills and updated detailed combustion phenomena. In case of diesel engines, computational models have been developed right from the fuel spray process starting with fuel injection, all the way down to the concentration of exhaust emissions. Spray characteristics in a combustion chamber strongly affect downstream diesel combustion processes and results. Hence, unrealistic spray models could lead to unphysical predictions in the combustion results. In addition, combustion modeling is one of the key issues in the computational investigations of an IC engine. Various CFD-based computational combustion models have been proposed for diesel combustion simulations such as the representative interactive flamelet model, shell/characteristic time combustion model, extended coherent flame model for three zones (ECFM-3Z), and direct integration of chemical kinetics. Finally, the prediction of exhaust gas composition from mineral diesel engine is important in the simulation of CI engines. In most studies, NO_x and soot emissions are modeled using Zeldovich mechanism and phenomenological models.

In order to model biodiesel engines with high accuracy, detailed physical properties of biodiesel are required along with appropriate spray models. Especially, mechanisms for combustion of biodiesel surrogate fuels are important in modeling ignition and combustion processes of biodiesel and blends.

In this section, diverse models are reviewed based on their suitability for modeling biodiesel fueled engine. It has been a challenge to model biodiesel combustion in CI engines due to high carbon number species present in biodiesel. There are very few combustion kinetics studies investigating biodiesel combustion modeling. Coniglio et al. [220] summarized research studies related to experimental and kinetic modeling aspects of biodiesel combustion in the last decade. Numerous experimental research studies of biodiesel oxidation were reviewed to validate biodiesel modeling results under different physical environments. However, proper and reliable reactor modeling was required to account for these physical conditions. At first, small carbon numbers (C_1–C_4) were used to model molecules of small methyl and ethyl esters, which was restricted to the use of high number of carbon species in kinetic models. While methyl butanoate (MB) was introduced as a surrogate fuel to biodiesel, it could not explain cool flames and negative temperature coefficient (NTC) regions. New surrogate components were suggested to account for the oxidation process in biodiesel having long-chain molecular structure. Comparison of various kinetic mechanisms of candidate surrogate fuels to biodiesel namely methyl hexanoate, methyl octanoate, methyl decanoate, methyl-5-, and methyl-9-decenoate was also carried out. Lai et al. [221] also considered MB kinetic reactions to model biodiesel combustion. They created two separate categories of biodiesel surrogate fuels: small carbon chain esters (up to five carbons) and large carbon chain esters (greater than five carbons). Although the MB modeling gave insight into the oxidation of methyl esters, it exhibited limitations in predicting the effects of larger molecules on biodiesel combustion. Methyl decanoate, which was selected as a surrogate fuel for biodiesel combustion, predicted the NTC trends against experimental results. However, larger number of reactions for large molecules severely limits its application to engine simulations. Finally, adequate understanding of reduction processes and further development of kinetic models to simulate biodiesel combustion are required. Biodiesel combustion modeling is still under evolution with an objective to precisely capture the combustion processes in comparison to experiments.

7.1 Physical Properties of Biodiesel and Spray Modeling. In order to model biodiesel spray atomization process, precise fuel properties are required for CFD simulations. In mineral diesel, spray modeling to obtaining precise fuel properties is challenging since mineral diesel is not a pure substance and is a mixture of large number of hydrocarbons. A surrogate fuel, tetradecane ($C_{14}H_{30}$), has been widely used to reproduce mineral diesel spray behavior traditionally [222–224]. Similarly, Biodiesels are also composed of several hydrocarbons. In addition, biodiesel is derived from many feedstock sources, e.g., Rapeseed, Palm, Coconut, and Soy [225]. The feedstock and the transesterification process determine the physical and chemical properties of biodiesels. Therefore, it is not straightforward to select a representative fuel to account for all biodiesels. Yuan et al. [226] suggested a methodology to estimate biodiesel properties by introducing methyl soyate as surrogate fuel. Since biodiesels contain six or seven fatty acid esters, therefore, it was reported that proper mixing rules could determine the mixture characteristics using pure components present in biodiesel. Critical fuel properties were calculated using Ambrose's method and Lydersen's method [227] based on the information of each pure constituent in order to improve the property prediction accuracy. Vapor pressure, latent heat of vaporization, liquid density, surface tension, and viscosity were derived based on temperature variation using various correlation formulae. Detailed equations and methodologies for this are listed in Table 9.

Researchers combined individual component species using mixing rules based on the mass fraction. The obtained values of biodiesel properties showed that the effects of composition of biodiesels were insignificant on the properties of interest, but the trend of variation with composition is clearly evident. It was further demonstrated that the results could be used as fundamental data for biodiesel spray and combustion modeling. Chakravarthy et al. [228] determined biodiesel's physical properties by calculating the physical properties of each constituent component based on mixing rules. Since biodiesel has simple fatty acid esters, they considered this method was feasible. For estimation of thermodynamic properties, group additivity and empirical formulations were used. The updated properties were used in computations in

Table 10 Assumed composition of Soy-biodiesel by for computational study [224]

Component	Amount (mol %)
Hexadecanoic acid, methyl ester	17
Octadecanoic acid, methyl ester	9
9-Octadecenoic acid, methyl ester	30
9, 12-Octadecadienoic acid, methyl ester	44

multidimensional CFD simulation, KIVA-3V. Under DI combustion mode, changed biodiesel properties generated lower evaporation rate and fuel-air mixing capability, which resulted from lower vapor pressure and higher heat capacity. These results, however, could not be validated by experiments. Ra et al. [224] estimated 11 physical properties of biodiesel by employing the same methodology as by Chakravarthy et al. [228]. They assumed that biodiesel is mainly composed of four esters found in Soy-biodiesel, which are listed in Table 10.

Based on the properties of biodiesel, sensitivity of numerical simulations to individual physical properties was evaluated under different engine operating conditions. Ra et al. [224] measured the changes in single droplet diameter under both stagnant and convective conditions. Among various physical properties, fuel density and vapor pressure were observed to strongly affect droplet evaporation. In addition, biodiesel and mineral diesel sprays in the engine cylinder were simulated using the updated data. Due to difference in fuel properties, biodiesel exhibited slower vaporization, thus increasing the mixing time and the ignition delay. However, as the SoI timing approached closer to TDC, the effect of fuel properties on mixing processes significantly reduced. Ismail et al. [229] performed fuel spray and combustion modeling of coconut methyl ester (CME), palm methyl ester (PME), and Soyabean methyl ester (SME) using the measured fuel properties. Since each methyl ester is from a different source, the composition of each ester was analyzed and the properties were measured for an individual biodiesel. For vapor pressure, three computed biodiesels showed lower vapor pressure than mineral diesel due to the absence of volatile species in them. Generally, biodiesel has lower vapor pressure compared to mineral diesel, but CME exhibited higher vapor pressure in a narrow temperature range of study, which affected spray considerably. They performed validation of fuel properties with respect to the spray structure in a constant volume chamber using an open source code. From their computational results, biodiesels showed slower evaporation rates and larger SMD compared to mineral diesel. The axial spray penetration length of all biodiesels was longer. Figure 23 shows the spray penetration length of biodiesel and mineral diesel along with comparison of experimental and computational results.

In comparison to experiments, simulation results of PME were in good agreement with the calculated physical properties. Although marginal errors occurred later in the simulations, vapor and liquid penetration lengths in the constant volume chamber were captured quite well. The liquid penetration length of biodiesels and mineral diesel were validated against PME and mineral diesel experiments. Penetration length of mineral diesel was overpredicted due to difference in properties between a surrogate fuel and a realistic mineral diesel. In addition, the effect of physical properties was observed in the other biodiesels' (PME, CME, and SME) liquid penetration length. In the case of CME, the behavior of evaporation and penetration trend was similar to that of mineral diesel. These results highly affected IC engine combustion environment. This is because the fuel-air mixing rate determined the combustion duration and engine performance. As mentioned earlier, biodiesel's physical properties were estimated using the mixing rules to express representative surrogate fuel. However, the discrete multicomponent (DMC) model developed by Ra and Reitz [230,231] allows researchers to consider various fuels together in the same domain. The DMC model allows preferential evaporation using specific properties of individual constituent species. Brakora et al. [232] conducted biodiesel modeling using this DMC model. They considered that biodiesel mainly composed of five methyl esters: methyl palmitate ($C_{17}H_{34}O_2$), methyl stearate ($C_{19}H_{38}O_2$), methyl oleate ($C_{19}H_{36}O_2$), methyl linoleate ($C_{19}H_{34}O_2$), and methyl linolenate ($C_{19}H_{32}O_2$). These components contained saturated and unsaturated structures with oxygen content, which were important biodiesel characteristics for investigating spray and combustion processes. The physical properties of each fuel constituent were obtained from various sources namely CHEMKIN code, Knovel Critical Tables online database, and Design Institute for Physical Property Research (DIPPR) database. They illustrated the distillation curve using five components (Fig. 24) wherein the simulation results were in close agreement with the experimental results. Dash-lines in Fig. 24 indicate the boiling point temperature of each fuel component.

Spray simulations were carried out using hybrid Kelvin–Helmholtz (KH)/Rayleigh–Taylor (RT) breakup models under constant volume chamber conditions [232]. The experimental study of Higgins et al. [233] was chosen as reference for validating the data. Proper breakup model constants were derived by comparing realistic liquid spray penetrations. As can be seen from

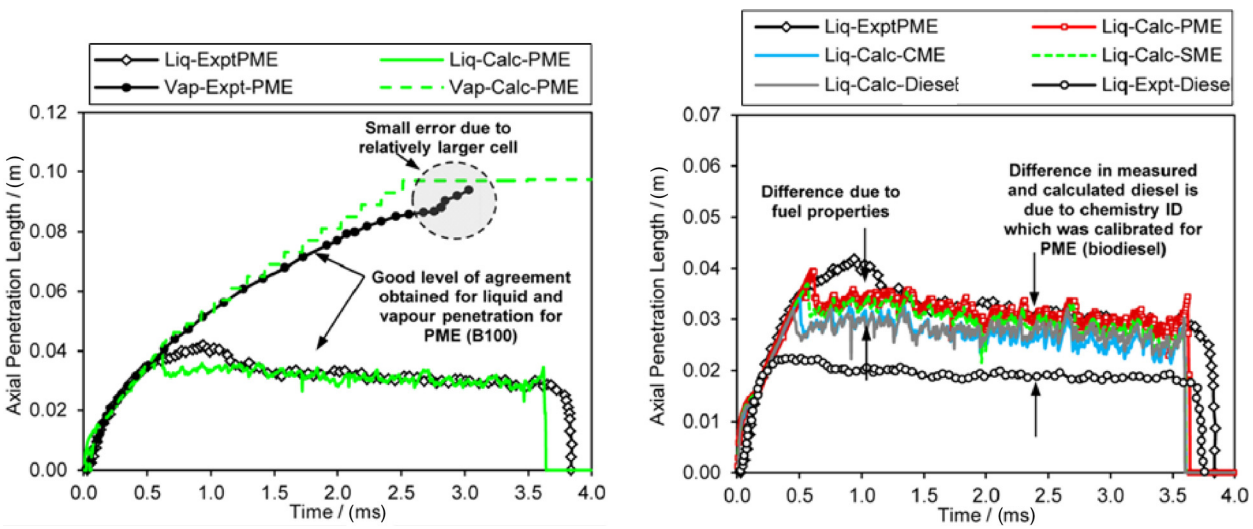

Fig. 23 Experimental and numerical axial penetration length for (*a*) PME vapor and liquid and (*b*) PME, CME, SME, and mineral diesel in liquid phase [229]

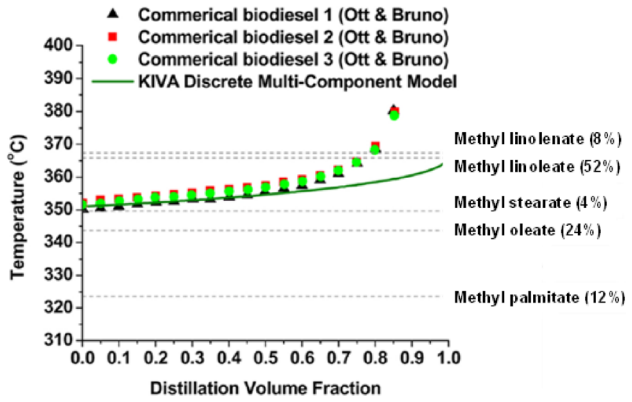

Fig. 24 Distillation curve using five-component fuel simulation for different commercial biodiesels [232]

Fig. 25, the updated constants could capture biodiesel spray characteristics based on reference results.

The modified breakup model depicted the spray development with larger droplets and shorter break-up length, which reflected the trend of biodiesel spray.

7.2 Mechanism for Combustion Modeling. Among variety of combustion models, the method of calculating chemical reactions has been highlighted to predict combustion and emission characteristics simultaneously. Combustion mechanism requires appropriate surrogate fuel to accurately express combustion. Expression of properties in terms of surrogate fuel is also needed because hydrocarbon fuel contains a number of species which undergo oxidation combustion. It is difficult to consider all the species and reactions in IC engine simulations. In the case of mineral diesel, *n*-heptane (C_7H_{16}) has been mainly used as the surrogate fuel in chemical reactions [234,235]. Although a single component was used as a surrogate fuel, it posed a huge challenge. The detailed mechanism of n-heptane is composed of 570 species and 2520 reactions, which is impractical to model an IC engine combustion. Therefore, many researchers proposed a reduced mechanism to shorten the computational time and still describe diesel combustion satisfactorily. Numerous researchers optimized the reduced diesel mechanism, which is used widely in the industry. Biodiesel includes long-chain hydrocarbon constituents and oxygen, which are important factors to demonstrate biodiesel combustion. Initially, methyl butanoate ($C_5H_{10}O_2$, MB) was proposed as a surrogate fuel for biodiesel due to its chemical structural features, although it did not have high molecular weight [236,237]. Detailed mechanism of MB contained 264 species and 1219 reactions, which was not very adaptable for engine simulation. Therefore, Brakora et al. [238] developed a reduced biodiesel mechanism using reduction processing, which included flux analysis, ignition sensitivity analysis, and optimization of reaction constants. They achieved the reduced biodiesel mechanism consisting of 41 species and 150 reactions. The small-size reactions for MB exhibited similar levels of accuracies in predicting ignition delay as that of original kinetics. Combination processes between reduced n-heptane and MB mechanisms were further performed to account for combustion of blends of mineral diesel and

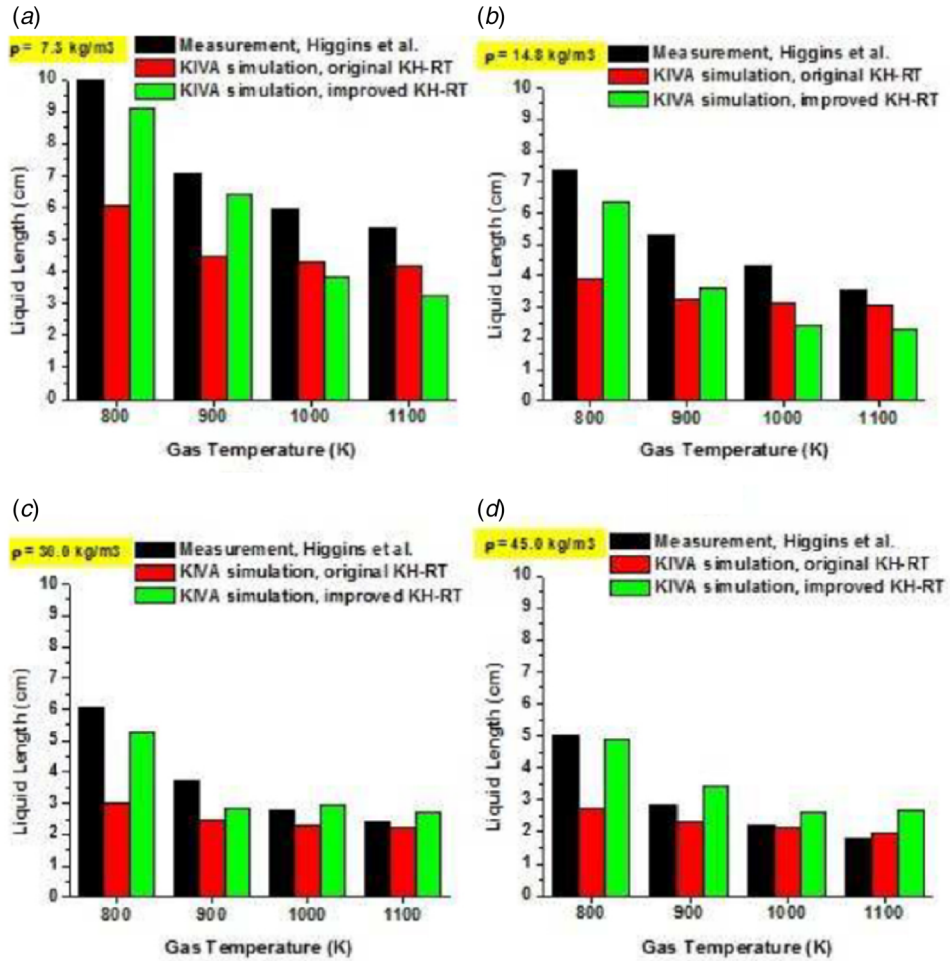

Fig. 25 Liquid spray penetration comparisons using original and improved KH-RT spray constants for biodiesel [233]

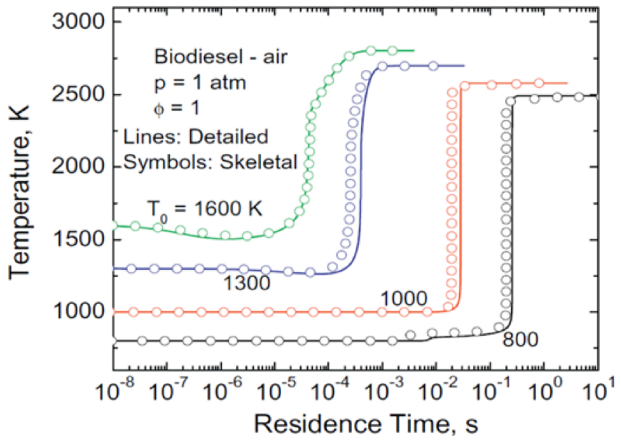

Fig. 26 Temperature profiles at different initial temperatures using 115-species skeletal mechanism and detailed mechanism, respectively [245]

biodiesel. Combined mechanism included 53 species and 156 reactions, which was a suitable size for engine simulation studies. In the multidimensional engine simulations, combined mechanism predicted the combustion pressure and heat release rate with high accuracy. However, NO_x emissions characteristics could not be captured well under low load conditions. Um et al. [239] also applied this mechanism to mineral diesel/biodiesel blends combustion in engine simulations. They modeled biodiesel blends derived from Ricebran oil. The developed chemistry described combustion characteristics with reasonable accuracy under different blending ratios. However, the emissions results showed large discrepancy vis-a-vis experimental results. To reduce the deviation of MB mechanism, new surrogate fuels were suggested. A mixture of methyl decanoate (MD), methyl-9-decenoate (MD9D), and n-heptane were proposed to describe biodiesel combustion accurately [240–242]. The new compiled mechanism had 3299 species and 10806 reactions. It was too large to implement in numerical study. Hence, Luo et al. [243] carried out reduction of this impractical mechanism for high temperature oxidation. The direct relation graph-aided sensitivity analysis and DRG were applied to obtain skeletal reactions to describe ignition delay under various ambient conditions in perfectly stirred reactors. In the new mechanism, three main fuels could account for various types of biodiesels by adjusting their fractions. Luo et al. [243] obtained a 118-species skeletal mechanism for describing of biodiesel combustion. However, these chemical reactions were derived for high temperature (>1000 K) oxidation. Later, Luo et al. [244,245] reported an updated mechanism with low

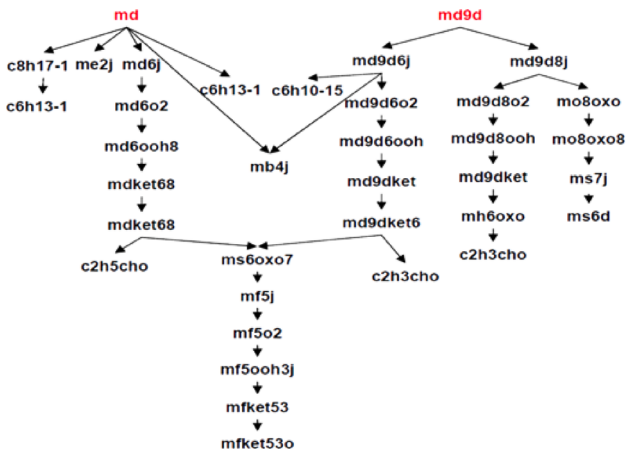

Fig. 27 Key pathway in the MD+MD9D mechanism [246]

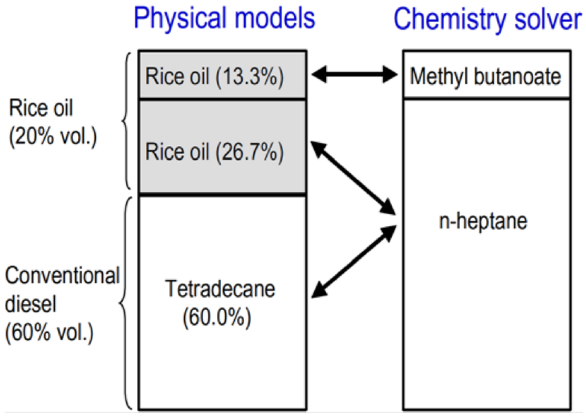

Fig. 28 Numerical composition of BD20 and the species information exchange between physical and chemistry models [239]

temperature reactions, which included the NTC. The final version of the reduced mechanism contained 115-species and 460 reactions, which was suitable for the three-dimensional engine simulation using biodiesel. The skeletal mechanism was validated against detailed mechanism as well as experimental results. As can be seen in Fig. 26, computed temperatures of auto-ignition under various initial temperatures were depicted accurately and were comparable to the results obtained from the detailed mechanism. Additionally, further validations were performed for various experimental conditions ranging from one-dimensional flames to three-dimensional turbulent spray combustion under CI engine conditions. It was concluded that 115-species skeletal mechanism was feasible to model biodiesel combustion.

Brakora [246] carried out reduction of mechanism using combined surrogate fuels; MD, MD9D, and n-heptane. This study targeted biodiesel derived from Soy for the use in CI engines. The reduction was initiated using the MD+MD9D detailed mechanism developed by Lawrence Livermore National Laboratory (LLNL). The number of species that participated in reactions was changed from 3299 to 85. Although the MD+MD9D mechanism was sufficient to describe biodiesel combustion process, the developed mechanism was combined with *n*-heptane reactions to expand on biodiesel applications. The key oxidation steps (Fig. 27) were transferred to the new mechanism. The minimizing process of the combined mechanism was also conducted up to 77 species and 216 reactions. Added n-heptane component improved the ignition characteristics and shared the same oxidation pathway with lower-level reactions of the MD+MD9D mechanism. In this study, it was suggested that the mole fractions of MD, MD9D, and n-heptane represent various types of biodiesel, e.g., RME would contain 2.5% MD and 47.5% MD9D; SME would have 8% MD and 42% MD9D; and PME would contain 24.5% MD and 25.5% MD9D. The remaining fraction was occupied by the *n*-heptane.

7.3 Biodiesel Fueled Compression Ignition Engine Modeling

7.3.1 Modeling of Engine Performance Characteristics. As mentioned previously, MB was proposed as a surrogate fuel to model biodiesel for describing biodiesel combustion characteristics in IC engines. Brakora et al. [238] and Um and Park [239] implemented combustion of biodiesel and its blends in CI engines with MB mechanism using KIVA/CHEMKIN codes to simulate multidimensional combustion. Brakora et al. [238] compared their engine simulation results with the experiments conducted on a Sandia CI optical research engine using 100% Soy-based biodiesel. Under four different load conditions, ignition timing and peak pressure were in good agreement. The research by Um et al. [239] used three test fuels namely 100% mineral diesel (D100), 20% (BD20), and 40% (BD40) biodiesel blends. The simulated

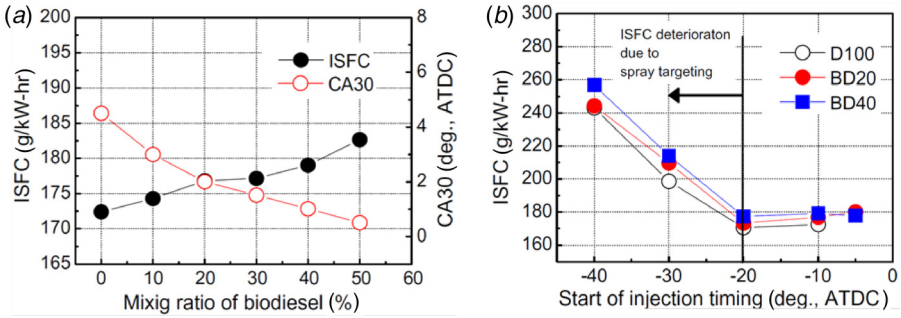

Fig. 29 Fuel consumption characteristics under different (*a*) mixing ratios of biodiesel and (*b*) injection timings [239]

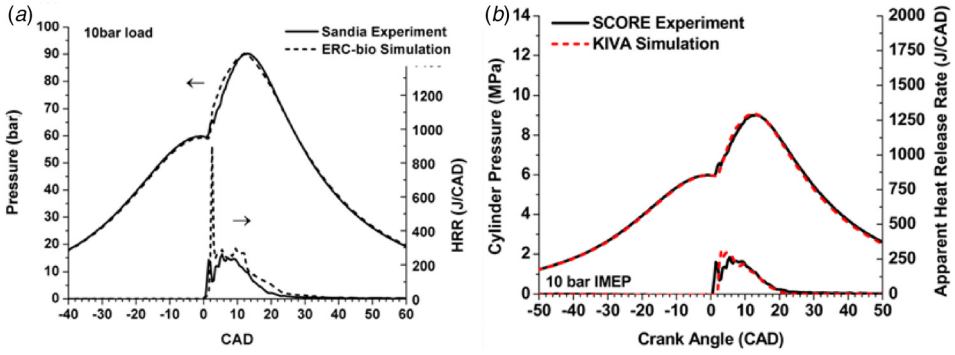

Fig. 30 Combustion pressure and heat release rate using (*a*) MB/*n*-heptane mechanism and (*b*) MD/MD9D/*n*-heptane mechanism with comparison to experimental results [232]

Table 11 Fuel composition using seven-component chemistry strategy for SME20 and PME20 [247]

SME20			PME20		
Property species	Chemistry species	Composition	Property species	Chemistry species	Composition
m.palmitate	MD	0.0132	m.palmitate	MD	0.0483
m.stearate	MD	0.0051	m.stearate	MD	0.0054
m.oleate	MD9D	0.0265	m.oleate	MD9D	0.0432
m.linoleate	MD9D	0.0577	m.linoleate	MD9D	0.0121
m.linolenate	MD9D	0.0087	m.linolenate	MD9D	0.0006
m.linoleate	nC7H16	0.1130	m.palmitate	nC7H16	0.1142
tetradecane	nC7H14	0.7757	tetradecane	nC7H14	0.7763

composition of BD20 was divided into physical and chemistry models to capture the fuel characteristics (Fig. 28). In this assumption, since MB could not represent biodiesel in terms of lower heating value, the combination of 1 mole MB and 2 moles *n*-heptane was necessary to compensate for the heating value.

The effect of biodiesel mixing ratio and injection timings on combustion characteristics was further investigated. Figures 29(*a*) and 29(*b*) show the fuel consumption depending on mixing ratio and operating conditions. The increase in biodiesel contents in mixed fuels deteriorates the indicated specific fuel consumption. This was because lower LHV of biodiesel required larger fuel quantity to generate the same power as that of mineral diesel. In Fig. 29(*a*), CA30 indicates the time by which 30% heat release has occurred. These results showed that biodiesel induced advanced ignition timings with increasing biodiesel content in blends. Figure 29(*b*) shows deterioration of fuel efficiency as the injection timing advanced. This was because the spray targeted the cylinder walls under advanced injection conditions. In addition, the increase in biodiesel quantity increases the consumption over the entire injection timing range compared to mineral diesel. Advanced ignition timing reduced the time available of fuel-air mixture formation.

The combined mechanism of MB and *n*-heptane was successful to model combustion of biodiesel and blends (with mineral diesel) in CI engines. However, other surrogate fuels were also widely used to model various biodiesels. Brakora et al. [232] validated the updated mechanism based on MB against experimental results. The developed mechanism used MD, MD9D, and *n*-heptane as surrogate fuels. As can be seen in Figs. 30(*a*) and 30(*b*), the new mechanism improved the prediction of biodiesel combustion pressure and heat release rate. Moreover, overpredicted heat release rate was alleviated using the developed chemistry.

In another study by the same authors [247], LTC of biodiesel was simulated. LTC simulation was implemented under injection timing of −32 deg, −26 deg, and −22 deg TDC using biodiesel, mineral diesel, and two biodiesel blends. In particular, they expressed SME and palm methyl ester (PME) blends with mineral diesel introducing different surrogate fuel compositions. Table 11 shows the specific fraction of compositions for SEM20 and PME20 (v/v). The composition of surrogate fuels was assigned based on realistic biodiesel component portions to describe the detailed combustion phenomena. Figure 31 represents the simulated pressure and heat release rate for biodiesel blends compared

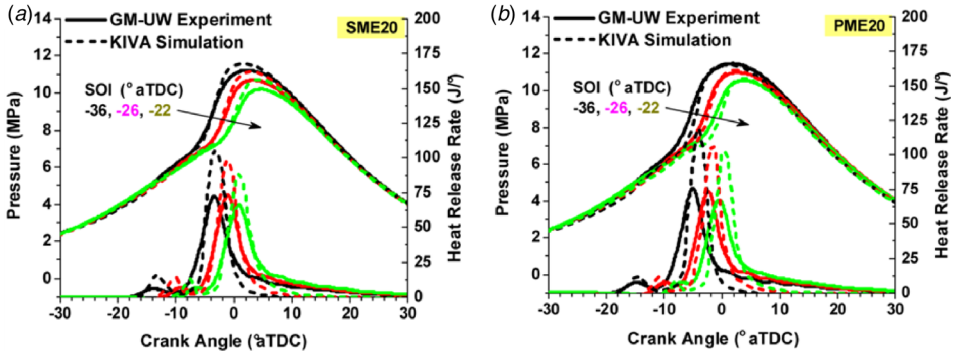

Fig. 31 Combustion pressure and heat release rate for (*a*) SME20 and (*b*) PME20 biodiesel blends [247]

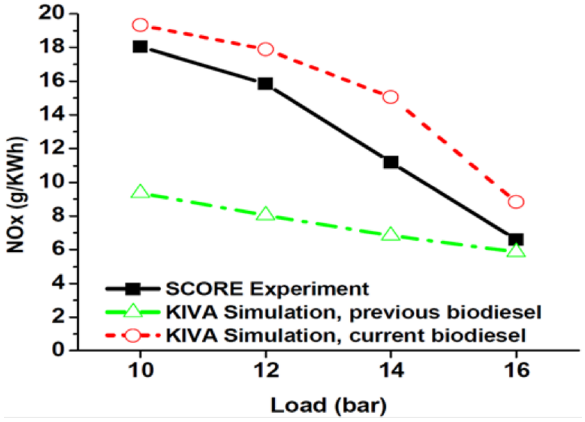

Fig. 32 Nitrogen oxides (NO_x) concentration for MB/*n*-heptane (green triangle) and MD/MD9D/n-heptane (red circle) mechanisms at various engine loads [247]

to experimental data. Although there are slight differences between simulations and experiments, the ignition timing and peak pressure values matched well for both fuels.

7.3.2 Modeling of Emissions Characteristics. Various emission models were developed to predict emissions using CI engine simulations. For NO_x modeling, reduced Gas Research Institute (GRI) NO_x model has been widely used [239]. This model contains four species and 9 or 12 steps to account for NO_x formation during the combustion process. Other emissions such as CO, CO_2, and unburned HCs are included in the reaction mechanism. For MB mechanism, the trends of CO and HC emissions were well predicted and compared to the experimental results. In the research by Um et al. [239], MB mechanism described CO and HC emission trends for various mixing ratios of biodiesel. However, NO_x emissions were not captured well as biodiesel content in the blended fuel increased. This result was also shown in the study of Brakora et al. [238,247]. MB mechanism (green triangle markers) exhibited large discrepancies between simulation and experimental results (Fig. 32). However, the MD/MD9D/n-heptane mechanism improved the predictions and further fine-tuning of the reaction constants enabled accurate prediction of exact NO_x concentrations in the exhaust.

Figures 33(*a*) and 33(*b*) show the comparative HC, CO, and NO_x emission results for SME20 and PME 20 using experiments as well as simulations. Numerical results matched well with experimental results and trends for varying injection timings. Since PME20 has higher cetane number than SME20, its earlier ignition and longer residence time at higher temperature led to higher NO_x emissions. Simulations also depicted this result [247].

Soot emission prediction is one of the important factor to model biodiesel combustion. However, reliable soot modeling for biodiesel still remains challenging. The theory of soot formation

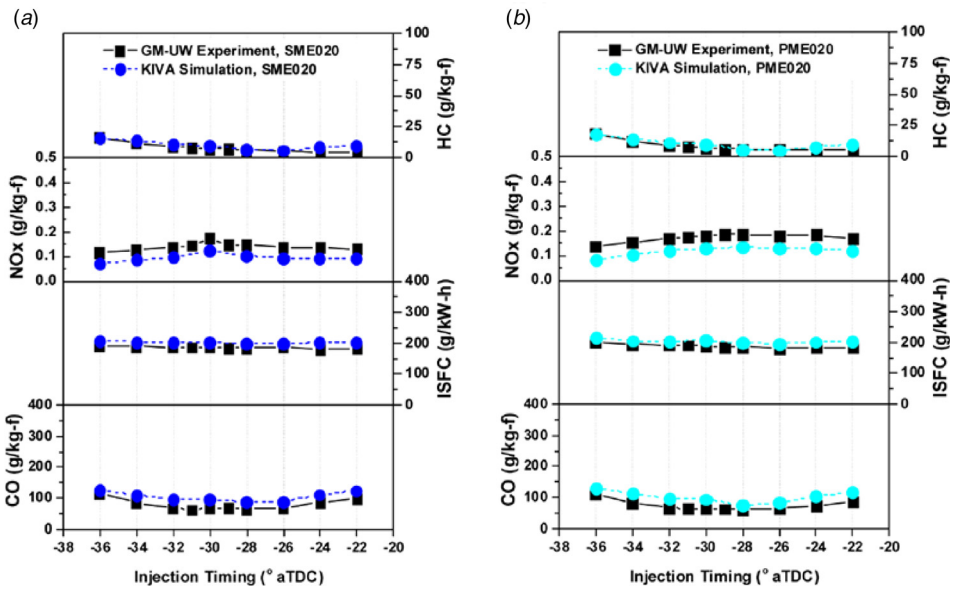

Fig. 33 Emissions concentration for (*a*) SME20 and (*b*) PME20 under LTC combustion conditions [247]

and oxidation of biodiesel is under investigation by numerous researchers and development of well accepted soot model for biodiesel still remains an elusive work, yet to be realized.

8 Conclusions

In this detailed review article, dependence of important biodiesel properties such as density, viscosity, surface tension, flash point, cetane number and heating values, and oxidation stability on chemical structure and feedstock is demonstrated.

Biodiesel density is usually higher than mineral diesel and depends on biodiesel's composition, purity, fatty acid content, molar mass, water content, and temperature. The density of blended fuels increases with increasing biodiesel blending ratios and decreasing temperatures. Viscosity of biodiesel is ~3.5–6.0 mm^2/s at 40 °C, which is higher than mineral diesel. Fuel viscosity affects both fuel spray characteristics and combustion of biodiesel. The viscosity of biodiesel decreases with increasing temperature. Surface tension of biodiesel is an important factor in the analysis of fuel spray, atomization and vaporization characteristics. The surface tension of mineral diesel and biodiesel are approximately 28.0 mN/m and 31.7 mN/m at 293 K, respectively. Higher biodiesel blends exhibit higher flash point temperature. Residual alcohol content in biodiesel significantly lowers the flash point temperature. Cloud and pour point of biodiesel is generally higher than mineral diesel. In cold weather conditions, one of the major concerns of biodiesel usage is its unfavorable cold-flow properties compared to mineral diesel. The freezing temperature of biodiesel is affected by structural properties of constituent chemical species such as chain length, degree of unsaturation, and branching.

In general, coefficient of friction involving biodiesels is significantly lower than mineral diesel, leading to lower friction and wear of fuel injection equipment components. Addition of as low as 1% biodiesel to ultralow-sulfur diesel compensates for the loss of lubrication properties due to reduction in fuel sulfur and meets the requirements set by EN590 standards. One of the major differences in chemical structure and composition between mineral diesel and biodiesel is the oxygen content of biodiesel. A significant advantage of biodiesels is that they have higher oxygen content (usually 11–12% w/w) in their molecular structure. As an indicator of ignition and combustion characteristics, the CN is related to the ignition delay and this property is dependent on composition and degree of unsaturation. Biodiesels have higher CN than mineral diesel and this tends to increase the peak combustion temperature. Relatively lower heating value of biodiesel tends to increase the brake-specific fuel consumption. When biodiesel is oxidized, fuel sediments have a tendency to form deposits on the injector and fuel pump components. In addition, changes in its properties due to oxidation cause an increase in acid value, fuel viscosity, and peroxide value, which deteriorates the fuel properties. Many investigated oxidation stability improving additives were found suitable for improving the shelf-storage life of biodiesels. A higher iodine value indicates that the biodiesel's feedstock oil is highly unsaturated and has a low cloud point. Higher iodine value values lead to shortened oxidative stability of the fuel.

Fuel spray and atomization characteristics are considerably affected by fuel properties as well as the injection conditions. Because of different fuel properties of biodiesel, spray behavior and spray breakup process are also different compared to mineral diesel. Higher density of biodiesel has an influence on the spray tip penetration and spray cone angle. Spray tip penetration of biodiesel is relatively longer and the spray cone angle is relatively narrower than mineral diesel. On the other hand, higher viscosity and surface tension of biodiesel leads to inferior atomization, leading to larger spray droplet size distribution. In addition, the exit flow velocity of biodiesel is relatively lower than mineral diesel in the near-field region.

Review of experimental investigations of biodiesel engine's performance parameters vis-à-vis mineral diesel shows that brake-specific fuel consumption generally increases with biodiesel addition to mineral diesel but BTE is not significantly affected by biodiesel blending. Biodiesel fueled engines exhibit relatively lower HC and CO emissions but NO_x emissions increase. Biodiesel usage leads to reduction in emission of aromatic and polyaromatic compounds. Some studies reported higher carbonyl emissions while others reported reduction in carbonyl emissions, hence the trend is not conclusive. Biodiesel fueled engines showed significant reduction in particulate mass as well as number emissions. Lower formaldehyde emissions and reduction in the toxicity potential of particulate bound PAHs were also observed in biodiesel blend fueled engines. Experimental investigations of combustion characteristics performed by in-cylinder pressure measurements and optical imaging indicated advanced start of injection timings and relatively earlier completion of combustion in the biodiesel fueled engines. Reduced concentration of soot particles in the exhaust is also observed because oxygen content of biodiesel helps in oxidation of particulates formed.

Recent studies on biodiesel combustion modeling show that physical and chemical models of atomization and combustion processes for biodiesel have improved significantly over time. It is now possible to model biodiesel engine performances and emissions by applying updated simulation-based physical properties and chemical mechanisms. In addition, skeletal mechanisms for biodiesel contribute in effectively calculating biodiesel combustion processes.

References

[1] Guo, Z., Guo, H., and Zeng, Q., 2018, "Investigation on Di-(2-Methoxypropyl) Carbonate Used as a Clean Oxygenated Fuel for Diesel Engine," ASME J. Energy Resour. Technol., **140**(1), p. 012201.

[2] Patil, V. V., and Patil, R. S., 2018, "Investigations on Partial Addition of n-Butanol in Sunflower Oil Methyl Ester Powered Diesel Engine," ASME J. Energy Resour. Technol., **140**(1), p. 012205.

[3] Mitchell, R. H., and Olsen, D. B., 2018, "Extending Substitution Limits of a Diesel–Natural Gas Dual Fuel Engine," ASME J. Energy Resour. Technol., **140**(5), p. 052202.

[4] Yadav, J., and Ramesh, A., 2018, "Comparison of Single and Multiple Injection Strategies in a Butanol Diesel Dual Fuel Engine," ASME J. Energy Resour. Technol., **140**(7), p. 072206.

[5] Buliński, Z., Szczygieł, I., Kabaj, A., Krysiński, T., Gładysz, P., Czarnowska, L., and Stanek, W., 2018, "Performance Analysis of the Small-Scale α-Type Stirling Engine Using Computational Fluid Dynamics Tools," ASME J. Energy Resour. Technol., **140**(3), p. 032001.

[6] Virsik, R., Rinderknecht, F., and Friedrich, H. E., 2018, "Free-Piston Linear Generator and the Development of a Solid Lubrication System," ASME J. Energy Resour. Technol., **140**(3), p. 032007.

[7] Abo-Elfadl, S., and Mohamed, A. A. E. S., 2018, "The Effect of the Helical Inlet Port Design and the Shrouded Inlet Valve Condition on Swirl Generation in Diesel Engine," ASME J. Energy Resour. Technol., **140**(3), p. 032203.

[8] Redtenbacher, C., Kiesling, C., Malin, M., Wimmer, A., Pastor, J. V., and Pinotti, M., 2017, "Potential and Limitations of Dual Fuel Operation of High Speed Large Engines," ASME J. Energy Resour. Technol., **140**(3), p. 032205.

[9] Carlanescu, R., Prisecaru, T., Prisecaru, M., and Soriga, I., 2018, "Swirl Injector for Premixed Combustion of Hydrogen–Methane Mixtures," ASME J. Energy Resour. Technol., **140**(7), p. 072002.

[10] Singh, A. P., Bajpai, N., and Agarwal, A. K., 2018, "Combustion Mode Switching Characteristics of a Medium-Duty Engine Operated in Compression Ignition/PCCI Combustion Modes," ASME J. Energy Resour. Technol., **140**(9), p. 092201.

[11] ASTM, 2012, "Standard Specification for Diesel Fuel Oils," American Society for Testing and Materials, West Conshohocken, PA, Standard No. ASTM D975-12a.

[12] ASTM, 2012, "Standard Specification for Biodiesel Fuel Blend Stock (B100) for Middle Distillate Fuels," American Society for Testing and Materials, West Conshohocken, PA, Standard No. ASTM D6751-15b.

[13] Tat, M. E., Van Gerpen, J. H., Soylu, S., Canakci, M., Monyem, A., and Wormley, S., 2000, "The Speed of Sound and Isentropic Bulk Modulus of Biodiesel at 21 °C from Atmospheric Pressure to 35 MPa," J. Am. Oil Chem. Soc., **77**(3), pp. 285–289.

[14] Martínez, G., Sánchez, N., Encinar, J. M., and González, J. F., 2014, "Fuel Properties of Biodiesel From Vegetable Oils and Oil Mixtures. Influence of Methyl Esters Distribution," Biomass Bioenergy, **63**, pp. 22–32.

[15] Giakoumis, E. G., 2013, "A Statistical Investigation of Biodiesel Physical and Chemical Properties, and Their Correlation With the Degree of Unsaturation," Renewable Energy, **50**, pp. 858–878.

[16] Meher, L. C., Kulkarni, M. G., Dalai, A. K., and Naik, S. N., 2006, "Transesterification of Karanja (Pongamia Pinnata) Oil by Solid Basic Catalysts," Eur. J. Lipid Sci. Technol.,**108**(5), pp. 389–397.
[17] Kumar, M. S., Ramesh, A., and Nagalingam, B., 2003, "An Experimental Comparison of Methods to Use Methanol and Jatropha Oil in a Compression Ignition Engine," Biomass Bioenergy, **25**(3), pp. 309–318.
[18] Pratas, M. J., Freitas, S. V., Oliveira, M. B., Monteiro, S. C., Lima, Á. S., and Coutinho, J. A., 2011, "Biodiesel Density: Experimental Measurements and Prediction Models," Energy Fuels, **25**(5), pp. 2333–2340.
[19] Baroutian, S., Aroua, M. K., Raman, A. A., and Sulaiman, N. M. N., 2008, "Density of Palm Oil-Based Methyl Ester," J. Chem. Eng. Data, **53**(3), pp. 877–880.
[20] Ivaniš, G. R., Radović, I. R., Veljković, V. B., and Kijevčanin, M. L., 2016, "Biodiesel Density and Derived Thermodynamic Properties at High Pressures and Moderate Temperatures," Fuel, **165**, pp. 244–251.
[21] Barabás, I., 2013, "Predicting the Temperature Dependent Density of Biodiesel–Diesel–Bioethanol Blends," Fuel, **109**, pp. 563–574.
[22] Prieto, N. M., Ferreira, A. G., Portugal, A. T., Moreira, R. J., and Santos, J. B., 2015, "Correlation and Prediction of Biodiesel Density for Extended Ranges of Temperature and Pressure," Fuel, **141**, pp. 23–38.
[23] Ramírez-Verduzco, L. F., García-Flores, B. E., Rodríguez-Rodríguez, J. E., and del Rayo Jaramillo-Jacob, A., 2011, "Prediction of the Density and Viscosity in Biodiesel Blends at Various Temperatures," Fuel, **90**(5), pp. 1751–1761.
[24] Ramírez Verduzco, L. F., 2013, "Density and Viscosity of Biodiesel as a Function of Temperature: Empirical Models," Renewable Sustainable Energy Rev., **19**, pp. 652–665.
[25] Yoon, S. H., Park, S. H., and Lee, C. S., 2007, "Experimental Investigation on the Fuel Properties of Biodiesel and Its Blends at Various Temperatures," Energy Fuels, **22**(1), pp. 652–656.
[26] Tate, R. E., Watts, K. C., Allen, C. A. W., and Wilkie, K. I., 2006, "The Densities of Three Biodiesel Fuels at Temperatures Up to 300 C," Fuel, **85**(7–8), pp. 1004–1009.
[27] Agarwal, A. K., Dhar, A., Gupta, J. G., Kim, W. I., Lee, C. S., and Park, S., 2014, "Effect of Fuel Injection Pressure and Injection Timing on Spray Characteristics and Particulate Size–Number Distribution in a Biodiesel Fuelled Common Rail Direct Injection Diesel Engine," Appl. Energy, **130**, pp. 212–221.
[28] Freitas, S. V., Segovia, J. J., Martín, M. C., Zambrano, J., Oliveira, M. B., Lima, Á. S., and Coutinho, J. A., 2014, "Measurement and Prediction of High-Pressure Viscosities of Biodiesel Fuels," Fuel, **122**, pp. 223–228.
[29] Shahabuddin, M., Kalam, M. A., Masjuki, H. H., Bhuiya, M. M. K., and Mofijur, M., 2012, "An Experimental investigation Into biodiesel Stability by Means of Oxidation and Property Determination," Energy, **44**(1), pp. 616–622.
[30] Ramírez-Verduzco, L. F., Rodríguez-Rodríguez, J. E., and del Rayo Jaramillo-Jacob, A., 2012, "Predicting Cetane Number, Kinematic Viscosity, Density and Higher Heating Value of Biodiesel From Its Fatty Acid Methyl Ester Composition," Fuel, **91**(1), pp. 102–111.
[31] Knothe, G., 2008, "Designer" Biodiesel: Optimizing Fatty Ester Composition to Improve Fuel Properties," Energy Fuels, **22**(2), pp. 1358–1364.
[32] Saiban, S., and Brown, T. C., 1997, "Kinetic Model for Cloud-Point Blending of Diesel Fuels," Fuel, **76**(14–15), pp. 1417–1423.
[33] Knothe, G., and Steidley, K. R., 2005, "Kinematic Viscosity of Biodiesel Fuel Components and Related Compounds. Influence of Compound Structure and Comparison to Petrodiesel Fuel Components," Fuel, **84**(9), pp. 1059–1065.
[34] Ejim, C. E., Fleck, B. A., and Amirfazli, A., 2007, "Analytical Study for Atomization of Biodiesels and Their Blends in a Typical Injector: Surface Tension and Viscosity Effects," Fuel, **86**(10–11), pp. 1534–1544.
[35] Ahmed, M. A., Ejim, C. E., Fleck, B. A., and Amirfazli, A., 2006, "Effect of Biodiesel Fuel Properties and Its Blends on Atomization," SAE Technical Paper No. 2006-01-0893.
[36] Shu, Q., Wang, J., Peng, B., Wang, D., and Wang, G., 2008, "Predicting the Surface Tension of Biodiesel Fuels by a Mixture Topological Index Method, at 313 K," Fuel, **87**(17–18), pp. 3586–3590.
[37] Pratas, M. J., Freitas, S., Oliveira, M. B., Monteiro, S. C., Lima, A. S., and Coutinho, J. A., 2010, "Densities and Viscosities of Fatty Acid Methyl and Ethyl Esters," J. Chem. Eng. Data, **55**(9), pp. 3983–3990.
[38] Davanlou, A., Lee, J. D., Basu, S., and Kumar, R., 2015, "Effect of Viscosity and Surface Tension on Breakup and Coalescence of Bicomponent Sprays," Chem. Eng. Sci., **131**, pp. 243–255.
[39] Phankosol, S., Sudaprasert, K., Lilitchan, S., Aryusuk, K., and Krisnangkura, K., 2014, "Estimation of Surface Tension of Fatty Acid Methyl Ester and Biodiesel at Different Temperatures," Fuel, **126**, pp. 162–168.
[40] Freitas, S. V., Oliveira, M. B., Queimada, A. J., Pratas, M. J., Lima, Á. S., and Coutinho, J. A., 2011, "Measurement and Prediction of Biodiesel Surface Tensions," Energy Fuels, **25**(10), pp. 4811–4817.
[41] Srivastava, A., and Prasad, R., 2000, "Triglycerides-Based Diesel Fuels," Renewable Sustainable Energy Rev., **4**(2), pp. 111–133.
[42] Soriano, N. U., Jr, Migo, V. P., and Matsumura, M., 2006, "Ozonized Vegetable Oil as Pour Point Depressant for Neat Biodiesel," Fuel, **85**(1), pp. 25–31.
[43] Boog, J. H. F., Silveira, E. L. C., De Caland, L. B., and Tubino, M., 2011, "Determining the Residual Alcohol in Biodiesel Through Its Flash Point," Fuel, **90**(2), pp. 905–907.
[44] Graboski, M. S., and McCormick, R. L., 1998, "Combustion of Fat and Vegetable Oil Derived Fuels in Diesel Engines," Prog. Energy Combust. Sci., **24**(2), pp. 125–164.
[45] Mejía, J. D., Salgado, N., and Orrego, C. E., 2013, "Effect of Blends of Diesel and Palm-Castor Biodiesels on Viscosity, Cloud Point and Flash Point," Ind. Crops Prod., **43**, pp. 791–797.
[46] Sarin, A., Arora, R., Singh, N. P., Sarin, R., Malhotra, R. K., and Kundu, K., 2009, "Effect of Blends of Palm-Jatropha-Pongamia Biodiesels on Cloud Point and Pour Point," Energy, **34**(11), pp. 2016–2021.
[47] Agarwal, A. K., 2007, "Biofuels (Alcohols and Biodiesel) Applications as Fuels for Internal Combustion Engines," Prog. Energy Combust. Sci., **33**(3), pp. 233–271.
[48] Guo, Y., Wei, H., Yang, F., Li, D., Fang, W., and Lin, R., 2009, "Study on Volatility and Flash Point of the Pseudo-Binary Mixtures of Sunflowerseed-Based Biodiesel+ Ethanol," J. Hazardous Mater., **167**(1–3), pp. 625–629.
[49] Alptekin, E., and Canakci, M., 2008, "Determination of the Density and the Viscosities of Biodiesel–Diesel Fuel Blends," Renewable Energy, **33**(12), pp. 2623–2630.
[50] Rashed, M. M., Kalam, M. A., Masjuki, H. H., Mofijur, M., Rasul, M. G., and Zulkifli, N. W. M., 2016, "Performance and Emission Characteristics of a Diesel Engine Fueled With Palm, Jatropha, and Moringa Oil Methyl Ester," Ind. Crops Products, **79**, pp. 70–76.
[51] Tiwari, A. K., Kumar, A., and Raheman, H., 2007, "Biodiesel Production From Jatropha Oil (Jatropha Curcas) With High Free Fatty Acids: An Optimized Process," Biomass Bioenergy, **31**(8), pp. 569–575.
[52] Agarwal, A. K., and Dhar, A., 2013, "Experimental Investigations of Performance, Emission and Combustion Characteristics of Karanja Oil Blends Fuelled DICI Engine," Renewable Energy, **52**, pp. 283–291.
[53] Lee, C. S., Park, S. W., and Kwon, S. I., 2005, "An Experimental Study on the Atomization and Combustion Characteristics of Biodiesel-Blended Fuels," Energy Fuels, **19**(5), pp. 2201–2208.
[54] Mosarof, M. H., Kalam, M. A., Masjuki, H. H., Alabdulkarem, A., Habibullah, M., Arslan, A., and Monirul, I. M., 2016, "Assessment of Friction and Wear Characteristics of Calophyllum Inophyllum and Palm Biodiesel," Ind. Crops Prod., **83**, pp. 470–483.
[55] Tomic, M., Savin, L., Micic, R., Simikic, M., and Furman, T., 2014, "Possibility of Using Biodiesel From Sunflower Oil as an Additive for the Improvement of Lubrication Properties of Low-Sulfur Diesel Fuel," Energy, **65**, pp. 101–108.
[56] Knothe, G., and Steidley, K. R., 2005, "Lubricity of Components of Biodiesel and Petrodiesel. The Origin of Biodiesel Lubricity," Energ. Fuel., **19**(3), pp. 1192–1200.
[57] Kinast, J. A., 2003, "Production of Biodiesels From Multiple Feedstocks and Properties of Biodiesels and Biodiesel/Diesel Blends: Final Report; Report 1 in a Series of 6," National Renewable Energy Lab., Golden, CO, Report No. NREL/SR-510-31460.
[58] Reddy, M. S., Sharma, N., and Agarwal, A. K., 2016, "Effect of Straight Vegetable Oil Blends and Biodiesel Blends on Wear of Mechanical Fuel Injection Equipment of a Constant Speed Diesel Engine," Renewable Energy, **99**, pp. 1008–1018.
[59] Cook, S., Barker, J., Reid, J., and Richards, P., 2012, "Possible Mechanism for Poor Diesel Fuel Lubricity in the Field," SAE Int. J. Fuels Lubr., **5**(2), pp. 711–720.
[60] Graboski, M. S., McCormick, R. L., Alleman, T. L., and Herring, A. M., 2003, "The Effect of Biodiesel Composition on Engine Emissions From a DDC Series 60 Diesel Engine," National Renewable Energy Laboratory, Golden, CO, Final Report No. NREL/SR-510-31461.
[61] Bechtold, R. L., 2002, *Alternative Fuels: Transportation Fuels for Today and Tomorrow*, SAE International, Warrendale, USA., pp. 63–73.
[62] Knothe, G., Matheaus, A. C., and Ryan, T. W., III, 2003, "Cetane Numbers of Branched and Straight-Chain Fatty Esters Determined in an Ignition Quality Tester," Fuel, **82**(8), pp. 971–975.
[63] Gülüm, M., and Bilgin, A., 2015, "Density, Flash Point and Heating Value Variations of Corn Oil Biodiesel–Diesel Fuel Blends," Fuel Process. Technol., **134**, pp. 456–464.
[64] Lapuerta, M., Armas, O., and Rodriguez-Fernandez, J., 2008, "Effect of Biodiesel Fuels on Diesel Engine Emissions," Prog. Energy Combust. Sci., **34**(2), pp. 198–223.
[65] Lopes, S. M., Furey, R., and Geng, P., 2013, "Calculation of Heating Value for Diesel Fuels Containing Biodiesel," SAE Int. J. Fuels Lubr., **6**(2), pp. 407–418.
[66] Shehata, M. S., Attia, A. M., and Razek, S. A., 2015, "Corn and Soybean Biodiesel Blends as Alternative Fuels for Diesel Engine at Different Injection Pressures," Fuel, **161**, pp. 49–58.
[67] Rathore, V., Tyagi, S., Newalkar, B., and Badoni, R. P., 2015, "Jatropha and Karanja Oil Derived DMC–Biodiesel Synthesis: A Kinetics Study," Fuel, **140**, pp. 597–608.
[68] Ali, O. M., Mamat, R., Abdullah, N. R., and Abdullah, A. A., 2016, "Analysis of Blended Fuel Properties and Engine Performance With Palm Biodiesel–Diesel Blended Fuel," Renewable Energy, **86**, pp. 59–67.
[69] Merlin, A. Z., Marcel, O. A., Louis Max, A. O., Salem, C., and Jean, G., 2015, "Development and Experimental Investigation of a Biodiesel From a Nonedible Woody Plant: The Neem," Renewable Sustainable Energy Rev., **52**, pp. 201–208.
[70] Agarwal, A. K., Dhar, A., Gupta, J. G., Kim, W. I., Choi, K., Lee, C. S., and Park, S., 2015, "Effect of Fuel Injection Pressure and Injection Timing of Karanja Biodiesel Blends on Fuel Spray, Engine Performance, Emissions and Combustion Characteristics," Energy Convers. Manage., **91**, pp. 302–314.
[71] Goodrum, J. W., and Geller, D. P., 2005, "Influence of Fatty Acid Methyl Esters From Hydroxylated Vegetable Oils on Diesel Fuel Lubricity," Bioresour. Technol., **96**(7), pp. 851–855.

[72] Patel, C., Lee, S., Tiwari, N., Agarwal, A. K., Lee, C. S., and Park, S., 2016, "Spray Characterization, Combustion, Noise and Vibrations Investigations of Jatropha Biodiesel Fuelled Genset Engine," Fuel, **185**, pp. 410–420.
[73] Koo, J. Y., and Martin, J. K., 1990, "Droplet Sizes and Velocities in a Transient Diesel Fuel Spray," SAE Trans., **99**(3), pp. 929–947.
[74] Jiotode, Y., and Agarwal, A. K., 2016, "In-Cylinder Combustion Visualization of Jatropha Straight Vegetable Oil and Mineral Diesel Using High Temperature Industrial Endoscopy for Spatial Temperature and Soot Distribution," Fuel Process. Technol., **153**, pp. 9–18.
[75] Gopinath, A., Puhan, S., and Nagarajan, G., 2009, "Theoretical Modeling of Iodine Value and Saponification Value of Biodiesel Fuels From Their Fatty Acid Composition," Renewable Energy, **34**(7), pp. 1806–1811.
[76] Benjumea, P., Agudelo, J., and Agudelo, A., 2008, "Basic Properties of Palm Oil Biodiesel–Diesel Blends," Fuel, **87**(10–11), pp. 2069–2075.
[77] Patel, C., Agarwal, A. K., Tiwari, N., Lee, S., Lee, C. S., and Park, S., 2016, "Combustion, Noise, Vibrations and Spray Characterization for Karanja Biodiesel Fuelled Engine," Appl. Therm. Eng., **106**, pp. 506–517.
[78] Guido, C., Beatrice, C., D., Iorio, S., Napolitano, P., Di, Blasio, G., Vassallo, A., and Ciaravino, C., 2011, "Assessment of Closed-Loop Combustion Control Capability for Biodiesel Blending Detection and Combustion Impact Mitigation for an Euro5 Automotive Diesel Engine," SAE Paper No. 2011-01-1193.
[79] Knothe, G., 2009, "Improving Biodiesel Fuel Properties by Modifying Fatty Ester Composition," Energy Environ. Sci., **2**(7), pp. 759–766.
[80] Zuleta, E. C., Baena, L., Rios, L. A., and Calderón, J. A., 2012, "The Oxidative Stability of Biodiesel and Its Impact on the Deterioration of Metallic and Polymeric Materials: A Review," J. Braz. Chem. Soc., **23**(12), pp. 2159–2175.
[81] Agarwal, A. K., and Khurana, D., 2013, "Long-Term Storage Oxidation Stability of Karanja Biodiesel With the Use of Antioxidants," Fuel Process. Technol., **106**, pp. 447–452.
[82] Marčič, M., 1999, "A New Method for Measuring Fuel-Injection Rate," Flow Meas. Instrum., **10**(3), pp. 159–165.
[83] Moser, B. R., 2016, "Fuel Property Enhancement of Biodiesel Fuels From Common and Alternative Feedstocks Via Complementary Blending," Renewable Energy, **85**, pp. 819–825.
[84] Zhao, H., 2009, *Advanced Direct Injection Combustion Engine Technologies and Development: Diesel Engines*, Vol. 2, Elsevier, Cambridge, UK.
[85] Park, S. H., Kim, H. J., Suh, H. K., and Lee, C. S., 2009, "A Study on the Fuel Injection and Atomization Characteristics of Soybean Oil Methyl Ester (SME)," Int. J. Heat Fluid Flow, **30**(1), pp. 108–116.
[86] Marčič, M., 2002, "Deformational Injection Rate Measuring Method," Rev. Sci. Instrum., **73**(9), pp. 3373–3377.
[87] Postrioti, L., Mariani, F., and Battistoni, M., 2012, "Experimental and Numerical Momentum Flux Evaluation of High Pressure Diesel Spray," Fuel, **98**, pp. 149–163.
[88] Arcoumanis, C., Baniasad, M. S., and Banias, M. S., 1993, "Analysis of Consecutive Fuel Injection Rate Signals Obtained by the Zeuch and Bosch Methods," SAE Trans., **102**(3), pp. 1371–1384.
[89] Tinprabath, P., Hespel, C., Chanchaona, S., and Foucher, F., 2015, "Influence of Biodiesel and Diesel Fuel Blends on the Injection Rate Under Cold Conditions," Fuel, **144**, pp. 80–89.
[90] Moon, S., Tsujimura, T., Gao, Y., Park, S., Wang, J., Kurimoto, N., Nishijima, Y., and Oguma, M., 2014, "Biodiesel Effects on Transient Needle Motion and Near-Exit Flow Characteristics of a High-Pressure Diesel Injector," Int. J. Engine Res., **15**(4), pp. 504–518.
[91] Doudou, A., and Maslouhi, A., 2007, "A Macro-Microscopic Investigation of High-Pressure Sprays Injected by a Common Rail System," J. Mech. Sci. Technol., **21**(8), pp. 1284–1292.
[92] Pickett, L. M., Kook, S., and Williams, T. C., 2009, "Visualization of Diesel Spray Penetration, Cool-Flame, Ignition, High-Temperature Combustion, and Soot Formation Using High-Speed Imaging," SAE Int. J. Engines, **2**(1), pp. 439–459.
[93] Genzale, C. L., Pickett, L. M., and Kook, S., 2010, "Liquid Penetration of Diesel and Biodiesel Sprays at Late-Cycle Post-Injection Conditions," SAE Int. J. Engines, **3**(1), pp. 479–495.
[94] Kostas, J., Honnery, D., Soria, J., Kastengren, A., Liu, Z., Powell, C. F., and Wang, J., 2009, "Effect of Nozzle Transients and Compressibility on the Penetration of Fuel Sprays," Appl. Phys. Lett., **95**(2), p. 024101.
[95] Agarwal, A. K., Som, S., Shukla, P. C., Goyal, H., and Longman, D., 2015, "In-Nozzle Flow and Spray Characteristics for Mineral Diesel, Karanja, and Jatropha Biodiesels," Appl. Energy, **156**, pp. 138–148.
[96] Chong, C. T., and Hochgreb, S., 2015, "Spray and Combustion Characteristics of Biodiesel: Non-Reacting and Reacting," Int. Biodeterior. Biodegrad., **102**, pp. 353–360.
[97] Mohan, B., Yang, W., Tay, K. L., and Yu, W., 2014, "Experimental Study of Spray Characteristics of Biodiesel Derived From Waste Cooking Oil," Energy Convers. Manage., **88**, pp. 622–632.
[98] Kuti, O. A., Nishida, K., and Zhu, J., 2013, "Experimental Studies on Spray and Gas Entrainment Characteristics of Biodiesel Fuel: Implications of Gas Entrained and Fuel Oxygen Content on Soot Formation," Energy, **57**, pp. 434–442.
[99] Liu, H., Huo, M., Liu, Y., Wang, X., Wang, H., Yao, M., and Chia-fon, F. L., 2014, "Time-Resolved Spray, Flame, Soot Quantitative Measurement Fueling n-Butanol and Soybean Biodiesel in a Constant Volume Chamber Under Various Ambient Temperatures," Fuel, **133**, pp. 317–325.
[100] Hong, C. H., Choi, W., Choi, B., and Lee, G., 2003, "Characteristics of High Pressure Bio-Diesel Fuel Spray," Trans. KSAE, **11**(2), pp. 56–62.
[101] Tinprabath, P., Hespel, C., Chanchaona, S., and Foucher, F., 2016, "Impact of Cold Conditions on Diesel Injection Processes of Biodiesel Blends," Renewable Energy, **96**, pp. 270–280.
[102] Mo, J., Tang, C., Li, J., Guan, L., and Huang, Z., 2016, "Experimental Investigation on the Effect of n-Butanol Blending on Spray Characteristics of Soybean Biodiesel in a Common-Rail Fuel Injection System," Fuel, **182**, pp. 391–401.
[103] Bayvel, L. P., 1993, *Liquid Atomization*, Taylor & Francis, Washington, DC.
[104] Park, S. H., Kim, H. J., Suh, H. K., and Lee, C. S., 2009, "Experimental and Numerical Analysis of Spray-[Atomization Characteristics of Biodiesel Fuel in Various Fuel and Ambient Temperatures Conditions," Int. J. Heat Fluid Flow, **30**(5), pp. 960–970.
[105] Manin, J., Bardi, M., Pickett, L. M., Dahms, R. N., and Oefelein, J. C., 2014, "Microscopic Investigation of the Atomization and Mixing Processes of Diesel Sprays Injected Into High Pressure and Temperature Environments," Fuel, **134**, pp. 531–543.
[106] Anantharaman, G., Krishnamurthy, S., and Ramalingam, V., 2013, "A Review on Combustion, Performance, and Emission Characteristics of Fuels Derived From Oil Seed Crops (Biodiesels)," Aust. J. Crop Sci., **7**(9), pp. 1350–1354.
[107] Tesfa, B., Mishra, R., Zhang, C., Gu, F., and Ball, A. D., 2013, "Combustion and Performance Characteristics of CI (Compression Ignition) Engine Running With Biodiesel," Energy, **51**, pp. 101–115.
[108] Gopal, K. N., Pal, A., Sharma, S., Samanchi, C., Sathyanarayanan, K., and Elango, T., 2014, "Investigation of Emissions and Combustion Characteristics of a CI Engine Fueled With Waste Cooking Oil Methyl Ester and Diesel Blends," Alexandria Eng. J., **53**(2), pp. 281–287.
[109] Gopal, K. N., and Karupparaj, R. T., 2014, "Effect of Pongamia Biodiesel on Emission and Combustion Characteristics of DI Compression Ignition Engine," Ain Shams Eng. J., **6**(1), pp. 297–305.
[110] Lin, B. F., Huang, J. H., and Huang, D. Y., 2009, "Experimental Study of the Effects of Vegetable Oil Methyl Ester on DI Diesel Engine Performance Characteristics and Pollutant Emissions," Fuel, **88**(9), pp. 1779–1785.
[111] Lahane, S., and Subramanian, K. A., 2015, "Effect of Different Percentages of Biodiesel–Diesel Blends on Injection, Spray, Combustion, Performance, and Emission Characteristics of a Diesel Engine," Fuel, **139**, pp. 537–545.
[112] Sinha, S., and Agarwal, A. K., 2007, "Experimental Investigation of the Combustion Characteristics of a Biodiesel (Rice-Bran Oil Methyl Ester)-Fuelled Direct-Injection Transportation Diesel Engine," Proc. Inst. Mech. Eng., Part D, **221**(8), pp. 921–932.
[113] Agarwal, A. K., Agarwal, A., and Singh, A. P., 2015, "Time Resolved in-Situ Biodiesel Combustion Visualization Using Engine Endoscopy," Measurement, **69**, pp. 236–249.
[114] Agarwal, A. K., Singh, A. P., Agarwal, A., Jeon, J., Lee, C. S., and Park, S., 2016, "Spatial Combustion Analysis of Biodiesel Fueled Engine Using Combustion Chamber Endoscopy and Modelling," Renewable Energy, **98**, pp. 292–303.
[115] Yoon, S. K., Kim, M. S., Kim, H. J., and Choi, N. J., 2014, "Effects of Canola Oil Biodiesel Fuel Blends on Combustion, Performance, and Emissions Reduction in a Common Rail Diesel Engine," Energies, **7**(12), pp. 8132–8149.
[116] Sathiyagnanam, A. P., and Saravanan, C. G., 2011, "Experimental Studies on the Combustion Characteristics and Performance of a Direct Injection Engine Fueled With Biodiesel/Diesel Blends With SCR," World Congress on Engineering (WCE), July 6–8, London, pp. 1–6.
[117] Labeckas, G., Slavinskas, S., and Mažeika, M., 2014, "The Effect of Ethanol–Diesel–Biodiesel Blends on Combustion, Performance and Emissions of a Direct Injection Diesel Engine," Energy Convers. Manage., **79**, pp. 698–720.
[118] How, H. G., Masjuki, H. H., Kalam, M. A., and Teoh, Y. H., 2014, "Engine Performance, Emission and Combustion Characteristics of a Common-Rail Diesel Engine Fuelled With Bioethanol as a Fuel Additive in Coconut Oil Biodiesel Blends," Energy Procedia, **61**, pp. 1655–1659.
[119] Dhar, A., and Agarwal, A. K., 2015, "Experimental Investigations of the Effect of Pilot Injection on Performance, Emissions and Combustion Characteristics of Karanja Biodiesel Fuelled CRDI Engine," Energy Convers. Manage., **93**, pp. 357–366.
[120] Nalgundwar, A., Paul, B., and Sharma, S. K., 2016, "Comparison of Performance and Emissions Characteristics of DI CI Engine Fueled With Dual Biodiesel Blends of Palm and Jatropha," Fuel, **173**, pp. 172–179.
[121] Liaquat, A. M., Masjuki, H. H., Kalam, M. A., Fattah, I. R., Hazrat, M. A., Varman, M., Mofijur, M., and Shahabuddin, M., 2013, "Effect of Coconut Biodiesel Blended Fuels on Engine Performance and Emission Characteristics," Procedia Eng., **56**, pp. 583–590.
[122] Rajaraman, S., Yashwanth, G. K., Rajan, T., Kumaran, R. T., and Raghu, P., 2009, "Experimental Investigations of Performance and Characteristics Emission Characteristics of Moringa Oil Methyl Ester and Its Diesel Blends in a Single Cylinder Direct Injection Diesel Engine," ASME Paper No. IMECE2009-11265.
[123] Mofijur, M., Masjuki, H. H., Kalam, M. A., Atabani, A. E., Arbab, M. I., Cheng, S. F., and Gouk, S. W., 2014, "Properties and Use of Moringa Oleifera Biodiesel and Diesel Fuel Blends in a Multi-Cylinder Diesel Engine," Energy Convers. Manage., **82**, pp. 169–176.
[124] Rahman, M. M., Hassan, M. H., Kalam, M. A., Atabani, A. E., Memon, L. A., and Rahman, S. A., 2014, "Performance and Emission Analysis of Jatropha Curcas and Moringa Oleifera Methyl Ester Fuel Blends in a Multi-Cylinder Diesel Engine," J. Cleaner Prod., **65**, pp. 304–310.

[125] Mofijur, M., Masjuki, H. H., Kalam, M. A., Atabani, A. E., Fattah, I. R., and Mobarak, H. M., 2014, "Comparative Evaluation of Performance and Emission Characteristics of Moringa Oleifera and Palm Oil Based Biodiesel in a Diesel Engine," Ind. Crops Prod., **53**, pp. 78–84.
[126] Al Dawody, M. F., and Bhatti, S. K., 2014, "Experimental and Computational Investigations for Combustion, Performance and Emission Parameters of a Diesel Engine Fueled With Soybean Biodiesel-Diesel Blends," Energy Procedia, **52**, pp. 421–430.
[127] Gautam, A., and Agarwal, A. K., 2013, "Experimental Investigations of Comparative Performance, Emission and Combustion Characteristics of a Cottonseed Biodiesel-Fueled Four-Stroke Locomotive Diesel Engine," Int. J. Engine Res., **14**(4), pp. 354–372.
[128] Dhar, A., and Agarwal, A. K., 2014, "Performance, Emissions and Combustion Characteristics of Karanja Biodiesel in a Transportation Engine," Fuel, **119**, pp. 70–80.
[129] Tüccar, G., Tosun, E., Özgür, T., and Aydın, K., 2014, "Diesel Engine Emissions and Performance From Blends of Citrus Sinensis Biodiesel and Diesel Fuel," Fuel, **132**, pp. 7–11.
[130] Azad, A. K., Rasul, M. G., Khan, M. M. K., Sharma, S. C., and Islam, R., 2015, "Prospect of Moringa Seed [Oil as a Sustainable Biodiesel Fuel in Australia: A Review," Procedia Eng., **105**, pp. 601–606.
[131] Tüccar, G., Özgür, T., and Aydın, K., 2014, "Effect of Diesel–Microalgae Biodiesel–Butanol Blends on Performance and Emissions of Diesel Engine," Fuel, **132**, pp. 47–52.
[132] Imdadul, H. K., Masjuki, H. H., Kalam, M. A., Zulkifli, N. W. M., Alabdulkarem, A., Rashed, M. M., Teoh, Y. H., and How, H. G., 2016, "Higher Alcohol–Biodiesel–Diesel Blends: An Approach for Improving the Performance, Emission, and Combustion of a Light-Duty Diesel Engine," Energy Convers. Manage., **111**, pp. 174–185.
[133] Prabu, A., 2018, "Engine Characteristic Studies by Application of Antioxidants and Nanoparticles as Additives in Biodiesel Diesel Blends," ASME J. Energy Resour. Technol., **140**(8), p. 082203.
[134] Wood, B. M., Kirwan, K., Maggs, S., Meredith, J., and Coles, S. R., 2015, "Study of Combustion Performance of Biodiesel for Potential Application in Motorsport," J. Cleaner Prod., **93**, pp. 167–173.
[135] Dhar, A., Kevin, R., and Agarwal, A. K., 2012, "Production of Biodiesel From High-FFA Neem Oil and Its Performance, Emission and Combustion Characterization in a Single Cylinder DICI Engine," Fuel Process. Technol., **97**, pp. 118–129.
[136] Paul, G., Datta, A., and Mandal, B. K., 2014, "An Experimental and Numerical Investigation of the Performance, Combustion and Emission Characteristics of a Diesel Engine Fueled With Jatropha Biodiesel," Energy Procedia, **54**, pp. 455–467.
[137] Prakash, R., Singh, R. K., and Murugan, S., 2015, "Experimental Studies on Combustion, Performance and Emission Characteristics of Diesel Engine Using Different Biodiesel Bio Oil Emulsions," J. Energy Inst., **88**(1), pp. 64–75.
[138] Roy, M. M., Wang, W., and Alawi, M., 2014, "Performance and Emissions of a Diesel Engine Fueled by Biodiesel–Diesel, Biodiesel–Diesel-Additive and Kerosene–Biodiesel Blends," Energy Convers. Manage., **84**, pp. 164–173.
[139] Can, Ö., 2014, "Combustion Characteristics, Performance and Exhaust Emissions of a Diesel Engine Fueled With a Waste Cooking Oil Biodiesel Mixture," Energy Convers. Manage., **87**, pp. 676–686.
[140] Yilmaz, N., 2012, "Comparative Analysis of Biodiesel–Ethanol–Diesel and Biodiesel–Methanol–Diesel Blends in a Diesel Engine," Energy, **40**(1), pp. 210–213.
[141] Yasin, M. H. M., Mamat, R., Yusop, A. F., Aziz, A., and Najafi, G., 2015, "Comparative Study on Biodiesel-Methanol-Diesel Low Proportion Blends Operating With a Diesel Engine," Energy Procedia, **75**, pp. 10–16.
[142] Yilmaz, N., Vigil, F. M., Benalil, K., Davis, S. M., and Calva, A., 2014, "Effect of Biodiesel–Butanol Fuel Blends on Emissions and Performance Characteristics of a Diesel Engine," Fuel, **135**, pp. 46–50.
[143] Balamurugan, T., and Nalini, R., 2014, "Effect of Blending Alcohol With Diesel on Performance, Combustion and Emission Characteristics of Four Stroke Diesel Engine-an Experimental Study," Int. J. ChemTech Res., **6**(1), pp. 750–762.
[144] Fang, Q., Fang, J., Zhuang, J., and Huang, Z., 2013, "Effects of Ethanol–Diesel–Biodiesel Blends on Combustion and Emissions in Premixed Low Temperature Combustion," Appl. Therm. Eng., **54**(2), pp. 541–548.
[145] Zhang, Z.-H., and Balasubramanian, R., 2014, "Influence of Butanol Addition to Diesel–Biodiesel Blend on Engine Performance and Particulate Emissions of a Stationary Diesel Engine," Appl. Energy, **119**, pp. 530–536.
[146] Nayak, S. K., and Pattanaik, B. P., 2014, "Experimental Investigation on Performance and Emission Characteristics of a Diesel Engine Fuelled With Mahua Biodiesel Using Additive," Energy Procedia, **54**, pp. 569–579.
[147] Can, Ö., Öztürk, E., Solmaz, H., Aksoy, F., Çinar, C., and Yücesu, H. S., 2016, "Combined Effects of Soybean Biodiesel Fuel Addition and EGR Application on the Combustion and Exhaust Emissions in a Diesel Engine," Appl. Therm. Eng., **95**, pp. 115–124.
[148] O., Mofijur, M., Rasul, M. G., and Hyde, J., 2015, "Recent Developments on Internal Combustion Engine Performance and Emissions Fuelled With Biodiesel-Diesel-Ethanol Blends," Procedia Eng., **105**, pp. 658–664.
[149] Singh, A. P., and Agarwal, A. K., 2018, "Evaluation of Fuel Injection Strategies for Biodiesel-Fueled CRDI Engine Development and Particulate Studies," ASME J. Energy Resour. Technol., **140**(10), p. 102201.
[150] Kittelson, D. B., 1998, "Engines and Nanoparticles: A Review," J. Aerosol. Sci., **29**(5–6), pp. 575–588.
[151] Dusek, U., and Amann, M., 2000, "Secondary Organic Aerosol–Formation Mechanisms and Source Contributions in Europe," International Institute for Applied Systems Analysis, Laxenburg, Austria, Report No. IR-00-066.
[152] Kawano, D., Ishii, H., Goto, Y., Noda, A., and Aoyagi, Y., 2006, "Application of Biodiesel Fuel to Modern Diesel Engine," SAE Technical Paper No. 2006-01-0233.
[153] Hare, C. T., Springer, K. J., and Bradow, R. L., 1976, "Fuel and Additive Effects on Diesel Particulate—Development and Demonstration of Methodology," SAE Trans., **85**(1), pp. 527–555.
[154] Müller, J. O., Su, D. S., Jentoft, R. E., Wild, U., and Schlögl, R., 2006, "Diesel Engine Exhaust Emission: Oxidative Behavior and Microstructure of Black Smoke Soot Particulate," Environ. Sci. Technol., **40**(4), pp. 1231–1236.
[155] Funkenbusch, E. F., Leddy, D. G., and Johnson, J. H., 1979, "The Characterization of the Soluble Organic Fraction of Diesel Particulate Matter," SAE Trans., **88**(2), pp. 1540–1560.
[156] Johnson, J. E., and Kittelson, D. B., 1994, "Physical Factors Affecting Hydrocarbon Oxidation in a Diesel Oxidation Catalyst," SAE Trans., **103**(3), pp. 1818–1835.
[157] Waldenmaier, D. A., Gratz, L. D., Bagley, S. T., Johnson, J. H., and Leddy, D. G., 1990, "The Influence of Sampling Conditions on the Repeatability of Diesel Particulate and Vapor Phase Hydrocarbon and PAH Measurements," SAE Trans. Journal of Engines, **99**(3), pp. 1431–1448.
[158] Phuleria, H. C., Geller, M. D., Fine, P. M., and Sioutas, C., 2006, "Size-Resolved Emissions of Organic Tracers From Light-and Heavy-Duty Vehicles Measured in a California Roadway Tunnel," Environ. Sci. Technol., **40**(13), pp. 4109–4118.
[159] Eastwood, P., 2008, *Particulate Emissions From Vehicles*, John Wiley & Sons, West Sussex, England.
[160] Nwafor, O. M. I., and Rice, G., 1995, "Performance of Rapeseed Methyl Ester in Diesel Engine," Renewable Energy, **6**(3), pp. 335–342.
[161] Singh, S. K., Agarwal, A. K., and Sharma, M., 2006, "Experimental Investigations of Heavy Metal Addition in Lubricating Oil and Soot Deposition in an EGR Operated Engine," Appl. Therm. Eng., **26**(2–3), pp. 259–266.
[162] Arana, C. P., Pontoni, M., Sen, S., and Puri, I. K., 2004, "Field Measurements of Soot Volume Fractions in Laminar Partially Premixed Coflow Ethylene/Air Flames," Combust. Flame, **138**(4), pp. 362–372.
[163] Rhead, M. N., Trier, C. J., and Petch, G. S., 1990, "The Development of a Radiolabelling Technique to Unequivocally Determine the Products of Combustion From Specific Components of Diesel Fuel," Fuels Automot. Diesel Engines, pp. 19–20.
[164] Martinot, S., Beard, P., Roesler, J., and Garo, A., 2002, "Comparison and Coupling of Homogeneous Reactor and Flamelet Library Soot Modeling Approaches for Diesel Combustion," SAE Paper No. 2001-01-3684.
[165] D'anna, A., and D'Alessio, A., 2000, "Modeling the Rich Combustion of Aliphatic Hydrocarbons," Combust. Flame, **121**(3), pp. 418–429.
[166] Curran, H. J., Fisher, E. M., Glaude, P.-A., Marinov, N. M., Pitz, W. J., Westbrook, C. K., Layton, D. W., Flynn, P. F., Durrett, R. P., Zur Loye, A. O., and Akinyemi, O. C., 2001, "Detailed Chemical Kinetic Modeling of Diesel Combustion With Oxygenated Fuels," SAE Paper No. 2001-01-0653.
[167] Wang, H., and Frenklach, M., 1997, "A Detailed Kinetic Modeling Study of Aromatics Formation in Laminar Premixed Acetylene and Ethylene Flames," Combust. Flame, **110**(1–2), pp. 173–221.
[168] Abbass, M. K., Andrews, G. E., Williams, P. T., and Bartle, K. D., 1989, "The Influence of Diesel Fuel Composition on Particulate PAH Emissions," SAE Technical Paper No. 892079.
[169] Agarwal, A. K., Gupta, T., Dixit, N., and Shukla, P. C., 2013, "Assessment of Toxic Potential of Primary and Secondary Particulates/Aerosols From Biodiesel Vis-a-Vis Mineral Diesel Fuelled Engine," Inhalation Toxicol., **25**(6), pp. 325–332.
[170] Tobias, H. J., Beving, D. E., Ziemann, P. J., Sakurai, H., Zuk, M., McMurry, P. H., Zarling, D., Waytulonis, R., and Kittelson, D. B., 2001, "Chemical Analysis of Diesel Engine Nanoparticles Using a Nano-DMA/Thermal Desorption Particle Beam Mass Spectrometer," Environ. Sci. Technol., **35**(11), pp. 2233–2243.
[171] Rogge, W. F., Hildemann, L. M., Mazurek, M. A., Cass, G. R., and Simoneit, B. R., 1993, "Sources of Fine Organic Aerosol. 2. "Noncatalyst and Catalyst-Equipped Automobiles and Heavy-Duty Diesel Trucks," Environ. Sci. Technol., **27**(4), pp. 636–651.
[172] Johnson, J. H., Bagley, S. T., Gratz, L. D., and Leddy, D. G., 1994, "A Review of Diesel Particulate Control Technology and Emissions Effects-1992 Horning Memorial Award Lecture," SAE Trans., **103**(3), pp. 210–244.
[173] Baumgard, K. J., and Johnson, J. H., 1992, "The Effect of Low Sulfur Fuel and a Ceramic Particle Filter on Diesel Exhaust Particle Size Distributions," SAE Technical Paper No. 920566.
[174] Opris, C. N., Gratz, L. D., Bagley, S. T., Baumgard, K. J., Leddy, D. G., and Johnson, J. H., 1993, "The Effects of Fuel Sulfur Concentration on Regulated and Unregulated Heavy-Duty Diesel Emissions," SAE Technical Paper No. 930730.
[175] Godlee, F., 1991, "Air Pollution—II: Road Traffic and Modern Industry," BMJ, **303**(6816), pp. 1539–1543.
[176] Agarwal, A. K., Gupta, T., Shukla, P. C., and Dhar, A., 2015, "Particulate Emissions From Biodiesel Fuelled CI Engines," Energy Convers. Manage., **94**, pp. 311–330.
[177] Gupta, T., Kothari, A., Srivastava, D. K., and Agarwal, A. K., 2010, "Measurement of Number and Size Distribution of Particles Emitted From a Mid-Sized Transportation Multipoint Port Fuel Injection Gasoline Engine," Fuel, **89**(9), pp. 2230–2233.

[178] Dolan, D. F., Kittelson, D. B., and Pui, D. Y. H., 1980, "Diesel Exhaust Particle Size Distribution Measurement Techniques," SAE Technical Paper No. 800187.
[179] Vuk, C. T., Jones, M. A., and Johnson, J. H., 1976, "The Measurement and Analysis of the Physical Character of Diesel Particulate Emissions," SAE Trans., **85**(1), pp. 556–597.
[180] Agarwal, J. K., and Sem, G. J., 1980, "Continuous Flow, Single-Particle-Counting Condensation Nucleus Counter," J. Aerosol Sci., **11**(4), pp. 343–357.
[181] Agarwal, A. K., Gupta, T., and Kothari, A., 2011, "Particulate Emissions From Biodiesel Vs Diesel Fuelled Compression Ignition Engine," Renewable Sustainable Energy Rev., **15**(6), pp. 3278–3300.
[182] Jung, H., Kittelson, D. B., and Zachariah, M. R., 2006, "Characteristics of SME Biodiesel-Fueled Diesel Particle Emissions and the Kinetics of Oxidation," Environ. Sci. Technol., **40**(16), pp. 4949–4955.
[183] Puzun, A., Wanchen, S., Guoliang, L., Manzhi, T., Chunjie, L., and Shibao, C., 2011, "Characteristics of Particle Size Distributions About Emissions in a Common-Rail Diesel Engine With Biodiesel Blends," Procedia Environ. Sci., **11**, pp. 1371–1378.
[184] Shukla, P. C., Gupta, T., Labhsetwar, N. K., and Agarwal, A. K., 2016, "Development of Low Cost Mixed Metal Oxide Based Diesel Oxidation Catalysts and Their Comparative Performance Evaluation," RSC Adv., **6**(61), pp. 55884–55893.
[185] Agarwal, A. K., Dhar, A., Srivastava, D. K., Maurya, R. K., and Singh, A. P., 2013, "Effect of Fuel Injection Pressure on Diesel Particulate Size and Number Distribution in a CRDI Single Cylinder Research Engine," Fuel, **107**, pp. 84–89.
[186] Ravindra, K., Sokhi, R., and Van Grieken, R., 2008, "Atmospheric Polycyclic Aromatic Hydrocarbons: Source Attribution, Emission Factors and Regulation," Atmos. Environ., **42**(13), pp. 2895–2921.
[187] Shukla, P. C., Gupta, T., and Agarwal, A. K., 2014, "A Comparative Morphological Study of Primary and Aged Particles Emitted From a Biodiesel (B20) Vis-à-Vis Diesel Fuelled CRDI Engine," Aerosol. Air Qual. Res., **14**, pp. 934–942.
[188] Zielinska, B., Goliff, W., McDaniel, M., Cahill, T., Kittelson, D., and Watts, W., 2003, "Chemical Analyses of Collected Diesel Particulate Matter Samples in the E-43 Project," National Renewable Energy Lab, Golden, CO.
[189] Kweon, C. B., Okada, S., Foster, D. E., Bae, M.-S., and Schauer, J. J., 2003, "Effect of Engine Operating Conditions on Particle-Phase Organic Compounds in Engine Exhaust of a Heavy-Duty Direct-Injection (DI) Diesel Engine," SAE Technical Paper No. 2003-01-0342.
[190] Gangwar, J. N., Gupta, T., and Agarwal, A. K., 2012, "Composition and Comparative Toxicity of Particulate Matter Emitted From a Diesel and Biodiesel Fuelled CRDI Engine," Atmos. Environ., **46**, pp. 472–481.
[191] Agarwal, A. K., Gupta, T., and Kothari, A., 2010, "Toxic Potential Evaluation of Particulate Matter Emitted From a Constant Speed Compression Ignition Engine: A Comparison Between Straight Vegetable Oil and Mineral Diesel," Aerosol. Sci. Technol., **44**(9), pp. 724–733.
[192] Macor, A., Avella, F., and Faedo, D., 2011, "Effects of 30% v/v Biodiesel/Diesel Fuel Blend on Regulated and Unregulated Pollutant Emissions From Diesel Engines," Appl. Energy, **88**(12), pp. 4989–5001.
[193] Sharp, C. A., Howell, S. A., and Jobe, J., 2000, "The Effect of Biodiesel Fuels on Transient Emissions From Modern Diesel Engines, Part I Regulated Emissions and Performance," SAE Technical Paper No. 2000-01-1967.
[194] Cheung, C. S., Di, Y., and Huang, Z., 2008, "Experimental Investigation of Regulated and Unregulated Emissions From a Diesel Engine Fueled With Ultralow-Sulfur Diesel Fuel Blended With Ethanol and Dodecanol," Atmos. Environ., **42**(39), pp. 8843–8851.
[195] Cheung, C. S., Zhu, L., and Huang, Z., 2009, "Regulated and Unregulated Emissions From a Diesel Engine Fueled With Biodiesel and Biodiesel Blended With Methanol," Atmos. Environ., **43**(32), pp. 4865–4872.
[196] McDonald, J. D., Barr, E. B., White, R. K., Chow, J. C., Schauer, J. J., Zielinska, B., and Grosjean, E., 2004, "Generation and Characterization of Four Dilutions of Diesel Engine Exhaust for a Subchronic Inhalation Study," Environ. Sci. Technol., **38**(9), pp. 2513–2522.
[197] Schauer, J. J., Kleeman, M. J., Cass, G. R., and Simoneit, B. R., 1999, "Measurement of Emissions From Air Pollution Sources: C1 through C30 Organic Compounds From Medium Duty Diesel Trucks," Environ. Sci. Technol., **33**(10), pp. 1578–1587.
[198] Schauer, J. J., Kleeman, M. J., Cass, G. R., and Simoneit, B. R., 2002, "Measurement of Emissions From Air Pollution Sources. 5. C1− C32 Organic Compounds From Gasoline-Powered Motor Vehicles," Environ. Sci. Technol., **36**(6), pp. 1169–1180.
[199] Grosjean, D., Grosjean, E., and Gertler, A. W., 2001, "On-Road Emissions of Carbonyls From Light-Duty and Heavy-Duty Vehicles," Environ. Sci. Technol., **35**(1), pp. 45–53.
[200] Pang, X., Shi, X., Mu, Y., He, H., Shuai, S., Chen, H., and Li, R., 2006, "Characteristics of Carbonyl Compounds Emission From a Diesel-Engine Using Biodiesel–Ethanol–Diesel as Fuel," Atmos. Environ., **40**(36), pp. 7057–7065.
[201] He, C., Ge, Y., Tan, J., You, K., Han, X., Wang, J., You, Q., and Shah, A. N., 2009, "Comparison of Carbonyl Compounds Emissions From Diesel Engine Fueled With Biodiesel and Diesel," Atmos. Environ., **43**(24), pp. 3657–3661.
[202] Karavalakis, G., Stournas, S., and Bakeas, E., 2009, "Light Vehicle Regulated and Unregulated Emissions From Different Biodiesels," Sci. Total Environ., **407**(10), pp. 3338–3346.
[203] Fontaras, G., Karavalakis, G., Kousoulidou, M., Ntziachristos, L., Bakeas, E., Stournas, S., and Samaras, Z., 2010, "Effects of Low Concentration Biodiesel Blends Application on Modern Passenger Cars—Part 2: Impact on Carbonyl Compound Emissions," Environ. Pollut., **158**(7), pp. 2496–2503.
[204] Magara-Gomez, K. T., Olson, M. R., Okuda, T., Walz, K. A., and Schauer, J. J., 2012, "Sensitivity of Hazardous Air Pollutant Emissions to the Combustion of Blends of Petroleum Diesel and Biodiesel Fuel," Atmos. Environ., **50**, pp. 307–313.
[205] Ho, S. S. H., Ho, K. F., Lee, S. C., Cheng, Y., Yu, J. Z., Lam, K. M., Feng, N. S. Y., and Huang, Y., 2012, "Carbonyl Emissions From Vehicular Exhausts Sources in Hong Kong," J. Air Waste Manage. Assoc., **62**(2), pp. 221–234.
[206] Di, Y., Cheung, C. S., and Huang, Z., 2009, "Experimental Investigation on Regulated and Unregulated Emissions of a Diesel Engine Fueled With Ultra-Low Sulfur Diesel Fuel Blended With Biodiesel From Waste Cooking Oil," Sci. Total Environ., **407**(2), pp. 835–846.
[207] Takada, K., Yoshimura, F., Ohga, Y., Kusaka, J., and Daisho, Y., 2003, "Experimental Study on Unregulated Emission Characteristics of Turbocharged DI Diesel Engine With Common Rail Fuel Injection System," SAE Paper No. 2003-01-3158.
[208] Ballesteros, R., Hernandez, J. J., Lyons, L. L., Cabanas, B., and Tapia, A., 2008, "Speciation of the Semivolatile Hydrocarbon Engine Emissions From Sunflower Biodiesel," Fuel, **87**(10-11), pp. 1835–1843.
[209] Correa, S. M., and Arbilla, G., 2008, "Carbonyl Emissions in Diesel and Biodiesel Exhaust," Atmos. Environ., **42**(4), pp. 769–775.
[210] Liu, Y.-Y., Lin, T. C., Wang, Y. J., and Ho, W. L., 2009, "Carbonyl Compounds and Toxicity Assessments of Emissions From a Diesel Engine Running on Biodiesels," J. Air Waste Manage. Assoc., **59**(2), pp. 163–171.
[211] Xue, J., Grift, T. E., and Hansen, A. C., 2011, "Effect of Biodiesel on Engine Performances and Emissions," Renewable Sustainable Energy Rev., **15**(2), pp. 1098–1116.
[212] Lea-Langton, A. R., Li, H., and Andrews, G. E., 2008, "Comparison of Particulate PAH Emissions for Diesel, Biodiesel and Cooking Oil Using a Heavy Duty DI Diesel Engine," SAE Paper No. 2008-01-1811.
[213] Zielinska, B., 2005, "Atmospheric Transformation of Diesel Emissions," Exp. Toxicol. Pathol., **57**, pp. 31–42.
[214] Karavalakis, G., Stournas, S., and Bakeas, E., 2009, "Effects of Diesel/Biodiesel Blends on Regulated and Unregulated Pollutants From a Passenger Vehicle Operated Over the European and the Athens Driving Cycles," Atmos. Environ., **43**(10), pp. 1745–1752.
[215] Pan, J., Quarderer, S., Smeal, T., and Sharp, C., 2000, "Comparison of PAH and Nitro-PAH Emissions Among Standard Diesel Fuel, Biodiesel Fuel, and Their Blend on Diesel Engines," 48th ASMS Conference on Mass Spectrometry and Allied Topics, Long Beach, CA, June 11–15.
[216] Kittelson, D. B., 1985, "Measurements of PAH in the Cylinders of an Operating Diesel Engine," Environmental Protection Agency, Washington, DC, Report No. 600/D-85/012.
[217] National Research Council, 1992, *Automotive Fuel Economy: How Far Can We Go?* The National Academies Press, Washington, DC.
[218] Jensen, T. E., and Hites, R. A., 1983, "Aromatic Diesel Emissions as a Function of Engine Conditions," Anal. Chem., **55**(4), pp. 594–599.
[219] Barbella, R., Bertoli, C., Ciajolo, A., and D'anna, A., 1988, "Soot and Unburnt Liquid Hydrocarbon Emissions From Diesel Engines," Combust. Sci. Technol., **59**(1–3), pp. 183–198.
[220] Coniglio, L., Bennadji, H., Glaude, P. A., Herbinet, O., and Billaud, F., 2013, "Combustion Chemical Kinetics of Biodiesel and Related Compounds (Methyl and Ethyl Esters): Experiments and Modeling–Advances and Future Refinements," Prog. Energy Combust. Sci., **39**(4), pp. 340–382.
[221] Lai, J. Y., Lin, K. C., and Violi, A., 2011, "Biodiesel Combustion: Advances in Chemical Kinetic Modelling," Prog. Energy Combust. Sci., **37**(1), pp. 1–14.
[222] Patterson, M. A., Kong, S. C., Hampson, G. J., and Reitz, R. D., 1994, "Modeling the Effects of Fuel Injection Characteristics on Diesel Engine Soot and NOx Emissions," SAE Trans., **103**(3), pp. 836–852.
[223] Kong, S. C., Han, Z., and Reitz, R. D., 1995, "The Development and Application of a Diesel Ignition and Combustion Model for Multidimensional Engine Simulation," SAE Trans., **104**(3), pp. 502–518.
[224] Ra, Y., Reitz, R. D., McFarlane, J., and Daw, C. S., 2009, "Effects of Fuel Physical Properties on Diesel Engine Combustion Using Diesel and Bio-Diesel Fuels," SAE Int. J. Fuels Lubr., **1**(1), pp. 703–718.
[225] Bajpai, D., and Tyagi, V. K., 2006, "Biodiesel: Source, Production, Composition, Properties and Its Benefits," J. OLEo Sci., **55**(10), pp. 487–502.
[226] Yuan, W., Hansen, A. C., and Zhang, Q., 2003, "Predicting the Physical Properties of Biodiesel for Combustion Modelling," Trans. ASAE, **46**(6), pp. 1487–1493.
[227] Reid, R. C., Prausnitz, J. M., and Poling, B. E., 1987, *The Properties of Gases and Liquids*, McGraw-Hill, New York.
[228] Chakravarthy, K., McFarlane, J., Daw, S., Ra, Y., Reitz, R. D., and Griffin, J., 2007, "Physical Properties of Bio-Diesel and Implications for Use of Bio-Diesel in Diesel Engines," SAE Trans., **116**(4), pp. 885–895.
[229] Ismail, H. M., Ng, H. K., Cheng, X., Gan, S., Lucchini, T., and D'Errico, G., 2012, "Development of Thermophysical and Transport Properties for the Cfd Simulations of in-Cylinder Biodiesel Spray Combustion," Energy Fuels., **26**(8), pp. 4857–4870.
[230] Ra, Y., and Reitz, R. D., 2009, "A Vaporization Model for Discrete Multi-Component Fuel Sprays," Int. J. Multiphase Flow, **35**(2), pp. 101–117.
[231] Ra, Y., and Reitz, R. D., 2011, "A Combustion Model for IC Engine Combustion Simulations With Multi-Component Fuels," Combust. Flame, **158**(1), pp. 69–90.

[232] Brakora, J. L., Ra, Y., and Reitz, R. D., 2011, "Combustion Model for Biodiesel-Fueled Engine Simulations Using Realistic Chemistry and Physical Properties," SAE Int. J. Engines, **4**(1), pp. 931–947.
[233] Higgins, B. S., Mueller, C. J., and Siebers, D. L., 1999, "Measurements of Fuel Effects on Liquid-Phase Penetration in DI Sprays," SAE Technical Paper No. 1999-01-0519.
[234] Curran, H. J., Gaffuri, P., Pitz, W. J., and Westbrook, C. K., 1998, "A Comprehensive Modeling Study of n-Heptane Oxidation," Combust. Flame, **114**(1–2), pp. 149–177.
[235] Patel, A., Kong, S. C., and Reitz, R. D., 2004, "Development and Validation of a Reduced Reaction Mechanism for HCCI Engine Simulations," SAE Technical Paper No. 2004- 01-0558.
[236] Fisher, E. M., Pitz, W. J., Curran, H. J., and Westbrook, C. K., 2000, "Detailed Chemical Kinetic Mechanisms for Combustion of Oxygenated Fuels," Proc. Combust. Inst., **28**(2), pp. 1579–1586.
[237] Golovitchev, V. I., and Yang, J., 2009, "Construction of Combustion Models for Rapeseed Methyl Ester Bio-Diesel Fuel for Internal Combustion Engine Applications," Biotechnol. Adv., **27**(5), pp. 641–655.
[238] Brakora, J. L., Ra, Y., Reitz, R. D., McFarlane, J., and Daw, C. S., 2009, "Development and Validation of a Reduced Reaction Mechanism for Biodiesel-Fueled Engine Simulations," SAE Int. J. Fuels Lubr., **1**(1), pp. 675–702.
[239] Um, S., and Park, S. W., 2010, "Modeling Effect of the Biodiesel Mixing Ratio on Combustion and Emission Characteristics Using a Reduced Mechanism of Methyl Butanoate," Fuel, **89**(7), pp. 1415–1421.
[240] Herbinet, O., Pitz, W. J., and Westbrook, C. K., 2010, "Detailed Chemical Kinetic Mechanism for the Oxidation of Biodiesel Fuels Blend Surrogate," Combust. Flame, **157**(5), pp. 893–908.
[241] Seshadri, K., Lu, T., Herbinet, O., Humer, S., Niemann, U., Pitz, W. J., Seiser, R., and Law, C. K., 2009, "Experimental and Kinetic Modeling Study of Extinction and Ignition of Methyl Decanoate in Laminar Non-Premixed Flows," Proc. Combust. Inst., **32**(1), pp. 1067–1074.
[242] Herbinet, O., Pitz, W. J., and Westbrook, C. K., 2008, "Detailed Chemical Kinetic Oxidation Mechanism for a Biodiesel Surrogate," Combust. Flame, **154**(3), pp. 507–528.
[243] Luo, Z., Lu, T., Maciaszek, M. J., Som, S., and Longman, D. E., 2010, "A Reduced Mechanism for High-Temperature Oxidation of Biodiesel Surrogates," Energy Fuels, **24**(12), pp. 6283–6293.
[244] Luo, Z., Plomer, M., Lu, T., Som, S., Longman, D. E., Sarathy, S. M., and Pitz, W. J., 2012, "A Reduced Mechanism for Biodiesel Surrogates for Compression Ignition Engine Applications," Fuel, **99**, pp. 143–153.
[245] Luo, Z., Plomer, M., Lu, T., Som, S., and Longman, D. E., 2012, "A Reduced Mechanism for Biodiesel Surrogates With Low Temperature Chemistry for Compression Ignition Engine Applications," Combust. Theory Modell., **16**(2), pp. 369–385.
[246] Brakora, J. L., 2012, "A Comprehensive Combustion Model for Biodiesel-Fueled Engine Simulations," Ph.D. thesis, The University of Wisconsin–Madison, Ann Arbor, MI.
[247] Brakora, J., and Reitz, R. D., 2013, "A Comprehensive Combustion Model for Biodiesel-Fueled Engine Simulations," SAE Technical Paper No. 2013-01-1099.